Abstract

Title of Dissertation: Forming Binary Near-Earth Asteroids From Tidal Disruptions

Kevin J. Walsh, Doctor of Philosophy, 2006

Dissertation directed by: Professor Derek C. Richardson
Department of Astronomy

We present simulations and observations as part of a model of the binary near-Earth asteroid population. The study of binary asteroid formation includes a series of simulations of near-Earth asteroid (NEA) tidal disruption, analyzed for bound, mutually orbiting systems. Discrete and solid particles held together only by self-gravity are employed to model a "rubble pile" asteroid passing Earth on a hyperbolic encounter. This is accomplished via N-body simulations, with multiple encounter and body parameters varied. We examine the relative binary production rates and the physical and orbital properties of the binaries created as a function of the parameters. We also present the overall relative likelihoods for possible physical and dynamical properties of created binaries.

In order to constrain the shape and spin properties of the bodies that feed the NEA population, an observing campaign was undertaken to observe lightcurves of small Main Belt asteroids ($D < 5$ km, SMBAs). Observations of 28 asteroids increases the overall number of SMBAs studied via lightcurves to 86. These observations allow direct comparison between NEAs and MBAs of a similar size.

The shape and spin for the SMBAs are incorporated into a Monte Carlo model of a steady-state NEA population, along with the binaries created by tidal disruption simulations. Effects from tidal evolution and binary disruption from close planetary encounters are included as a means of altering or disrupting binaries. We find that with the best known progenitor (small Main Belt asteroids) shape and spin distributions, and current

estimates of NEA lifetime and encounter probabilities, that tidal disruption should account for approximately 1–2% of NEAs being binaries. Given the observed estimate of an $\sim$ 15% binary NEA fraction, we conclude that there are other formation mechanisms that contribute significantly to this population.

Forming Binary Near-Earth Asteroids From Tidal Disruptions

by

Kevin J. Walsh

Dissertation submitted to the Faculty of the Graduate School of the
University of Maryland at College Park in partial fulfillment
of the requirements for the degree of
Doctor of Philosophy
2006

Advisory Committee:

Professor Derek C. Richardson, advisor
Professor Michael F. A'Hearn
Professor William D. Dorland
Professor Douglas P. Hamilton
Professor M. Coleman Miller
Professor Andrew S. Rivkin

© Kevin J. Walsh 2006

Preface

Much of the work in this dissertation is published, or in the process of being published. Chapter 2 appeared in the planetary-science journal *Icarus*, in nearly the same form as presented here (Walsh & Richardson 2006). The work in Chapter 4 was recently submitted to the same journal, and is under review. Together, and with the results from Chapter 3, this dissertation presents an ongoing study into the binary NEA population. As a whole it provides details on the role that tidal disruption plays in creating the binary NEA population, and builds a framework for further studies in this field.

Over the course of these studies the known population of binary asteroids in the Solar System has more than doubled. New discovery techniques have been used, and old techniques have been applied to different populations. Because of the rapidly changing landscape, this work is quite timely and relevant to the latest observations and theoretical work being done. Beyond the answers provided about tidal disruption, the steady-state model will be able to incorporate new binary formation mechanisms as they become better understood.

To all those who helped along the way...

Acknowledgements

I would not have made it to this point in my education without significant amounts of help and inspiration along the way. I would like to thank as many as possible, starting with everyone at YMCA Camp Eberhart, where I first learned to use a telescope. Prof. Rettig at Notre Dame helped me immensely by directing my first research projects and by keeping me working at the observatory. Thanks to Derek for supplying plenty of freedom and support as my advisor throughout my time at Maryland, from my second year project all the way through to my dissertation. He never hesitated to send me to a conference or a telescope, and always encouraged my numerous side projects, which substantially enhanced my educational experience. I also owe many thanks to the faculty, staff and students at Maryland for making my time here both fun and enriching. Thanks to the UMD-KPNO collaboration for supplying me with observing time and funding in support of my dissertation.

Contents

List of Tables **viii**

List of Figures **ix**

1 Introduction **1**
1.1 Scientific Motivation 1
1.1.1 Why binary asteroids are interesting 1
1.1.2 Binary near-Earth asteroids 2
1.1.3 Binary Main-Belt asteroids 6
1.2 Binary Formation Mechanisms 9
1.2.1 Capture 12
1.2.2 Collisions 12
1.2.3 Rotational disruption 14
1.3 Shape and Spin Distributions for NEAs and MBAs 17
1.3.1 Existing lightcurve data 17
1.3.2 Recent studies 18
1.3.3 Motivation for work on small MBAs 19
1.4 Steady-State Models of the NEA Population 20
1.4.1 Near-Earth asteroid population dynamics 21
1.5 Background 22
1.5.1 Tidal disruption 22
1.5.2 Rubble piles 24
1.6 This Dissertation 25

2 Formation of Binary Asteroids via Tidal Disruption of Rubble Piles **26**
2.1 Overview 26
2.2 Method 27
2.2.1 Simulations 27
2.2.2 Progenitors 27
2.2.3 Tidal encounters and initial conditions 30
2.2.4 Analysis 32

2.3 Results and Discussion . . . 33
2.3.1 Bulk results . . . 33
2.3.2 T-PROS and T-EEBs . . . 45
2.3.3 Classes of disruption . . . 47
2.3.4 3 h spin rate subset . . . 47
2.3.5 Triples and hierarchical systems . . . 50
2.3.6 Tidal evolution and eccentricity damping . . . 50
2.4 Conclusion . . . 55

3 Lightcurve Observations of Small Main Belt Asteroids 57
3.1 Overview . . . 57
3.2 Observations . . . 58
3.3 Data Reduction and Photometry . . . 60
3.3.1 Phase dispersion minimization . . . 61
3.4 Results and Discussion . . . 62
3.4.1 Well-determined lightcurves . . . 63
3.4.2 Detections with significant constraints . . . 64
3.4.3 Marginal detections . . . 66
3.4.4 Spin and shape properties among small MBAs and NEAs . . . 74
3.5 Conclusions . . . 78

4 Steady-State Model of the Binary Near-Earth Asteroid Population 80
4.0.1 Previous work . . . 81
4.1 Steady-State Model . . . 83
4.1.1 Initial shape and spins . . . 83
4.1.2 NEA lifetimes and planetary encounters . . . 84
4.1.3 Binary evolution . . . 88
4.1.4 Migrating binary MBAs . . . 92
4.2 Steady-State Results and Discussion . . . 95
4.2.1 Nominal case . . . 95
4.2.2 Influence of MBA binary percentage . . . 96
4.2.3 Influence of MBA shape/spin properties . . . 101
4.2.4 Influence of tidal evolution . . . 101
4.2.5 Estimates on the properties of binary NEAs formed by tidal disruption . . . 103
4.2.6 Estimates of migrated binaries' numbers and properties . . . 104
4.2.7 Doublet craters . . . 105
4.3 Conclusion . . . 105

5 Conclusions 108
5.1 Future Work . . . 109

A Parameter Tests **113**
A.1 Bulk Density of Progenitor 113
A.2 Resolution of Progenitor 115
A.3 Packing Efficiency of Progenitor 116
A.4 Conclusions on Parameter Tests 118

Bibliography **121**

List of Tables

1.1 Binary NEA properties. 5
1.2 Binary MBA properties. 11

2.1 Binary formation statistics. 33

3.1 Diameter estimates from H. 59
3.2 Orbital, physical and lightcurve parameters for all targets. 68

4.1 Lifetimes for binary NEAs. 90
4.2 Binary fractions for all simulations. 103

A.1 Number of binaries produced at varying resolutions. 116

List of Figures

1.1 Binary NEA and MBA properties. 10

2.1 Initial spin and shape parameters. 29
2.2 Distribution of v_∞ for NEA close encounters. 31
2.3 Snapshots of a tidal disruption. 32
2.4 Probability of binary formation for each parameter. 34
2.5 Binaries formed compared to mass of the largest remnant. 36
2.6 Binary orbital properties. 38
2.7 Binary size ratio, obliquity and spin period. 41
2.8 Primary body shape statistics. 43
2.9 T-PROS and T-EEBs 46
2.10 Comparison of S-, B-, and M-class disruptions. 48
2.11 Spin periods of 3 h spin subset. 49
2.12 Tidal evolution of semi-major axis. 53
2.13 Eccentricity damping timescales. 54

3.1 Lightcurve plots 69
3.2 Lightcurve plots 70
3.3 Lightcurve plots 71
3.4 Lightcurve plots 72
3.5 Lightcurve plots 73
3.6 Shape and spin distributions for different sized MBAs 75
3.7 NEA and SMBA lightcurve distribution comparison 76
3.8 NEA and SMBA lightcurve distribution comparison, $H < 17$ 77

4.1 Lightcurves periods and amplitudes for NEAs, MBAs and SMBAs 85
4.2 NEA lifetimes 86
4.3 Test of 3-body simulations 91
4.4 MBA binary properties 94
4.5 Number of binaries in nominal simulation 97
4.6 Properties of binaries in nominal simulation 98
4.7 Lifetimes of binaries in nominal simulation 99

4.8 Percentage of migrated binaries 100
4.9 Influence of tidal evolution on simulations 102

5.1 Preliminary YORP spinup results 111

A.1 Results from simulations with varying resolution. 117

Chapter 1

Introduction

1.1 Scientific Motivation

1.1.1 Why binary asteroids are interesting

The discovery and observation of binary asteroids over the past decade has provided new ways to study the properties of Solar System bodies. Before the 1993 discovery of Ida's companion Dactyl in the main asteroid belt by the *Galileo* mission, there were only unconfirmed detections and theoretical speculation about binary asteroids. The inventory of binary minor planets has now eclipsed 100, there are known triple and even quadruple systems, and detailed radar shape models are being produced for some nearby binaries (see Richardson & Walsh 2006 for a review). Of particular interest for this dissertation are binaries in the Main-Belt and near-Earth populations.

The reason astronomers have searched for binary asteroids since the discovery of (1) Ceres is that binary asteroids can provide extensive insight into the physical properties of the bodies. They can also provide information about past and present dynamics affecting small bodies in the inner Solar System. A binary system typically allows for estimation

of the system mass M by way of Kepler's Third Law,

$$P^2 = 4\pi^2 a^3 / GM \tag{1.1}$$

with period P and mean separation a typically directly measured, and G is the gravitational constant. In most situations component sizes and shapes can be modeled allowing for a rare measurement of asteroid density. When coupled with a spectroscopic estimate of asteroidal composition, estimates on porosity and internal structure can be made.

The dynamical mechanisms affecting various populations of small bodies can also be studied by way of binary asteroids. Binaries have been discovered in nearly every dynamical population of minor planets, with large numbers among trans-Neptunian objects (or Kuiper Belt Objects), one binary Jovian Trojan, two binary Centaurs, and a plethora of binary Main Belt and near-Earth asteroids. Adding to this inventory are recent discoveries of complex systems such as the additional satellites of Pluto, a triple KBO 2003 EL_{61}, and a triple Main-Belt asteroid (MBA) system (87) Sylvia. Since each population boasts dramatically different dynamical, collisional and thermal environments, the existence and detailed study of binaries will be quite valuable.

1.1.2 Binary near-Earth asteroids

The known binary near-Earth asteroids (NEAs) have been discovered from a combination of lightcurve and radar observations. Lightcurve studies, where an asteroid's magnitude is plotted over time, have been conducted on a large number of bodies. However, certain orbital properties (asynchronous orbit and favorable geometry) are needed to make an unambiguous assessment of the state of the binary (Weidenschilling et al. 1989; Pravec & Hahn 1997). The secondaries must be large enough ($\sim$20% of the primary) for their nonsynchronous periods to be observed above any noise in the lightcurve of the primaries. Observations must also capture occultations/eclipses over multiple revolutions of the sec-

ondary body, which requires extensive observations at a viewing angle near the binary orbital plane.

Radar observations require the close approach of an asteroid to Earth, but can provide detailed physical and orbital information about the binary. The signal–to–noise ratio (SNR) of radar measurements is proportional to $R_{\rm tar}^{-4}$ and $D_{\rm tar}^{3/2}$, where $R_{\rm tar}$ and $D_{\rm tar}$ are the distance to and diameter of the target body respectively. The SNR is also proportional to $P^{1/2}$, the square root of the rotation period. Thus radar observations are more likely to discover nearby, larger, slower-rotating secondaries (Ostro et al. 2002).

The currently known NEA binaries share similar physical and orbital traits. All currently known or suspected binaries have primary bodies with a diameter ($D_{\rm pri}$) less than 4 km, normal for NEAs but significantly smaller than large MBAs (see Table 1.1). All primaries with measured rotations, with the exceptions of NEAs (69230) Hermes and 2000 UG_{11}, have rotation periods among the fastest observed between 2.2 and 3.6 h. These rotation rates are very near the critical spin limit for a spherical strengthless body given approximately by

$$P_{\rm crit} \approx \frac{3.3}{\sqrt{\rho}}({\rm h}) \tag{1.2}$$

where ρ, the bulk density of the body, is in g cm^{-3}. For a body with ρ = 2.2 g cm^{-3}, $P_{\rm crit}$ $\approx$ 2.2 h, which defines the lower limit for primary spin rate currently observed (Pravec & Harris 2000). Asteroids spinning above the critical rate are not stable as material at their equator feel more outward centrifugal acceleration than the acceleration from its own self gravity.

All the primaries have similar lightcurve amplitudes, typically below 0.2 magnitudes. The amplitude of a primary's lightcurve (Δm) has a simple relationship with the body's shape

$$\Delta m \sim 2.5 \log \frac{a}{b} \tag{1.3}$$

where a and b are the long and intermediate length axes of a tri-axial ellipsoid. Thus

the largest lightcurve amplitudes observed, ~ 0.2 magnitudes, imply a 1.2:1.0 axis ratio. The entire population of NEAs has a much larger range of lightcurve amplitudes; 0.2 is relatively close to spherical in comparison (Pravec et al. 2002).

The secondaries typically have diameters between 0.2 and 0.6 times $D_{\rm pri}$. Again, the exception is Hermes which is a suspected synchronously rotating binary with equal-sized components, as well as the radar-discovered (1862) Apollo with a secondary 1/20th the size of its primary[1]. All others are asynchronous systems, with the primary rotating much faster than the orbital period of the secondary (Pravec et al. 2004b). An observational limit exists for bodies below 0.2 $D_{\rm pri}$, but between 0.6 and 1.0 $D_{\rm pri}$, where few systems are observed, no biases are known. The secondaries are also consistent in their separation from the primary, with most being within 6 primary radii ($R_{\rm pri}$). The exception is 1998 ST_{27} with a separation ~ 10 $R_{\rm pri}$, which also has a relatively fast-spinning secondary (period < 6 h) and a high eccentricity ($e > 0.3$). Other than ST_{27}, the few eccentricities that are known are all below 0.1. Few rotations of secondaries are well known, though they appear mostly synchronized with the orbital motion, with 1998 ST_{27} again being an exception (Pravec et al. 2004b). No correlations are seen between properties and primary mass or asteroid spectral classification Pravec et al. (2006).

The lightcurve survey of binary NEAs determined that 15 ± 4% of NEAs larger than 0.3 km are binaries with $D_{\rm sec}/D_{\rm pri} \geq 0.18$ (Pravec et al. 2006). Among the fastest spinning NEAs with rotation rates between 2–3 h, the binary percentage is 66^{+10}_{-12}%. These estimates include the detection limitations of the lightcurve techniques, which are strongly biased against discovering binaries with wide separations (Pravec et al. 2006).

[1]Synchronization timescales for a binary like Hermes are expected to be below 10 Myr, possibly even below 1 Myr. See Section 2.3.6 for a detailed treatment of tidal evolution.

Table 1.1. Binary NEA properties.

Binary	a (AU)	e	D_{pri} (km)	P_{pri} (h)	a km	D_{sec} (km)	P_{orb} (d)	Disc.	ref
(66391) 1999 KW_4	0.64	0.68	1.2	2.77	2.5	0.4	0.73	R	[1,2]
1998 ST_{27}	0.81	0.53	0.8	3.0	4.0	0.12		R	[3,4]
1999 HF_1	0.81	0.46	3.5	2.32	7.0	0.8	0.58	L	[2,5]
(5381) Sekhmet	0.94	0.29	1.0	2.7	1.5	0.3	0.52	R	[6,7]
(66063) 1998 RO_1	0.99	0.72	0.8	2.49	1.4	0.38	0.60	L	[2,8]
1996 FG_3	1.05	0.35	1.5	3.59	2.6	0.47	0.67	L	[2,9,10]
(88710) 2001 SL_9	1.06	0.27	0.8	2.40	1.4	0.22	0.68	L	[2,11]
1994 AW_1	1.10	0.07	1.0	2.52	2.1	0.5	0.93	L	[2,12]
2003 YT_1	1.10	0.29	1.0	2.34	2.7	0.18	1.25	L/R	[2,13]
(35107) 1991 VH	1.13	0.14	1.2	2.62	3.2	0.44	1.36	L	[2,14]
2000 DP_{107}	1.36	0.37	0.8	2.77	2.6	0.3	1.76	R	[2,15,16,17]
(1862) Apollo	1.47	0.56	1.6	3.06	3.0	0.08		R	[33]
(65803) Didymos	1.64	0.38	0.8	2.26	1.1	0.17	0.49	L/R	[2,18]
(69230) Hermes	1.65	0.62	0.6	13.89			0.54	R	[2,19]
1990 OS	1.67	0.46	0.3		0.6	0.05	0.88	R	[20]
(5407) 1992 AX	1.83	0.27	3.9	2.55	6.8	0.78	0.56	L	[2,21]
2002 BM_{26}	1.83	0.44	0.6	2.7		0.1		R	[22]
(85938) 1999 DJ_4	1.85	0.48	0.4	2.51	1.5	0.17	0.74	L	[2,23,24]
2000 UG_{11}	1.92	0.57	0.2	4.44	0.4	0.08	0.77	R	[2,25]
2003 SS_{84}	1.93	0.57	0.1			0.06		R	[26]
2002 KK_8	1.95	0.46	0.5			0.1		R	[27]
(31345) 1998 PG	2.01	0.39	0.9	2.52	1.5	0.3		L	[2,28]
(3671) Dionysus	2.19	0.54	1.5	2.71	3.8	0.3	1.16	L	[2,29]
2002 CE_{26}	2.23	0.55	3.0	3.29	5.1	0.21	0.67	R	[2,30]
1994 XD	2.35	0.73	0.6		1.0	0.15	0.67	R	[32]
2005 AB	3.21	0.65		3.33			0.75	L	[31]

Note. — Orbital and physical properties for well-observed or suspected NEA binaries. The discovery techniques are (L) lightcurve and (R) radar. References: [1] Benner et al. (2001b); [2] Pravec et al. (2006); [3] Benner et al. (2001a); [4] Benner et al. (2003); [5] Pravec et al. (2002); [6] Nolan et al. (2003b); [7] Neish et al. (2003); [8] Pravec et al. (2003b); [9] Pravec et al. (2000b); [10] Mottola & Lahulla (2000); [11] Pravec et al. (2001); [12] Pravec & Hahn (1997); [13] Nolan et al. (2004); [14] Pravec et al. (1998); [15] Ostro et al. (2000); [16] Pravec et al. (2000a); [17] Margot et al. (2002); [18] Pravec et al. (2003a); [19] Margot et al. (2003); [20] Ostro et al. (2003); [21] Pravec et al. (2000b); [22] Nolan et al. (2002a); [23] Pravec et al. (2004a); [24] Benner et al. (2004); [25] Nolan et al. (2000); [26] Nolan et al. (2003a); [27] Nolan et al. (2002b); [28] Pravec et al. (2000b); [29] Mottola et al. (1997); [30] Shepard et al. (2004); [31] Reddy et al. (2005); [32] Benner et al. (2005); [33] Ostro et al. (2005),

1.1.3 Binary Main-Belt asteroids

Recent discoveries among small Main-Belt asteroids (MBAs) using lightcurve observations have started to remove the observational biases that previously obscured any similarities between binary MBAs and NEAs (Pravec & Harris 2006). At first they were discovered primarily using two distinct techniques, lightcurves for NEAs and high-resolution direct imaging for MBAs. These two techniques preferentially discover entirely different kinds of binaries, with lightcurves only sensitive to binaries with small separation and moderate (1.0-0.2) size ratios, whereas direct imaging is primarily sensitive to binaries with a large separation and can cover a wider range of size ratios.

A limiting factor, which plagues both discovery methods, is primary size. This is a complication regardless of observing technique, as a 1 km body in the Main Belt is substantially more difficult to study than one in the near-Earth population. Despite recent lightcurve discoveries among MBAs with $D < 5$km, sub-kilometer discoveries of any kind would require substantial time on very large telescopes. Discoveries with both methods point to two seemingly different groups within the binary MBA population, each formed from different mechanisms. Hence, we describe the binaries discovered by each method separately.

High-resolution imaging discoveries

The binary MBAs discovered via direct imaging always have relatively distant companions that must be observed outside of the point spread function of the brighter primary. However, these observations are sensitive to large brightness differences, for example (45) Eugenia's moon Petit Prince was 7 magnitudes dimmer at discovery than its primary (Merline et al. 2002c). These two effects demand that the observed MBA binaries have large separations but allow a wide range of size ratios. Even the smallest binaries discov-

ered with AO or HST, down to diameters below 5 km, have very wide separations, usually over 100 km.

Starting with (45) Eugenia in 1999, the first binaries discovered in the Main Belt population shared few similarities with the binary NEAs. First, they were observed to have a much smaller percentage of occurrence ($\sim$ 2–3%) than NEA binaries ($\sim$ 15%) (Pravec et al. 1999; Margot et al. 2002; Merline et al. 2002c). Even accounting for different discovery techniques and observing scenarios there is a significant, sizable difference in relative numbers. Second, all have primaries that are larger than 4.5 km, with nearly half larger than 100 km. Thus nearly all the primaries for known MBA binaries are larger than the largest NEA (this is largely a selection effect due to the difficulty of observing distant small bodies).

Third, the primaries' spin period of binary MBAs are spread between 2.6 and 16.5 h, with only three with periods below 4.0 h (see Fig. 1.1, Table 1.2). This differs significantly from the very tight grouping of primary spin for NEAs. Fourth, the secondaries are between 0.04 and 1.0 times the size of the primaries, going well below the 0.2 size threshold for NEA binaries (the 0.2 size threshold is likely an observational bias for NEAs, rather than a physical limit). Fifth, the observed separations are quite large, ranging from 2–100 primary radii, well beyond any observed for NEAs.

Primary spin rate is a quantity which should not be biased in AO observations, though it is not directly measured during discovery and therefore sometimes not reported. The differences in primary spin between MBA and NEA binaries (before the recent binary MBA lightcurve discoveries, see next section) was commonly cited as the main evidence for different formation scenarios. With no correlation in spin rates, and large ranges in secondary sizes and separations, it has generally been considered likely that the original MBA binaries result from collisions in the Main Belt.

Lightcurve discoveries

A lightcurve is simply the measure of an asteroid's brightness over time. The first binaries in the Main Belt discovered via lightcurve observations were synchronous systems, with a secondary orbital period equal to the primary rotation period (Behrend et al. 2006). This survey studied bodies with absolute magnitudes, $9 < H < 15$, equivalent to diameters from 10–50 km. The binaries had orbital and rotational periods from 16–37 h, starkly different from the fast-spinning NEA primaries. However, the separations for the systems mirrored the NEAs, ranging from 1.7 to 2.6 $R_{\rm pri}$. All of these systems have primaries larger than 10 km, significantly larger than the NEAs.

Pravec & Harris (2006) reported on survey results among MBAs with diameters smaller than 5 km, discovering multiple binaries. These systems, unlike those of Behrend et al. (2006), were found to resemble the NEA population in nearly every way. They had similar separations, size ratios, and the primaries were spinning almost as rapidly. The binary NEAs, with only a few exceptions, have primaries rotating at or below a 3 h period. The newly discovered small MBA binaries do not show such uniform rapid rotation, though most have rotations faster than 6 h. The overall number of discoveries among MBAs with diameter < 10 km is still very small, and it is possible that the NEA-like binaries discovered by Pravec & Harris (2006) and the slightly larger binaries found by Behrend et al. (2006) belong to the same population in which the primary spin rate depends strongly on primary size.

Any asteroid discovery made via lightcurves suffers the same biases, with systems having close separations and larger secondaries being preferentially discovered. The strongest diagnostic from lightcurve observations is the primary spin, as that is determined with great accuracy with this method, and has already proven to vary widely in different populations, and for different sized primaries.

Comparison with binary NEAs

The application of lightcurve techniques to small MBAs may define the role that asteroid size plays in binary fractions and properties. These recent discoveries suggest the previously perceived differences between NEA and MBA binaries may have been dominated by the relative difference in size of observed bodies as well as the fundamental observing biases affecting each. If the small MBA binaries have very similar properties to NEAs, then a similar formation mechanism will be needed for both MBAs and NEAs, and potential transport of MBAs to the NEA population will be important. These newly discovered binary small MBAs with rapidly rotating primaries, small size-ratios and small separations suggest that the formation mechanism for binary NEAs may also be creating binaries of a similar sort in the Main Belt.

1.2 Binary Formation Mechanisms

Until very recently different formation mechanisms were typically invoked to explain binary NEAs and MBAs: rotational spin-up and collisional processes respectively. Tidal disruption, as a means of rotational disruption, fit the binary NEAs, as encounters with large planetary bodies are unique to that region and frequent enough to affect a large percentage of the population. In the Main Belt collisional lifetimes are shorter than dynamical lifetimes, providing a framework for the formation of the diverse population of binary MBAs. The recent work on small binary MBAs calls into question these separate formation mechanisms and may demand a new formation mechanism which will affect small bodies in both populations. Below we discuss the main binary formation mechanisms expected to be acting throughout the inner Solar System.

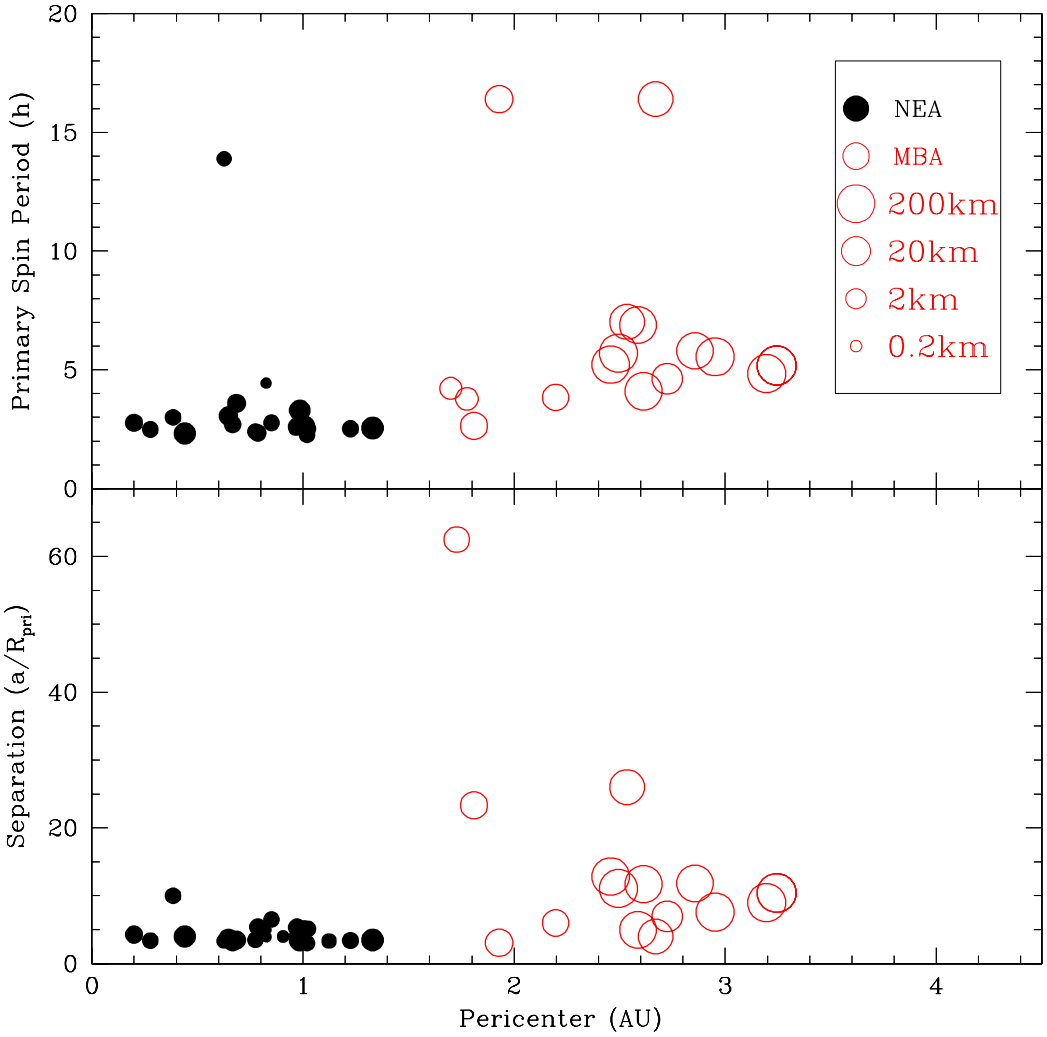

Figure 1.1: (Top) The primary rotation period of the known NEA (filled) and MBA (open) binaries as a function of the pericenter of the binary's orbit. (Bottom) The component separations of the same binaries as a function of pericenter. In both panels, each point represents one binary, with the size of the point indicating the size of the primary.

Table 1.2. Binary MBA properties.

Binary	a (AU)	e	D_{pri} (km)	P_{pri} (h)	a km	D_{sec} (km)	P_{orb} (d)	Disc.	ref
(4674) Pauling	1.86	0.07	8		250	2.5		AO	[1]
(1509) Esclangona	1.87	0.03	12	2.64	140	4		AO	[2,3]
(9069) Hovland	1.91	0.11	3	4.22		0.9		L	[4]
(5905) Johnson	1.91	0.07	3.6	3.783		1.44	1.16	L	[4,5]
(76818) 2000 RG_{79}	1.93	0.10	3.6	3.166		1.1	0.59	L	[36]
(1089) Tama	2.21	0.13	13	16.44	20	(9)	0.68	L	[6]
(3749) Balam	2.24	0.11	7		350	1.5	100	AO	[7,8]
(3703) Volkonskaya	2.33	0.13	3	3.23		1.2	1	L	[36]
(854) Frostia	2.36	0.17					1.57	L	[9]
(3782) Celle	2.41	0.09	6.1	3.84	36.57	2.6	1.52	L	[10,11]
(11264) Claudiomaccone	2.58	0.23	4	3.18		1.2	0.63	L	[36]
(1313) Berna	2.65	0.20		25.46			1.061	L	[12]
(45) Eugenia	2.72	0.08	215	5.70	1190	13	4.69	AO	[8,13]
(4492) Debussy	2.76	0.17		26.59			1.11	L	[14]
(22899) 1999 TO_{14}	2.84	0.08	4.5		170	1.5		HST	[15]
(17246) 2000 GL_{74}	2.84	0.02	4.5		230	2		HST	[16]
(243) Ida	2.86	0.05	31	4.63	108	1.4	1.54	SC	[8,17]
(22) Kalliope	2.91	0.10	181	4.14	1020	38	3.58	AO	[18,19,20]
(283) Emma	3.04	0.15	148	6.88	600	12	3.36	AO	[21,22,23]
(130) Elektra	3.12	0.21	182	5.22	1250	4	3.9	AO	[21,24,25]
(379) Huenna	3.13	0.19	92	7.02	3400	(7)	81	AO	[23,26,27]
(90) Antiope	3.16	0.16	85	16.50	170	85	0.69	AO	[8,28]
(762) Pulcova	3.16	0.09	137	5.84	810	20	4.0	AO	[8,29]
(121) Hermione	3.43	0.14	209	5.55	775	13	2.57	AO	[30,31,32,33]
(107) Camilla	3.47	0.08	223	4.84	1240	9	3.71	HST	[8,34]
(87) Sylvia	3.49	0.07	261	5.18	1360	18	3.65	AO	[8,35,37]
(87) Sylvia	3.49	0.07	261	5.18	710	7	1.38	AO	[37]

Note. — Orbital and physical properties for well-observed or suspected MBA binaries. The discovery techniques are (L) lightcurve, (AO) adaptive optics, (T) ground-based telescope, and (SC) for spacecraft. References: [1] Merline et al. (2004); [2] Merline et al. (2003b); [3] Warner (2004); [4] Warner et al. (2005a); [5] Warner et al. (2005b); [6] Behrend et al. (2004b); [7] Merline et al. (2002a); [8] Merline et al. (2002c); [9] Behrend et al. (2004a); [10] Ryan et al. (2003); [11] Ryan et al. (2004); [12] Behrend et al. (2004c); [13] Merline et al. (1999); [14] Behrend (2004); [15] Merline et al. (2003d); [16] Tamblyn et al. (2004); [17] Belton & Carlson (1994); [18] Merline et al. (2001); [19] Margot & Brown (2001); [20] Marchis et al. (2003); [21] Marchis et al. (2005a); [22] Merline et al. (2003c); [23] Stanzel (1978); [24] Merline et al. (2003e); [25] Magnusson (1990); [26] Margot (2003); [27] Harris et al. (1992); [28] Merline et al. (2000b); [29] Merline et al. (2000a); [30] Merline et al. (2002b); [31] Merline et al. (2003a); [32] Marchis et al. (2004a); [33] Marchis et al. (2004b); [34] Storrs et al. (2001); [35] Brown et al. (2001); [36] Pravec et al. (2006); [37] Marchis et al. (2005b).

1.2.1 Capture

In this scenario two asteroids become mutually bound during a close encounter. Required during this encounter are relative speeds that are below their mutual escape speeds. For the small bodies of the NEA population the escape speeds are generally on the order of m s^{-1}, while encounter speeds are on the order of km s^{-1}. As well the time between encounters is longer than the dynamical lifetime for the bodies. Capture is similarly unlikely in the Main Belt, eliminating the possibility of a captured system in this population migrating into the NEA population. As well, captured binaries would be expected to be only loosely bound, and would have a very short lifetime in the NEA population before a planetary encounter disrupted the system. The capture scenario is best suited to very wide binaries observed in the Kuiper Belt.

1.2.2 Collisions

Both catastrophic and subcatastrophic impacts can create a debris field capable of reaccumulating secondaries around a massive central remnant, or having debris leaving the system become bound to each other. Hypothesized by van Flandern et al. (1979) and Weidenschilling et al. (1989) as a possible mechanism for binary formation, it needs to overcome the fundamental problem that debris leaving the surface of a spherically-symmetric asteroid will have its bound orbit pass through the surface of the asteroid. Weidenschilling et al. (1989) posited that dense debris fields with accumulated secondaries whose final orbit is determined by their mean angular momentum is a possible solution.

After the discovery of Ida's satellite, Dactyl, numerical simulations of an expanding debris field resulting from a collision and disruption of an asteroid found that many different kinds binary systems were created (Durda 1996). Using assumed ejecta patterns and mass distributions, numerous binary configurations were observed, with a wide range

of size ratios, including contact-binary formations.

In the course of modeling asteroid family formation via reaccumulation of debris following a catastrophic impact, Michel et al. (2001, 2004) found many companions of the largest remnant. The works were focused on, and matched, many dynamical and physical properties of some asteroid families, but no comprehensive analysis of any binaries was completed.

Durda et al. (2004) simulated large-scale (100 km diameter target body) catastrophic collisions of asteroids to determine the efficiency of forming binaries via collision. Similar to Michel et al. (2001, 2004) these simulations used a smoothed particle hydrodynamics (SPH) code to model the collision and an *N*-body code to simulate the post-collision evolution and re-accumulation of the fragments. The collisions were efficient at creating bound systems out of the re-accumulated debris and many of the binaries produced are qualitatively similar to those observed in the Main Belt. Two main types of outcomes from these simulations were observed and classified as SMATS (SMAshed Target Satellites) and EEBs (Escaping Ejecta Binaries). The SMATS consist of re-accumulated fragments orbiting the largest remnant from the collision, whereas the EEBs are small and usually similar-sized fragments that have escaped from the largest remnant and become bound to each other.

Of the observed MBA binaries discovered via high-resolution imaging most are similar to SMATS, with primaries significantly larger than the secondaries. Some binaries with small, nearly equal-sized components and large separations are suspected EEBs (see (4674) Pauling, (1509) Esclangona, (22899) 199 TO_{14}, and (17246) GL_{74} in Table 1.2).

In the NEA population the collisional lifetimes are significantly longer than the very short dynamical lifetimes ($\sim$10 Myr as determined through numerical simulations), making collisions an unlikely local source of binaries. The binaries observed in collision simulations typically have larger separations than is observed with NEA binaries. How-

ever, understanding the mechanism is important as collisionally formed binaries in the Main Belt may migrate to the NEA population.

1.2.3 Rotational disruption

Rotational disruption has been credited with a large role in binary formation among NEAs due to some of the prominent similar properties shared by these binaries (Merline et al. 2002c; Margot et al. 2002). Rapidly-rotating primaries, very near the theoretical breakup limit for strengthless bodies, have been a signature of binary NEAs and have recently been seen among small MBAs. The fastest-rotating NEAs have periods no shorter than $\sim$ 2 h, and the primaries of the observed binaries nearly all have periods below 3 h. Thus a formation related to rotational disruption when an asteroid is made to spin faster than the critical limit has been favored for this population.

Tidal disruption

Tidal disruption of a rubble pile has been invoked to explain the disruption of Comet D/Shoemaker–Levy 9 (SL9) and has also been applied to asteroid studies. SL9 disrupted when the comet passed within $\sim 1.36\ R_J$ of Jupiter on 1992 July 7. The comet was torn apart and $\sim$ 21 fragments or reaccumulated clumps were later observed. *N*-body studies have since matched many of the comet's basic post-disruption features (train length, position angle and morphology) using a strengthless rubble pile model (Solem 1994; Asphaug & Benz 1996; Walsh et al. 2003).

Solem & Hills (1996) used similar *N*-body techniques to simulate the change in elongation (ratio of long axis to short axis length) of an asteroid due to a planetary close approach. Citing 1620 Geographos as an extreme case with an elongation of 2.7, encounters with Earth between close approach distance q = 1.02 and 2.03 Earth radii ($R_\oplus$) were sampled with a range of v_∞ (the speed at infinity of a hyperbolic encounter) between $\sim$

15 and 25 km s^{-1}. The models represented the progenitors with 135 particles, and some simulations produced outcomes more elongated than Geographos, providing a potential means of creating very elongated solar system bodies.

Bottke & Melosh (1996a) simulated splitting of contact binaries to explain doublet craters on Earth, Venus and Mars. In this model a binary asteroid is formed during a close encounter with a planet, and the binary's separation grows through subsequent encounters. Eventually the binary hits a planet, making a doublet crater. This scenario depends on a constant refreshing of the NEA binary population via tidal disruptions, and predicts that $\sim$ 15% of NEAs may be binaries at any given time.

Simulations of NEA tidal disruption by Richardson et al. (1998) covered a large parameter space of elongated rotating bodies (constructed with 247 particles) passing Earth at various q and v_∞. The study was designed to quantify disruption and mass loss for tidal encounters, but noted binary formation as an observed outcome and suggested that tidal disruption could explain up to $\sim$ 15% of the NEAs being binaries. The simulations sparsely covered the parameters of q, v_∞, progenitor elongation, progenitor spin rate and long axis alignment. Basic trends in disruption were observed, with increasing disruption for closer approaches, slower approach speeds, and faster prograde rotation rates. More subtle results were seen as a function of body elongation and long axis alignment at close approach.

Functionally tidal disruption is an impulsive event that both elongates and torques a body. A spherical body will be elongated and then spun-up during a passage by a planet, whereas a previously elongated body may be reshaped or just spun-up more dramatically depending on the long-axis alignment during close approach. In the closest and most catastrophic encounters a strengthless body is pulled into a long string of particles, similar to the SL9 event, and numerous clumps form along the string. A less dramatic event will simply involve a body appearing to have been spun-up to the point that some mass escapes

off the equator or off one end of a prolate body.

Bottke et al. (1999) compared the shape of 1620 Geographos, obtained from delay–Doppler measurements, to that of a tidal encounter outcome. The well-defined shape of Geographos matched many features of the simulation output, including the cusped ends, an opposed convex side, and a nearly concave side with a large hump. This study was similar in approach to Solem & Hills (1996), but matched the high-quality images with high-resolution ($\sim$ 500-particle) simulations.

Thermal Spinup

An alternative mechanism for rotational disruption is the YORP thermal effect (see Bottke et al. 2006 for a review). This effect, related to the Yarkovsky effect, relies on re-emission of absorbed solar radiation to provide a very small thermal thrust. This thrust, over long timescales, provides a torque which can alter the asteroid's obliquity and spin rate. This effect depends heavily on the size of the asteroid, and is expected to be quite powerful for sub-kilometer bodies (with spin rate doubling timescales on the order of 0.5 Myr) and ineffective for diameters larger than 40 km. Suggested as possibly responsible for the excess in fast and slow rotators among small asteroids, YORP has been shown in one dramatic case to re-orient spin axes. Vokrouhlický et al. (2003) demonstrated that the combination of thermal torques from YORP and spin-orbit resonances created a collection of similar spin periods and obliquities among Koronis family members, matching observations perfectly.

Despite these detailed studies of the YORP effect, binary creation from thermal spin-up has yet to be studied in detail. Any detailed study relies on various assumptions about an asteroid's shape and thermal properties, as well as the dynamics of a body that has reached and passed its critical spin frequency. The discovery of binaries in the Main Belt, resembling those in the NEA population, strongly suggest that a thermal force is helping

to create or change binaries within both populations.

1.3 Shape and Spin Distributions for NEAs and MBAs

The shape and spin distributions for NEAs and MBAs tells a significant story about each population. The first theories that asteroids may be strengthless, or even rubble piles, came from analysis of the spin periods derived from lightcurves (Burns 1975; Harris 1996). As well, it was concerted campaigns to collect lightcurves of NEAs which started discovering binaries (Pravec & Hahn 1997). The spin and shape of asteroids has also proven to be important parameters in determining the outcome of tidal disruption simulations (Richardson et al. 1998), which is why they are of interest in this work. From the measured lightcurve, an asteroid's rotational period can be estimated assuming that any normal elongation will produce a double-peaked periodic curve. The amplitude of this curve is related to the axis ratio of the asteroid via equation 1.3.

1.3.1 Existing lightcurve data

The repository for published asteroid lightcurves contains the best parameters for all observed small bodies (Harris et al. 2005a). A rating system is employed to differentiate between data of different quality,

0 Result later proven incorrect. This appears only on records of individual observations.

1 Result based on fragmentary lightcurve(s), may be completely wrong.

2 Result based on less than full coverage, so that the period may be wrong by 30 percent or so. Also, a quality of 2 is used to note results where an ambiguity exists as to the number of extrema per cycle or the number of elapsed cycles between lightcurves. Hence the result may be wrong by an integer ratio.

3 Denotes a secure result with no ambiguity and full lightcurve coverage.

4 In addition to full coverage, denotes that a pole position is reported.

Significant temporal coverage of an asteroid's rotation period is required to estimate the period with any certainty, and, as the rating system implies, even extensive observations can still leave certain parameters in doubt. When compiling statistics about different population's shape and spin from lightcurve data, the rating system is an important tool in understanding previously published data.

Currently in the lightcurve repository there are 60 Main Belt objects with a diameter < 5 km for which a minimum quality (**Q**) of 2 is listed. There are 225 such observations for bodies with diameter $D < 10$ km and 480 with $D < 20$ km. From this list none of the small ($D < 5$ km) MBAs are binary asteroids, and there are 289 NEAs listed in the repository, among which 15 are binaries.

1.3.2 Recent studies

Binzel et al. (1992) presented the results of a dedicated survey of MBAs smaller than $D < 5$ km. The survey covered 32 objects and presented 30 periods and 32 amplitudes from lightcurves. Overall the results suggested that the sample had a rotational frequency faster than the population of larger MBAs. This was the first survey of this kind, and no similar dedicated survey of small MBAs (SMBAs) lightcurves has followed.

Pravec et al. (2002) summarizes asteroid rotations highlighting how spin rate varies with size. Using a running box statistical method they report that the geometric mean spin period for $D > 40$ km is $\sim$13 h, and decreases to $\sim$ 6 h for $D \sim 10$ km. The distribution for asteroids with $D > 40$ km, is fit well with a maxwellian distribution, whereas for 0.15 $< D < 10$ km is not. This group of smaller asteroids, which includes NEAs, has strong populations of slow ($\sim$30 h) and fast ($\sim$3.5 h) rotators, with an apparent maximum spin

barrier around 2.2 h. The excess of both fast and slow rotators in the NEA population has been suggested as a possible manifestation of the YORP thermal effect (Pravec et al. 2002; Bottke et al. 2006).

Scheeres et al. (2004) analyzed the nature of rotation changes due to the close encounters with planets that NEAs undergo. This study quantified the overall increase in spin rate that a population would gain through these encounters by modeling a steady-state system where Main Belt asteroids become NEAs, have encounters over their lifetime and are then replaced by new MBAs. This Monte Carlo simulation used the rotation rates from Donnison & Wiper (1999) derived from collisional experiments as the initial MBA rotation rate distribution. This distribution was then compared to the steady-state distribution of NEAs that evolved over time through planetary encounters. Overall a slight spin-up of rotation rates was noted, and the maximum spin achieved from an encounter was near the classical critical breakup limit of 2 h. This study confirmed that the NEA population will have a spin-rate distribution different from its parent bodies in the Main Belt.

1.3.3 Motivation for work on small MBAs

Due to observational constraints it is significantly more difficult to obtain lightcurves for kilometer-sized MBAs than for the closer NEAs. Thus direct comparisons between similarly sized NEAs and MBAs is nearly impossible, as the number of lightcurves for small MBAs is currently inadequate. Each population has differing dynamical environments, with short lifetimes and frequent planetary encounters for NEAs and much shorter collisional than dynamical lifetimes in the Main Belt. They also have differing thermal environments, with the more distant MBAs less affected by the Yarkovsky or YORP thermal effects. Because of the sometimes powerful effects these phenomena may have on the shape and spin of small asteroids, detailed studies of lightcurves are potentially diag-

nostic.

Recent results have demonstrated that the effectiveness of tidal disruption at binary formation has a strong dependence on the shape and spin of a strengthless asteroid encountering a planet (Walsh & Richardson 2006, Chapter 2). In order to place tidal disruption simulations into a larger model of MBA-NEA binary formation and evolution it is necessary to understand the properties of small MBAs ($D < 5$ km, SMBAs). The NEA population is roughly a steady-state population with asteroids being removed via encounters/collisions with planets and the Sun, and being refilled by eccentricity-pumping resonances in the Main Belt (Bottke et al. 2002). Though there are many NEA lightcurves that are well characterized, these will represent the shape and spin of bodies which may have already had their spin state altered due to close encounters with planets (Scheeres et al. 2004). The lightcurves of SMBAs however, should provide the spin and shape distribution of asteroids which first encounter planets after entering an NEA orbit.

Photometric lightcurves have successfully discovered $\sim$ 17 binary asteroids in the NEA population, and $\sim$ 13 in the Main Belt (Pravec et al. 2006). Up until 2004 all MBA binaries had been discovered via high-resolution ground- or space-based imaging, whereas most NEA binaries were discovered via lightcurve observations.

1.4 Steady-State Models of the NEA Population

The NEAs are essentially a transient population, with short lifetimes on the order of 10 Myr, but roughly constant overall numbers due to migration of asteroids from the Main Belt (Bottke et al. 2002). Comparison of binary formation simulations with the observed population requires the properties of the simulated binaries, as well as inclusion of the dynamic lifetimes of the bodies and any known evolutionary effects. The modeled population changes over time, as binaries are created and evolve, and are replaced by

single bodies at the end of their lifetime. The steady-state population that evolves can then be compared with the observed population, revealing the importance of tidal disruption in forming binary NEAs.

1.4.1 Near-Earth asteroid population dynamics

The NEA population consists of those asteroids with perihelion distances $q \leq 1.3$ AU and aphelion distances $Q \geq 0.983$ AU (Rabinowitz 1994; Bottke et al. 2002). Earth and Moon cratering records suggest an impact flux that has remained roughly constant over the past 3 Gyr, implying that the NEA population has not varied drastically in numbers over that time (Grieve & Shoemaker 1994). Therefore bodies being removed from the NEA population (via collision with a planet or the Sun, or by ejection from the inner solar system) must be replaced to keep the population constant.

Prior to the first studies indicating that resonances can cause significant increases in an asteroid's eccentricities, it was thought that many NEAs were extinct cometary nuclei. However, eccentricity-boosting resonances provide a means for MBAs to migrate onto planet-crossing orbits and eventually into near-Earth space (Wetherill 1979; Wisdom 1983). It was thought that frequent catastrophic collisions or large impacts with ejected debris would cause material to be injected into two powerful resonances in the inner Main Belt: the ν_6 secular resonance with Saturn and the 3:1 mean motion resonance (MMR) with Jupiter. Once material is injected into these resonances, it will have its eccentricity pumped and enter an Earth-crossing orbit on a short timescale. Monte Carlo simulations of the asteroid transport into these two resonances and subsequently into near-Earth space traced the evolution of asteroids into NEAs, but did not account for the inherently chaotic environment later revealed with the first numerical investigations (Wetherill 1988; Rabinowitz 1997a,b; Gladman et al. 2000).

A series of works has suggested that Mars-crossing asteroids can be considered as

another intermediate source of NEAs in addition to the two previously cited resonances. Migliorini et al. (1998) asserted that the Mars-crossers that are not NEAs ($q > 1.3$ AU) have histories inconsistent with an origin from the 3:1 MMR or the ν_6 secular resonance. It was also shown that a series of weak mean-motion resonances with Jupiter or Mars, along with three-body mean-motion resonances with Jupiter and Saturn, can increase an asteroid's eccentricities until it is on a Mars-crossing orbit (Morbidelli & Nesvorny 1999). From a Mars-crossing orbit an asteroid can evolve into an NEA on timescales of only tens of millions of years (Migliorini et al. 1998; Michel et al. 2000).

Bottke et al. (2002) modeled the transport of asteroids from 5 different source populations in the Main Belt, matching their resultant NEA orbits to a debiased NEO population fit to Spacewatch data. This work found that the majority ($\sim$61%) of the NEA population migrates from the inner Main Belt ($a < 2.5$ AU), with the central Main Belt ($2.5 < a < 2.8$ AU) contributing $\sim$24%. This established the NEA population as a steady-state population consisting mostly of inner Main Belt asteroids that migrated via one of three main sources; the two inner Main Belt resonances or from intermediate Mars-crossers.

1.5 Background

1.5.1 Tidal disruption

The model for a tidal disruption of a small, non-rotating, liquid satellite in orbit around a massive body was initially provided by Roche (1847) (see Chandrasekhar 1969). This work solved for the orbital radius inside of which the small body on a circular orbit cannot maintain an equilibrium figure under the strain of tidal forces. This limit is

$$r_{Roche} = 1.52\left(\frac{M_p}{\rho_s}\right)^{1/3} = 2.46R_p\left(\frac{\rho_p}{\rho_s}\right)^{1/3} \tag{1.4}$$

where M_p, R_p and ρ_p are the mass, radius and density of the planet, and ρ_s is the density

of the satellite in question. For an asteroid of density 2.0 g cm^{-3}, the Roche limit would be $\sim 3.45\ R_{\oplus}$ about Earth.

In an attempt to extend this limit to solid bodies, Jeffreys (1947) considered internal strength. He applied his solution to asteroids breaking up around the Earth and Jupiter, as well as the formation of the rings of Saturn from objects with the consistency of ice. His calculations estimated high internal strengths, and therefore determined that tidal forces, which increase with size, could only be effective on objects with a diameter roughly $>$ 200 km. After the discovery of Comet Ikeya-Seki in 1965, Opik (1966) considered models of tidal disruption for the sun grazing family of comets, and included self-gravity. Opik (1966) suggested that Ikeya-Seki may have had a rubble-pile structure and even made qualitative arguments about the effect that the direction of the axis of rotation could have on a tidal disruption.

In their study of self-gravitating, non-rotating viscous bodies during parabolic encounters with planets Sridhar & Tremaine (1992) showed that small bodies can shed mass or disrupt entirely. They determined a pericenter distance inside of which disruption or mass loss would occur

$$r_{disrupt} < 1.69 R_p \left(\frac{\rho_p}{\rho_s} \right)^{1/3} \tag{1.5}$$

which is smaller than the classical Roche limit. For non-viscous bodies that are held together by self-gravity they determined that the bodies would behave approximately like the viscous fluid.

Richardson et al. (1998) used rubble pile models to simulate tidal disruption of Earth–crossing asteroids. These simulations explored a parameter space which included the asteroid's hyperbolic encounter (periapse q and encounter velocity with Earth v_∞), spin period P and shape–orientation conditions. The outcomes were parametrized by the mass stripped off during the disruption, or the distortion of the body.

1.5.2 Rubble piles

The evidence for non-monolithic solar system objects is of considerable importance for tidal disruption scenarios, as internal strength can frustrate disruptions. Evidence for a significant population of strengthless bodies dates to work by Burns (1975), where they examined the spin angular momentum of 70 asteroids and compared the centrifugal accelerations to the bodies' self-gravity. The critical spin period scales with $\rho^{-1/2}$ thus demanding a shorter period for denser objects. For all asteroids in the sample with an assumed density of 3 g cm^{-3} the gravitational force exceeded that of the centrifugal thus permitting these objects to be held together strictly by self-gravity. The lack of objects with a very rapid rotation rate suggests that internal structures do not allow rapid rotation.

A huge database of asteroid light curves (688) was used by Harris (1996) to evaluate possible rubble pile structure of asteroids. The lack of objects with very fast spin period again suggests an overall trend of asteroids of very low internal strength. The cutoff in rotation rate is at the critical spin rate for a density of $\sim$ 2.7g cm^{-3}, a density thought to be typical for asteroids, suggesting that no faster rotation rates are observed because in general these asteroids have no internal strength.

In a review of the studies on strengthless bodies, Richardson et al. (2002) established terminology stating that a rubble pile is moderately porous, strengthless body with constituents bound only by their own self-gravity. This differs from a shattered, or fractured body, which may have no strength, but also low porosity. A numerical model of a "perfect" rubble pile, will by necessity have moderate porosity (at least $\sim$30%), and currently no techniques incorporate strength. Citing evidence from cometary breakup, crater chains on planetary moons, doublet craters, asteroids spin rates, low asteroid densities, giant craters on asteroids, linear grooves on surfaces and binary asteroids, this work provided a strong case for the theory that many or most bodies between the sizes of $\sim$100 m and

$\sim$100 km are rubble piles.

1.6 This Dissertation

This dissertation was designed to investigate the role of tidal disruption in the formation of binary NEAs. At the heart of this work is the attempt to answer the following three questions,

1. What are the properties of tidal-disruption-formed binaries and how do they compare to the observed NEA binaries?

2. What is the spin and shape distribution for small MBAs, how does it compare to NEAs and large MBAs?

3. What is the overall steady-state binary fraction for NEAs caused by tidal disruption?

We present theoretical and observational studies to address all three questions in the following chapters. First, in Chapter 2, we describe our models of the tidal disruption of strengthless "rubble pile" asteroids, using N-body simulations. Results from many simulations covering a large parameter space are presented, with characterization of the binaries formed.

In Chapter 3 an observing campaign designed to study the shape and spin of small MBAs is presented. Observations of 28 asteroids are combined with previously published lightcurves to determine the shape and spin distribution for small MBAs.

The results from the observations in Chapter 3 are used along with the simulation results in Chapter 2, to create a steady-state model of the binary NEA population presented in Chapter 4. This model tracks binary NEAs as they are formed, evolve and eventually replaced when they reach the end of their lifetime.

In Chapter 5 we summarize the main results and present conclusions.

Chapter 2

Formation of Binary Asteroids via Tidal Disruption of Rubble Piles

Walsh & Richardson, 2006, Formation of Binary Asteroids via Tidal Disruption of Rubble Piles, *Icarus* 180, 201–216

2.1 Overview

In this chapter we adopt numerical techniques similar to those of previous *N*-body rubble pile simulations, and cover parameters previously shown to produce catastrophic tidal encounters, but in much greater detail. This study is unique in the large number of simulations performed and detailed investigation into the physical and orbital attributes of the resulting binaries. In Section 2.2 the details of the simulations and analysis are explained, and the results are discussed in Section 2.3. Conclusions and future work are presented in Section 2.4.

2.2 Method

2.2.1 Simulations

All simulations were done using `pkdgrav`, a parallelized tree code designed for efficient N-body gravitational and collisional simulations (Richardson et al. 2000; Leinhardt et al. 2000; Stadel 2001; Leinhardt & Richardson 2002; Richardson et al. 2005). The simulations used a timestep of 10^{-5} yr/2π, (about 50 seconds, or $\sim$ 2% of the dynamical time for the particles) and all simulations were initially run for 10,000 timesteps ($\sim$ 5.8 days). Simulations that produced binaries or systems of bound bodies were run an additional 20,000 timesteps to reach a total of 30,000 timesteps ($\sim$ 17.4 days). The collisions of individual particles were governed by coefficients of restitution, both normal (ε_n) and tangential (ε_t), which determine how much energy is dissipated during collisions. The normal coefficient of restitution, ε_n, was fixed at 0.8 in these simulations, similar to previous studies, and ε_t was fixed at 1.0 (no surface friction). Previous work has shown that ε_n has little effect on the outcome of a tidal disruption so long as $\varepsilon_n < 1.0$ (Richardson et al. 1998).

2.2.2 Progenitors

The rubble pile models used in these simulations consist of identical rigid spheres bound to one another by gravity alone. There were five separate progenitors used in the simulations, each with different elongations: 1.0, 1.25, 1.5, 1.75, and 2.0 (here elongation is defined as $e = a/c$ with a, b and c representing the long, intermediate and short axis length of a tri-axial ellipsoid; in our simulations, b was set to $\sim c$). The bodies were all constructed using particles with an internal density of 3.4 g cm^{-3}, but the bulk density of the body would vary depending on its packing efficiency, which was usually around

$\sim$ 60%, making a bulk density of $\sim$ 2.0 g cm^{-3}. Each progenitor consisted of approximately 1,000 particles; the exact number varied between 991 and 1021 depending on the final overall shape[1]. Recent work by Richardson et al. (2005) shows that the resolution of a rubble pile simulation can have an effect on the outcome: as resolution increases, the granular behavior becomes more fluid-like, aiding disruption. To justify our use of 1000 particles, we assume the smallest building block for rubble piles in the inner solar system is $\sim$150 m, based on SPH collision studies and the observed spin rate cutoff of km-sized asteroids (Benz & Asphaug 1999; Pravec et al. 2002). With 150 m particles, a spherical close-packed rubble pile with 1000 particles is $\sim$ 3.3 km in diameter. This diameter is nearly as large as the largest observed NEA binary primary, but also has enough resolution to model ejected fragments which may remain bound to each other, and to allow accurate measurement of size ratios.

The progenitors were given one of four rotation rates: 3, 4, 6, or 12 h periods. Large asteroid ($D > 40$ km) spin rates have been shown to follow a Maxwellian distribution, but small asteroids ($D < 10$ km) have an excess of fast and slow rotators (Pravec et al. 2002). Studies have attempted to fit the population of small asteroids with 3 different Maxwellians, with a combination of fast, moderate, and slow rotation rates of $\sim$ 6.4, 11.3, and 27.5 h (Donnison & Wiper 1999). However, with the large proportion of fast-rotating NEAs (possibly as high as 50%) observed to be primaries of binary systems, they may have already experienced a tidal disruption and had their spin state altered (Margot et al. 2002; Scheeres et al. 2004). Our selections were made to sample fast rotators (3, 4 h), as well as some moderate ones (6, 12 h). No spin periods longer than 12 h were simulated

[1]The packing algorithm uses hexagonal closest packing, which depends on a certain level of symmetry to construct bodies out of a finite number of perfect spheres. This results in variation in the number of particles for various shapes. Similarly, due to boundary algorithms and the finite size of the building blocks, the bulk density can vary slightly.

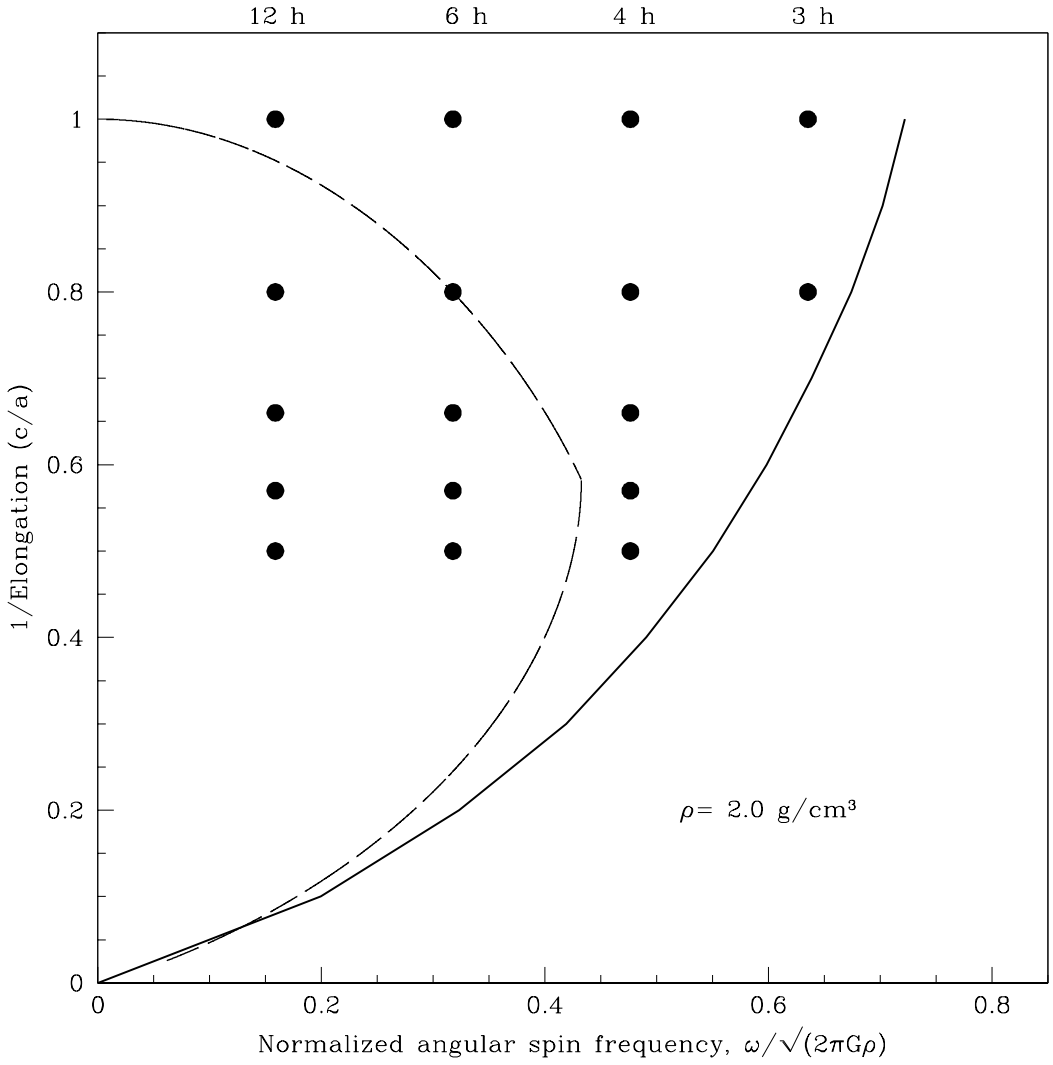

Figure 2.1: Progenitor initial parameters of the reciprocal of elongation (c/a) and normalized angular spin frequency ($\omega/\sqrt{2\pi G\rho}$) are plotted as points. (solid line) This is compared with the limiting curve for a cohesionless granular proloid with friction angle $\phi = 40°$ (Holsapple 2001; Richardson et al. 2005). (dashed line) The solutions for Jacobi and Maclaurin sequences representing theoretical axis ratios for rotating fluids.

due to the small contribution rotation actually makes to tidal disruption at slower spins (Richardson et al. 1998).

The 3 h spin rate simulations were only carried out for progenitors with an elongation of 1.0 and 1.25. Comparison to Richardson et al. (2005), as well as separate tests, indicate that bodies with elongation of 1.5 or greater would be unstable at a 3 h spin rate, thus

shedding mass and distorting prior to encountering the tidal forces of Earth (Fig. 2.1). The subset of results for 3 h will be presented independent of the bulk of the studies.

The progenitors used in this work are all below the limit for cohesionless granular proloids with friction angle $\phi = 40^\circ$ (Holsapple 2001). This limit, verified by Richardson et al. (2005) as a rotational stability limit for numerical models of rubble piles, differs from the Maclaurin/Jacobi limits for fluid bodies (essentially a sequence of allowed equilibrium shapes). The Maclaurin/Jacobi sequence can be derived analytically and provides a useful fiducial for comparing less idealized models. For example Guibout & Scheeres (2003) determined that when a body is spinning beyond the Jacobi limit, the flow of material on the surface of the body is towards the equator, whereas below the limit, the flow is towards the poles.

2.2.3 Tidal encounters and initial conditions

The hyperbolic encounters asteroids have with planets can be described by the close approach distance q and the relative speed at infinity v_∞. When $v_\infty \gg v_{esc}$ (where $v_{esc} = \sqrt{2GM/R}$), close approach is distributed with likelihood increasing as the square of the distance. This means that an asteroid is four times more likely to encounter Earth at 4 $R_{\oplus}$ than at 2 $R_{\oplus}$. The v_∞ of these encounters depends on the bodies' pre-encounter orbits. A distribution of expected encounter statistics was taken from a series of N-body simulations of NEA migration from major source regions in the Main Belt (3:1 mean-motion resonance with Jupiter, ν_6 secular resonance, Mars crossers; Bottke et al. 2002, Bottke 2004 personal communication; the distribution is similar to the impact speed distribution of Bottke et al. 1994). This was used to determine the expected v_∞ for the hyperbolic encounters with Earth (Fig. 2.2). Simulated parameters were selected to cover the most frequently occurring encounters and those previously shown to create very disruptive encounters likely to form binaries, all sampled at a frequency to balance detail with compu-

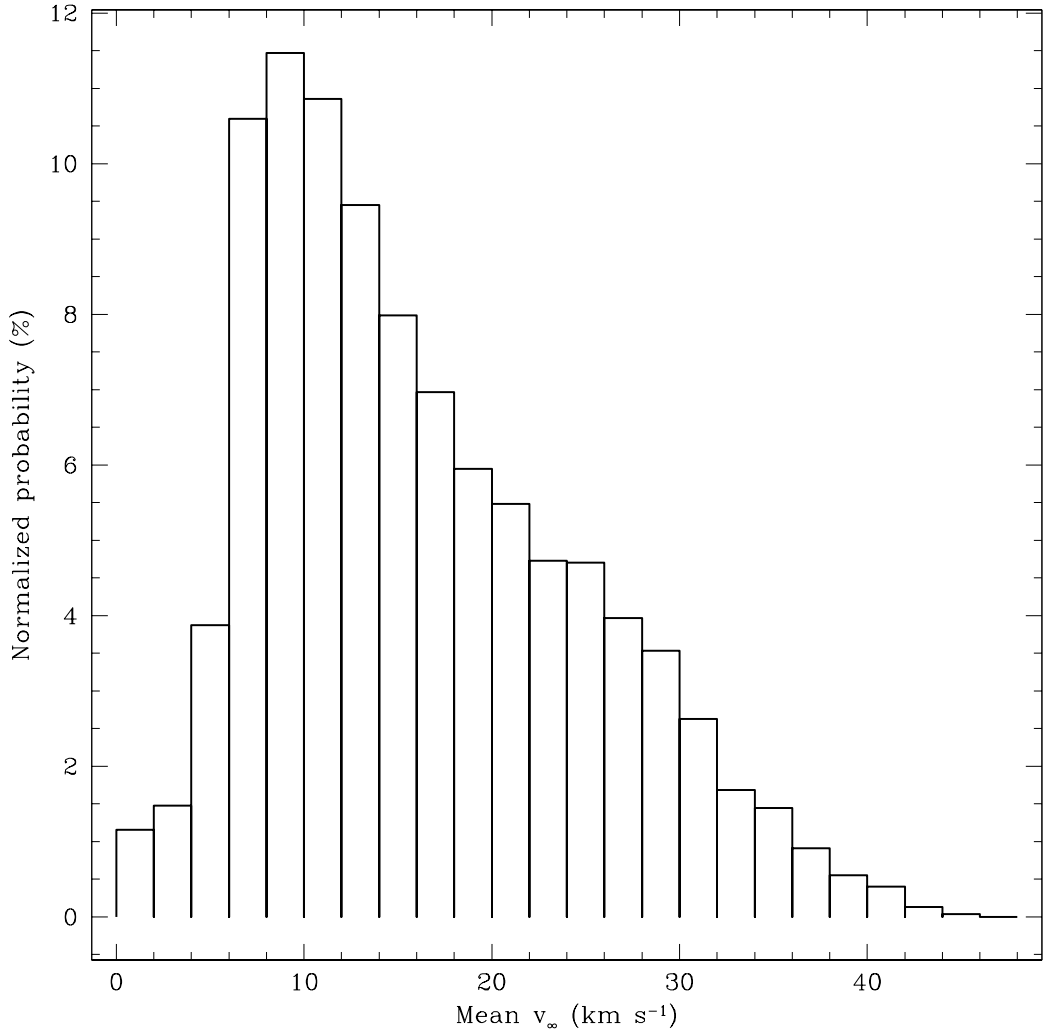

Figure 2.2: The distribution of v_∞ for close hyperbolic encounters with Earth, with v_∞ in km s^{-1} and the y-axis indicating the normalized probability for each v_∞ bin (Bottke 2004, personal communication).

tational expediency: q=1.2, 1.4, 1.6, 1.8, 2.0, 2.2, 2.4, 2.6, 2.8, 3.0, 3.5, 4.0 and 4.5 $R_{\oplus}$ and v_∞= 8, 12, 16, 20, and 24 km s^{-1}.

Richardson et al. (1998) determined that the orientation of a non-spherical body can have a significant effect on the outcome of a tidal disruption. Specifically when the leading long axis of a body is rotating towards or away the planet, disruption is enhanced or suppressed respectively. Near perigee the equipotential surface of the body is stretched in

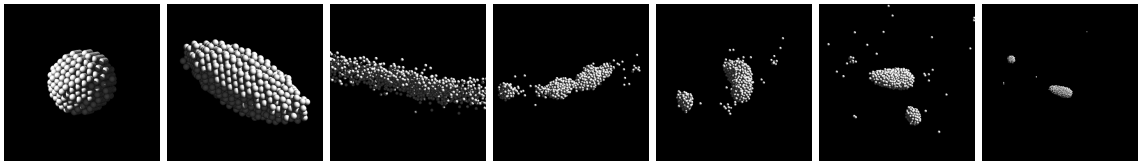

Figure 2.3: Snapshots of a tidal disruption simulation that led to the formation of a binary asteroid. The frames span about 72 h.

the direction of Earth, and particles may rearrange to fill that shape (see Fig. 2.3 for a representative disruption). So if the long axis is rotating away from the planet, the rotation of the body opposes the movement of the particles. Instead of parameterizing the specifics of body axis alignment, a compromise was made: for each set of encounter (q and v_∞) and body (elongation and spin rate) parameters, the simulation was run 100 times, each time randomizing the orientation of the body's spin axis. Thus, given that the hyperbolic encounters were always in the same plane, some bodies were spinning prograde and some retrograde with respect to the encounter with Earth, depending on the randomization outcome. The long axis position at perigee was also random. This means that each set of parameters has a distribution of possible outcomes rather than one unique solution.

2.2.4 Analysis

Identification of orbiting systems was done using the `companion` code (Leinhardt & Richardson 2005). This code is optimized for extremely fast searches over all simulations, identifying and analyzing those with bound systems. First, each simulation was searched for re-accumulated clumps of particles (Leinhardt et al. 2000). Once the clumps were identified, those consisting of more than three particles were fed into `companion` to search for systems. Any bound clumps were then analyzed to obtain important physical parameters, such as spin vector, elongation, mass, radius and position/velocity vectors.

The code `companion` sorts binaries according to identification of the primary and secondary clumps. In a situation where a specific clump has multiple secondaries, it will

Total Binaries	T-PROS	T-EEBs	Prolate	Oblate	S-class	B-class	M-class
4939	4556	383	4692	246	226	2299	2414
3 h spin periods; 1.0 and 1.25 elongations only							
798	702	96	740	58	59	357	382

Table 2.1: Cumulative statistics from all 110,500 simulations. Total binaries is simply a count of all systems observed in the simulations. T-PROS and T-EEBs represent the total binaries split into dynamical groups (see Section 2.3.2). Prolate and Oblate columns separate the binaries according the shape of the primary body (see Section 2.3.1). The binaries are also separated according to the class of disruption in which they were formed, S-class being the most disruptive, followed by B-Class and M-Class (see Section 2.3.3).

be listed once for each. Thus a triple, or larger, system may result in the same primary being counted multiple times in the statistics presented. The situation of an hierarchical system, where a secondary body itself has an orbiting clump, will result in that body being counted as both a secondary and a primary.

2.3 Results and Discussion

2.3.1 Bulk results

The bulk results covered 1,105 sets of parameters, which encompasses 110,500 total simulations. From these simulations a total of 5,737 bound systems were found after 30,000 timesteps (see Table 2.1 for a summary of bulk statistics). Of all the binaries, 798 were formed in the subset of 3 h, low-elongation simulations (to be referred to as the 3 h subset, and not included in plots or tables unless specifically mentioned; see Section 2.2.2 and Section 2.3.4).

Figure 2.4 shows the relative contributions each parameter made to binary production. The trends are consistent with the findings of Richardson et al. (1998). The lower the v_∞, the more disruptive the outcome, and hence more binary formation results. Likewise binary production falls off very smoothly as q increases. The spin period distribution

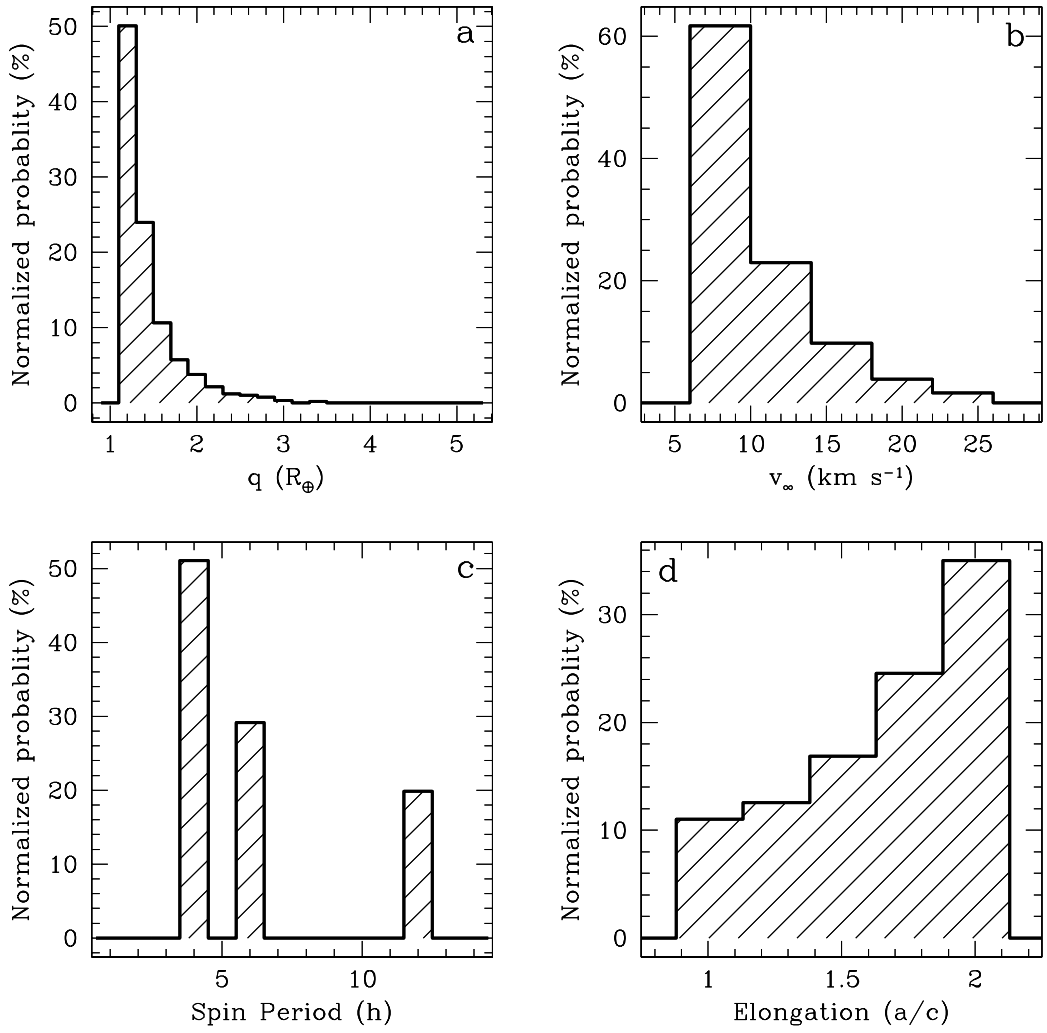

Figure 2.4: Normalized probability of binaries formed versus (a) q, (b) v_∞, (c) initial spin rate and, (d) initial elongation.

shows the dramatic increase in production at high spin rates, as bodies with 4 h periods were nearly 60% more likely to create a system than those with a 6 h period. Similarly, elongated bodies were significantly more efficient at producing binaries, with elongations of 2.0 making nearly 3 times the number of binaries as elongations of 1.0 or 1.25.

Figure 2.5 displays the number of binaries formed as a function of the mass of the largest remnant divided by the mass of the progenitor, basically a measure of how disrup-

tive the encounter was. This measure was used by Richardson et al. (1998) to delineate 3 classes of tidally disruptive encounters:

1. S-class disruption: Named for an SL9-type disruption where the largest remnant has no more than 50% of the progenitor's mass. This class of disruptions is the most dramatic, as the progenitor is stretched into a long trail of particles before numerous clumps take shape. Binaries can be created if two clumps form close enough to become bound, or if a clump has accreted multiple fragments.

2. B-class disruption: A rotational breakup where the largest remnant contains between 50% and 90% of the mass of the progenitor. A B-class breakup involves a similar situation as the S-class, but less extreme, allowing a central large clump to form from the distorted and stretched progenitor.

3. M-class disruption: A mild breakup with less than 10% of the mass of the progenitor lost during the disruption. As the body is spun up, it is stretched along its long axis, particles slide to the equator of the body, and many are launched off the main body. Unlike the more disruptive breakups where a long chain of particles separates into separate clumps, the M-class encounters appear more like a body that starts spinning too fast (beyond the Jacobi and related cohesionless granular proloid limits), distorts, and then sheds mass from its equator.

Binary production peaks for encounters classified as M-class, with the largest remnant containing 90% to 95% of the mass of the progenitor. With a large percentage of the mass contained in the largest remnant, the binaries formed are limited to small size ratios. B-class and M-class outcomes account for nearly equal amounts of the binaries created and about 95% of the total created.

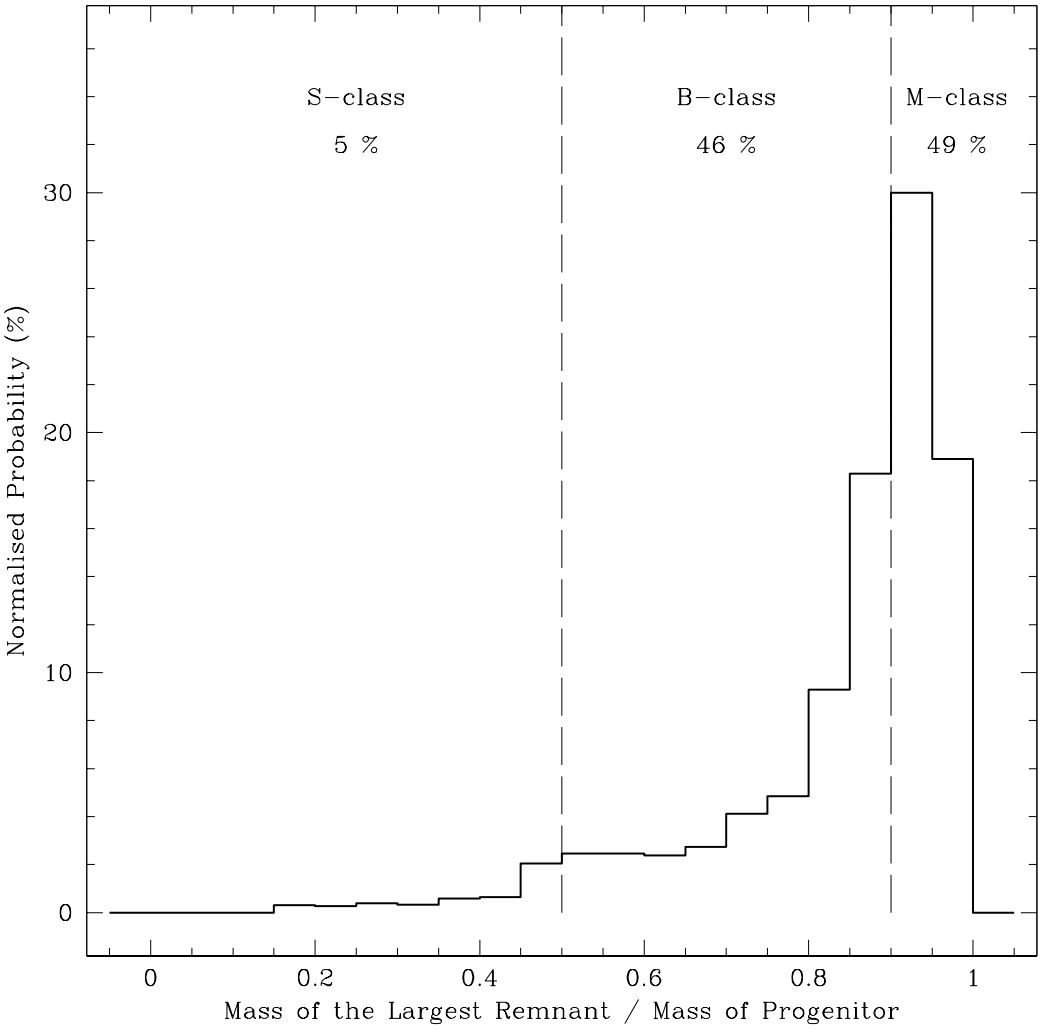

Figure 2.5: Normalized probability of binaries formed versus the mass of the largest remnant divided by the mass of the progenitor. The vertical lines separate the disruptions into defined classes, with S-class being most disruptive, followed by B-class and M-class (Richardson et al. 1998). The percentages represent the total number of binaries in each class

Orbital properties

The eccentricity distribution in the simulations is dominated by high ($e > 0.1$) eccentricities, and has similar morphology to the eccentricity distribution in Durda et al. (2004) found in binaries formed after MBA collisions (Fig. 2.6a). However, the known binary NEAs with measured eccentricity are usually found to have eccentricity below 0.1. Such systems are formed at one tenth the rate of those with $e > 0.9$ in our simulations and account for only $\sim$ 3% of the total results. This difference might be explained by lightcurve studies possibly being more likely to discover low-eccentricity secondaries or by evolutionary eccentricity damping (Weidenschilling et al. 1989; Murray & Dermott 1999). Tidal dissipation mechanisms are expected to damp eccentricities, where the timescales are dependent on Q (the tidal dissipation parameter for the secondary), the diameter of the secondary, and the semi-major axis of the orbit (see Section 2.3.6).

The semi-major axis distribution is relatively smooth, peaked around 5 $R_{\rm pri}$ and extending out to nearly 1000 $R_{\rm pri}$ (Fig. 2.6b). The Hill sphere radius, $r_H \sim a(M_{\rm pri}/3M_\odot)^{1/3}$, where $M_\odot$ is the mass of the Sun, and a = 1 AU at Earth, equates to $r_H \approx 130\ R_{\rm pri}$. Thus inclusion of the Sun in these simulations would eventually eliminate many of the systems with very large separation, as Hamilton & Burns (1991) showed that circular prograde orbits are stable with respect to solar tides only out to $\sim r_H/2$, and retrograde orbits are stable to $\sim r_H$. The small number of binaries with $a < 2R_{\rm pri}$ are expected to have extremely short lifetimes against collision with the primary (Scheeres 2002). Observed NEA binaries nearly all have $a/R_{\rm pri}$ between 3 and 10, which is also the most likely outcome seen in the simulations. However, the simulations create many systems with larger separations that are not observed in the NEA population, suggesting a possible strong observational selection effect or an evolutionary/survival property. Nearly half the simulations produced a separation of over 10 $R_{\rm pri}$, which may suggest that we are only currently observing half of the NEA binaries.

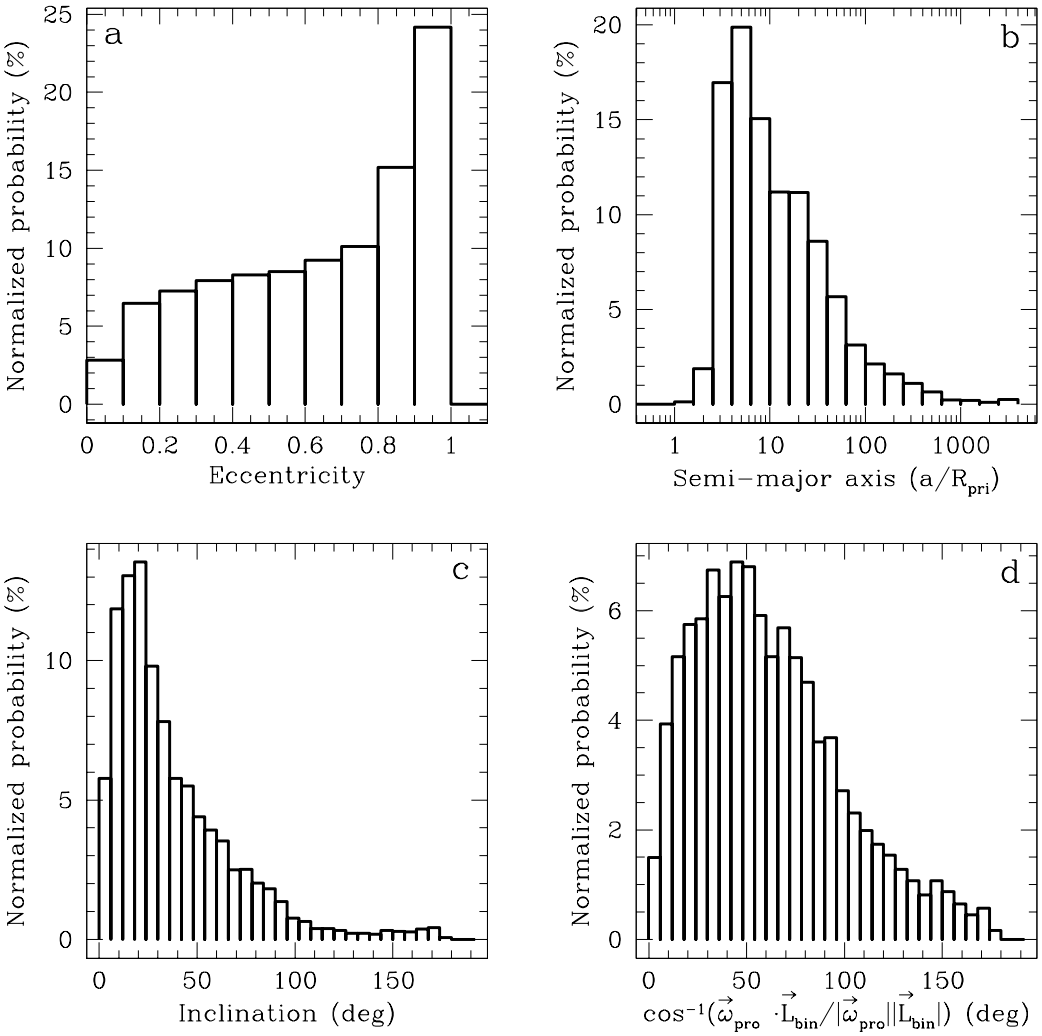

Figure 2.6: (a) Satellite eccentricity and (b) semi-major axis (in terms of primary radii, $R_{\rm pri}$) distributions for binaries formed by tidal disruption. (c) Inclination of the orbit with respect to the encounter orbital plane, $i = \cos^{-1}((L_{\rm bin}L_{\rm enc})/(|L_{\rm bin}||L_{\rm enc}|))$. (d) Angle between the progenitor's spin axis, $\omega_{\rm pro}$, and the binary angular momentum, $L_{\rm bin}$.

The inclination of the binary favors an alignment with the progenitor's encounter orbit (0°), where inclination is measured as the angle between the plane of the encounter orbit and the plane of the binary orbit (see Fig. 2.6c). The inclination distribution peaks around 20°, and has some cases with values between 90° and 180°, which describe outcomes where the binary orbit is retrograde with respect to the progenitor's encounter with Earth. This could have come about if a progenitor had retrograde spin with respect to the encounter, or via a chance post-disruption circumstance, most likely involving a very small secondary.

The rest of the angular momentum of the system comes from the spin of the progenitor, which is quantified by measuring the angle between the spin axis of the progenitor and the binary's angular momentum vector ($\omega_{\rm pro}$ and $L_{\rm bin}$; see Fig. 2.6d). This has a peak around 45° degrees falling off towards 0° and 90°, with very small contributions between 90° and 180°. This result suggests that neither progenitor spin nor encounter orbit will dominate the resultant binary inclination but that the encounter orbit is slightly more important. The encounter scenario likely determines which factor dominates, with a fast spinning progenitor disrupting at a distant q having the plane of the binary determined by the progenitor's spin, whereas a slow spinning, low q encounter placing debris mostly in the plane of the encounter.

Body properties

The size ratio between secondary and primary bodies is strongly peaked between 0.1 and 0.2 (Fig. 2.7a). This is a slightly lower and narrower peak than that observed for NEA binaries, for which size ratios typically range between 0.2 and 0.6, with one notable exception being Hermes, with a size ratio very near 1.0 (Margot et al. 2003; Pravec et al. 2003c). The lowest size ratios in the simulations were < 0.05, which is limited by the arbitrary requirement we imposed that three particles are needed to make a clump, and

various complications of measuring the elongated shapes of rubble piles. These two main disparities with observations, the width and position of the simulation size ratio peak, may potentially be an effect of the simulation resolution. If resolution affects resultant size ratios, and, as was discussed in Section 2.2.2, progenitors are constructed out of 150–200 m diameter building blocks, then smaller progenitors would require lower resolution. This effect could potentially account for both the higher observed size ratios and their wide range, as a range in progenitor sizes might generate a wider peak in simulated size ratios. Another problem is potential irregular shapes and sizes of building blocks, which may differ significantly from the perfect hard spheres used for computation simplicity. On the other hand, lightcurve studies are limited by the size ratio, and cannot detect secondaries below 0.2 times the size of the primary (Merline et al. 2002c).

The spin of the primary in the simulations is bracketed between 3.5 and 6.0 h spin periods, while the secondary has a peak around 6 h and falls off slowly out to 20 h and greater (Fig. 2.7c). The spin of the primary has been exceptionally consistent in observed NEA binaries, with nearly all measured to have spin periods between 2.2 and 3.6 h. This disparity between our simulations and the observations is potentially caused by our choice of parameters. The fastest progenitor spin period simulated was 3 h and likely does not represent the fastest spinning NEAs that encounter Earth. For the densities used in the simulations, and following the work of Richardson et al. (2005), the critical spin period for a spherical rubble pile of the density we used is approximately 2.7 h (see Eq. 1). This is significantly slower than the shortest observed periods in the NEA population; however, the observed distribution of spin rates for NEAs does not suggest that an overwhelming number have periods less than 3.0 h (Pravec et al. 2002). Some of the disparity may be the numerical simplifications needed for the simulations, notably perfect spherical particles, which could artificially inflate porosity and decrease critical spin rate. This could make the idealised rubble piles disrupt at a slower spin rate than observed. The bulk density of

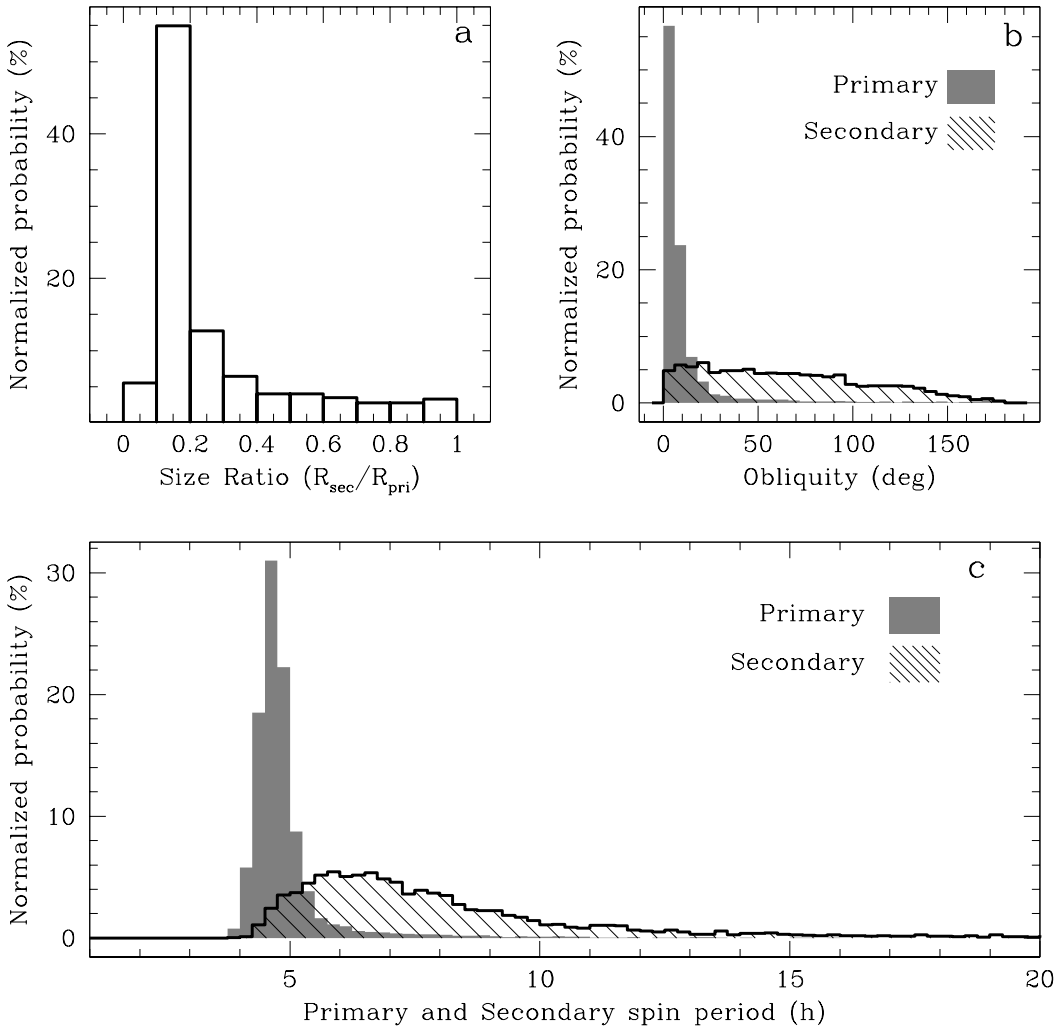

Figure 2.7: (a) Normalized probability of binaries formed as a function of secondary-to-primary size ratio. (b) Primary (shaded) and secondary (cross-hatch) obliquity. (c) Primary (shaded) and secondary (cross-hatch) spin period.

the progenitor is ~ 2.0 g cm^{-3} with a porosity of 35%, neither of which are extreme for observed NEAs. However, any tensile forces or mechanical strength which could push critical spin rate faster, even very briefly, may contribute to the very fast spinning primary. Further work is needed to show whether these caveats are responsible for the difference between the observed and simulated spin rate distributions.

The obliquity of the primary in simulations is quite low (where obliquity is the angle

between $\omega_{\rm pri}$ and $L_{\rm bin}$), with close to 90% of the binaries having an obliquity less than 20°. The obliquity of the secondary has no such relation, being nearly flat between 0° and 90°, and falling off from 90° to 180° (Fig. 2.7b). With many secondaries formed from accreting material in orbit around the primary, retaining an aligned spin axis appears to be unlikely for a secondary.

Shape of the primary

The shape of the primary was measured along the body's three principal axes, *a*, *b*, and *c* for the longest, intermediate and shortest axis length. Nearly all primaries are in a principal axis rotation state, rotating around the shortest axis. Thus the shape irregularities which are associated with a rotational lightcurve are a result of a difference between the long axis, *a* and the intermediate axis, *b*. If the intermediate axis, *b*, equals *a* or *c*, the body is either oblate ($b = a$) or prolate ($b = c$). However, few bodies approach such perfect classification, so for the sake of simplicity we define a shape index

$$I = (a-b)/(a-c)$$

where I = 1 means prolate, and I = 0 oblate.

The progenitor bodies were created to be simple prolate ellipsoids ($b = c$), with different values of *a*/*c* for varying amounts of elongation. The resulting primaries, as shown in Figure 2.8a, have a distribution of *a*/*c* concentrated between 1.0 and 3.0. The progenitor elongations used in the simulation were only varied between 1.0 and 2.0, so elongation was significantly enhanced during the binary-forming encounters.

The distribution of *a*/*b* is a more valuable comparison to the shape derived via lightcurve studies for bodies rotating around their shortest principal axis. This distribution has the same peak as *a*/*c*, at 1.95, but a larger concentration of objects near 1.0 (Fig. 2.8b). When the distribution is separated into bodies with $I < 0.5$ and > 0.5 (more oblate-like or

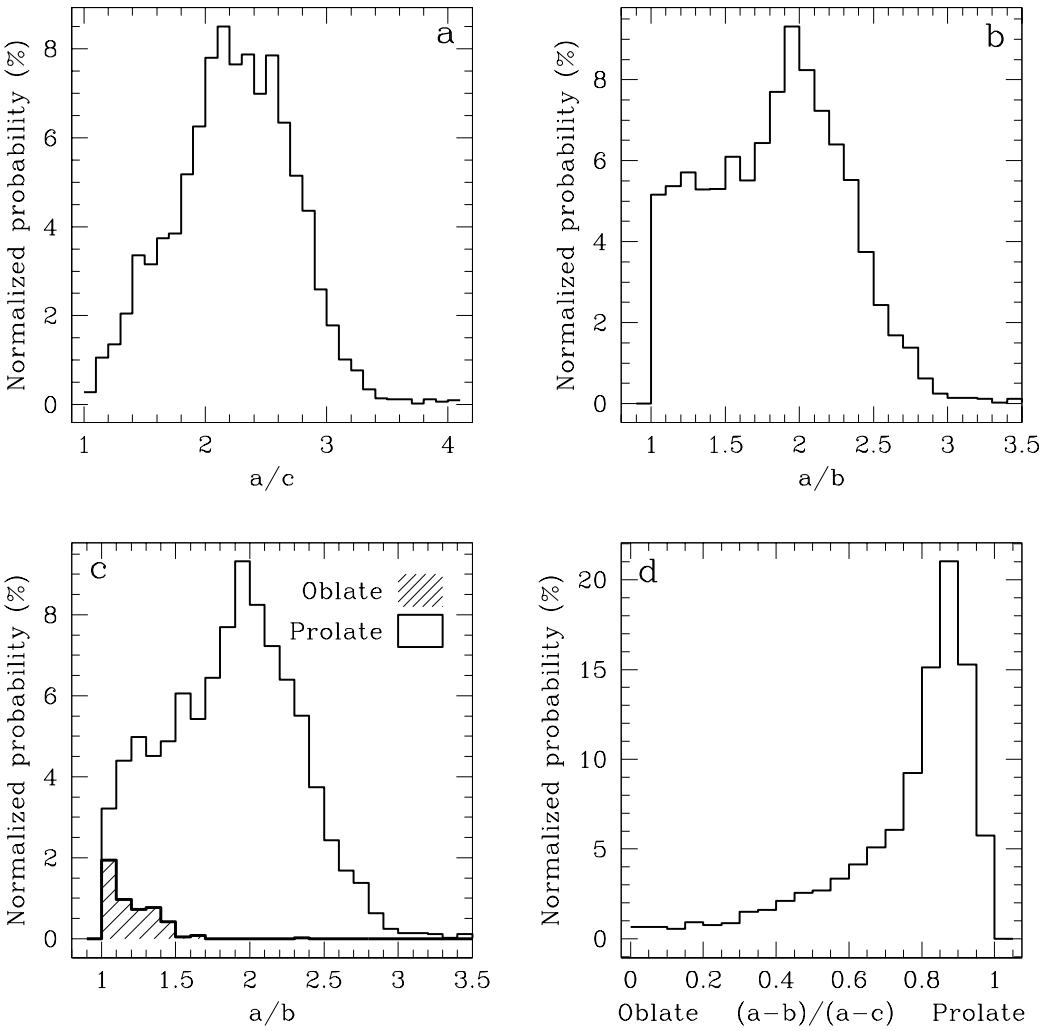

Figure 2.8: (a) Ratio of axes *a*/*c* for primaries of resultant binary systems. (b) Ratio of axes *a*/*b*. (c) Ratio of axes *a*/*b* separated into prolate (thin lines) and oblate (thick lines, cross hatch fill). (d) Ratio of $I = (a\text{-}b)/(a\text{-}c)$, showing whether the intermediate axis *b* is closer to *a*, making the body oblate-like, or closer to *c*, making the body prolate-like.

prolate-like), the oblate-like bodies account for nearly half of these that have $a/b < 1.2$; few oblate-like bodies have $a/b > 1.5$ (Fig. 2.8c).

As mentioned above, virtually no bodies were perfectly oblate or prolate. The value I was computed for all primaries, which describes how near the body was to being exactly prolate or oblate (Fig. 2.8d). The plot shows that many bodies are very nearly completely prolate with b nearly equal to c. Conversely oblate-like primaries are frequently only mildly oblate, with b nearly evenly between a and c.

The observed population of NEA binaries typically have quite spherical primaries, where in most cases amplitude of the lightcurve is used to interpret the shape of the body. Some elongations could potentially be larger if the lightcurve amplitudes are artificially low due to non-ideal viewing angles. The simulations produce some low-elongation primaries, but relatively few in comparison with high-elongation bodies with elongation above 2.0. Furthermore, the simulated low-elongation primaries have a high probability of appearing oblate. When isolated, the low-elongation primaries show no properties suggesting that they are more likely to have small separation or other properties related to the observed binary population. They have a slight trend toward lower eccentricity, possibly suggesting that the lack of observed high elongation primaries may be more related to survival, as opposed to formation. For example, how many of the currently observed binaries could survive with a primary of elongation 1.5 or 2.0? With all observed binaries having similarly small separations, studying orbital stability around irregularly shaped primaries is appropriate. An answer may be found in large-separation NEA binaries (when/if they are discovered), where elongated primaries would have a less significant impact on the dynamics of the binary orbit, so the binaries may have a better chance of surviving long enough to be observed.

2.3.2 T-PROS and T-EEBs

Durda et al. (2004) introduced terminology to differentiate between two types of satellites formed in a collision. The SMAshed Target Satellites (SMATS) form from debris orbiting around a remaining target body. The Escaping Ejecta Binaries (EEBs) form from fragments escaping the collision and becoming bound to one another. Similar analogs exist in the case of a tidal disruption. We have dubbed systems that form around the largest remnant of the disruption "Tidal PROgenitor Satellites" (T-PROS), and those that form from escaping debris "Tidal Escaping Ejecta Binaries" (T-EEBs). As seen in the collisional cases, there are distinct differences between the two groups. The strongest difference is in size ratio, where the T-PROS have a high probability of having a size ratio between 0.1 and 0.2, while the T-EEBs have a strong chance of being 0.8 and higher (Fig. 2.9a). Some of this effect may be due to the resolution of the simulations, where if most of the 1000 particles are invested in the largest remnant, there are only limited remaining particles to create a T-EEB, which will then necessarily have size ratio near unity (to be considered, a clump must have at least 3 particles). This was also observed by Durda et al. (2004), where many of the EEBs are the lowest-resolution particles, thus having a size ratio of exactly 1. With only one NEA binary (Hermes) with a size ratio above 0.7, T-EEBs may not be common; in the simulations they made up only $\sim$ 10% of the total systems created, and have even stronger tendencies to come from extreme disruptions with low q and v_∞ (Fig. 2.9c,d).

There is also a distinct difference in the spin axis alignments for the two types (Fig. 2.9b). The T-PROS' primary spin axes are typically closely aligned with the binary orbital angular momentum, while the T-EEBs' primaries have only a slight correlation with the orbit. The T-PROS distribution matches that for the overall distribution, with close to 90% being aligned within 20° of the binaries' orbits. T-EEBs show only a slight alignment with

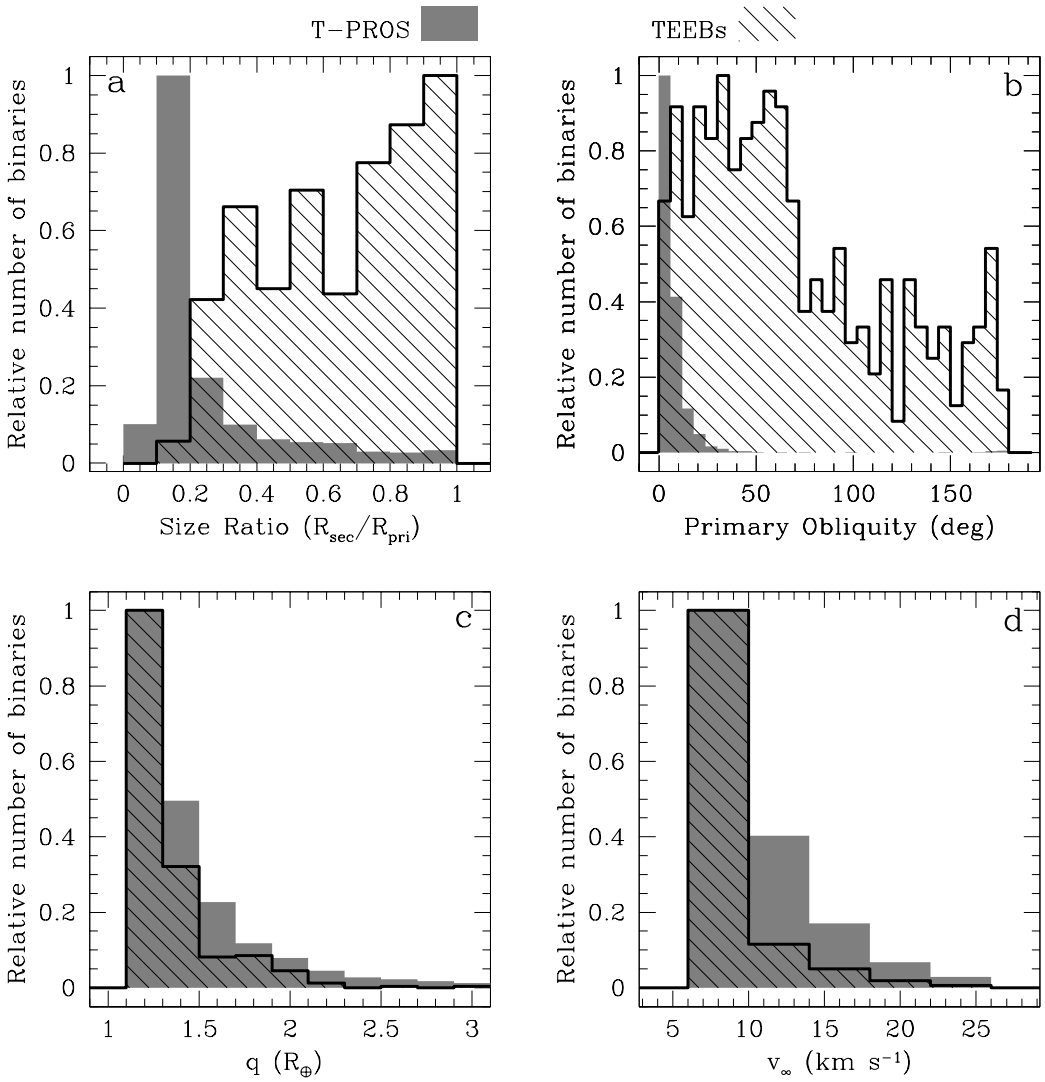

Figure 2.9: Plots comparing T-PROS (shaded) with T-EEBs (bold lines) in terms of relative number, meaning each distribution is normalized independently due to large disparity in overall numbers: (a) secondary-to-primary size ratio; (b) primary obliquity; (c) relative binary formation as a function of encounter conditions q and (d) v_∞.

the binary orbit, and has significant contributions out near 180°. The spin rates for the primaries of the T-EEBs are much more distributed than for T-PROS, and the secondaries have a similar distribution to that of all secondaries (not shown).

2.3.3 Classes of disruption

The three classes of disruption (S-, B-, and M-class; see Section 2.3.1) form binaries which have different properties. As well, each class of disruption prefers to form binaries from different types of encounters. First, the more disruptive the encounter, the more likely it was to have been produced by a low q or low v_∞ encounter. Figures 2.10a,b show the relative contributions each of the three classes made as a function of q and v_∞. The resultant binaries from each class had some physical differences, mostly in eccentricity and size ratio. Mild encounters had a stronger peak in high eccentricity, as compared to the S-class disruptions where a 0.95 eccentricity was only slightly more likely to occur than anything > 0.25 (Fig. 2.10c). This trend continues in size ratio with mild encounters producing a strong peak between 0.1 and 0.2, while disruptive S-class encounters were peaked at 0.9–1.0 (Fig. 2.10d).

2.3.4 3 h spin rate subset

The subset of simulations run with a progenitor 3 h spin period was done to investigate the relationship between the progenitor spin and the binary primary spin period. Of the 3 h simulations run, using only elongations of 1.0 and 1.25, 798 binaries were formed from 13,000 simulations. The 3 h subset produced a similar primary spin distribution to that of the entire set of simulations, with none below 3.7 h period (Fig. 2.11). Overall the periods for the primary and secondary were essentially the same for the full parameter simulation. This result suggests that primary spin is not strongly dependent on progenitor spin, and is likely dominated by other factors such as bulk density, particle shape or small internal

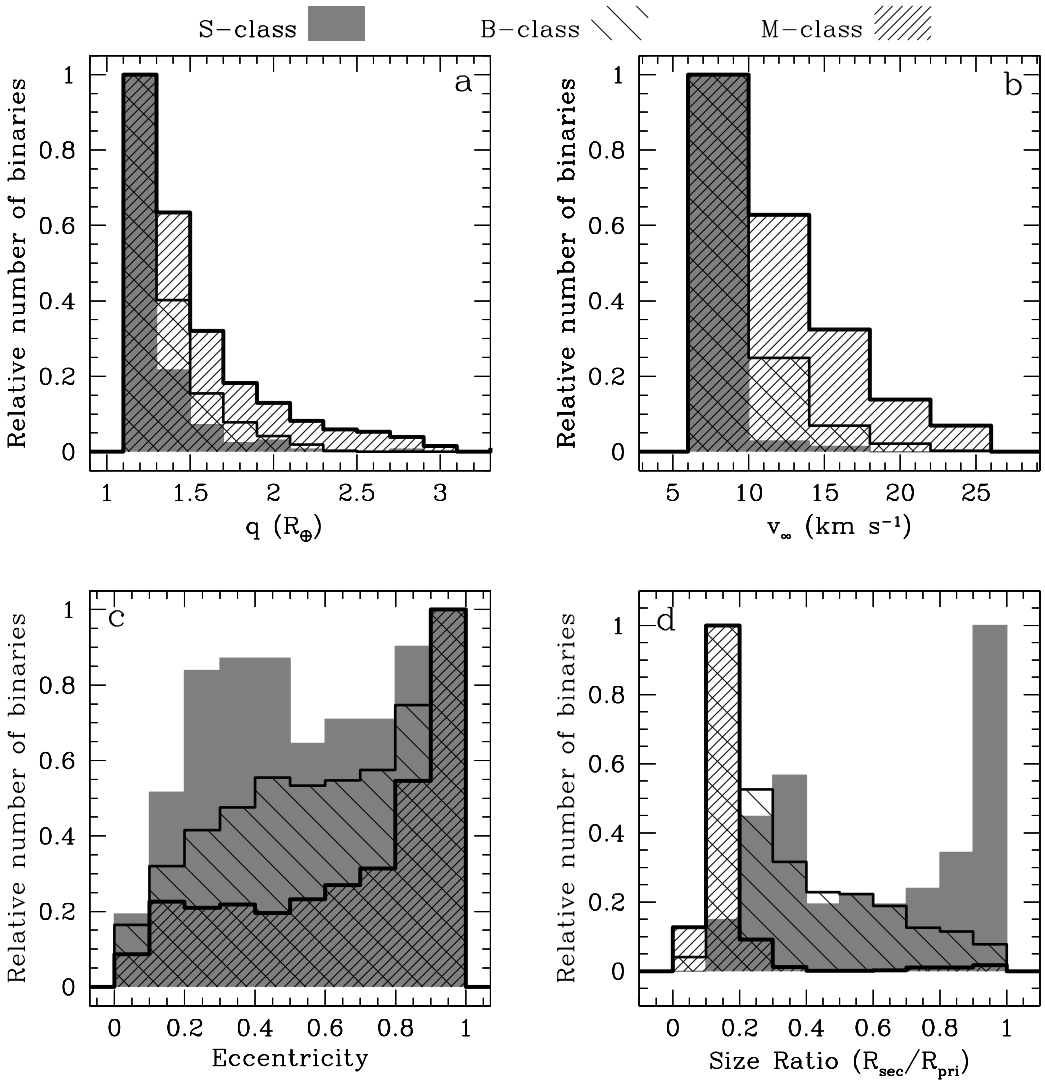

Figure 2.10: Comparison of S-class (gray fill), B-class (wide cross-hatch) and M-class (small cross hatch) tidal disruptions in terms of relative number of binaries formed for each class. (a) The three classes are plotted as a function of close approach q and (b) v_∞. The binaries produced within each class are also plotted as a function of (c) eccentricity and (d) size ratio of the secondary to the primary.

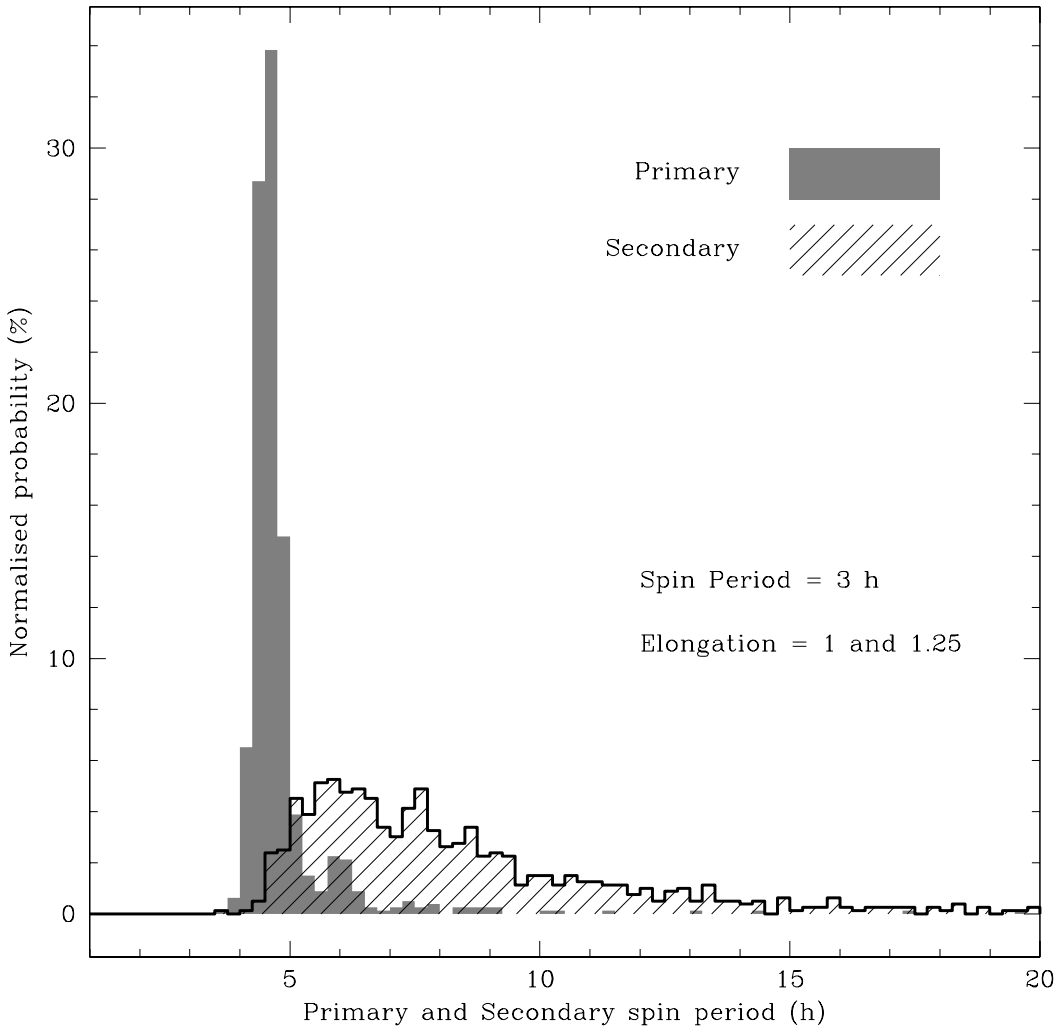

Figure 2.11: Histograms of the primary (shaded) and secondary (cross-hatch) spin periods for the binaries produced in the 3 h spin subset.

strength.

2.3.5 Triples and hierarchical systems

In general, triple systems (a system with two secondaries orbiting one primary) are likely to be unstable on short timescales in the inner solar system. Currently one Main-Belt asteroid has been observed in this state ((87) Sylvia, and its satellites Romulus and Remus). However, the simulations produced these and more complicated systems with $N > 3$. The simplest case of two satellites orbiting the largest remnant was found in 757 of the simulations with another 357 having three or more satellites in orbit.

Some unique situations involved multiple systems formed around the second, third, and fourth largest remnant. There were 5 simulations with at least 2 secondaries around the second largest remnant, 6 that produced them around the third largest, and 1 simulation that produced them around the fourth largest remnant. These situations almost exclusively originated from very close encounters ($q < 1.6\ R_{\pm\bigcirc}$) and fast-spinning primaries (4 h).

A hierarchical system, where a secondary has a bound companion, was a rare outcome. A total of 102 simulations produced these systems. These were typically simple situations with a satellite bound to the second-largest remnant, which in turn was bound to the largest remnant. Though no similar systems have been observed among asteroids, they do occur immediately post-disruption in simulations.

2.3.6 Tidal evolution and eccentricity damping

The simulations represent snapshots of binary properties immediately after formation. Subject to tidal interactions, planetary encounters, and thermal effects, the binaries will evolve with time. Tidal forces between the primary and secondary will affect the binary in most cases by: changing the semi major axis of the secondary's orbit, synchronizing the secondary's rotation with its orbital period, and changing the eccentricity of the secondary. Weidenschilling et al. (1989) determined the change of the semi-major axis of a

tidally evolving asteroid binary to be given by,

$$\left(\frac{a_f}{R_{\rm pri}}\right)^{13/2} - \left(\frac{a_o}{R_{\rm pri}}\right)^{13/2} = \frac{312\pi^{3/2}G^{3/2}\rho^{5/2}(R_{\rm sec}/R_{\rm pri})^3(1+(R_{\rm sec}/R_{\rm pri})^3)^{1/2}R_{\rm pri}^2}{19\sqrt{3}\mu Q}\Delta t \tag{2.1}$$

where a_o and a_f are the initial and final semi-major axes of the binary's orbit, G is the gravitational constant, ρ is the bulk density, μ is a measure of the rigidity of the body in dyne cm^{-2}, Q is the tidal dissipation factor, and Δt is time. The *effective* rigidity of a body, $\tilde{\mu}$, is defined as

$$\tilde{\mu} = \frac{19\mu}{2\rho g R} \tag{2.2}$$

where $g = GM/R^2$ is the surface gravity of a body (Murray & Dermott 1999).

Margot et al. (2002) obtained a value of $\tilde{\mu}$ = 1.66 $\times$ 10^4 for the radar-observed binary NEA 2000 DP$_{107}$ by assuming the secondary had evolved from nearly touching the primary to its present separation over the median NEA lifetime of 10 Myr[2].

For the known properties of 2000 DP$_{107}$ ($D_{\rm pri}$ = 800 m, ρ = 1.7 g cm^{-3}) and a commonly estimated value of Q = 100, the rigidity value is then μ = 2.26 $\times$ 10^6 dyne cm^{-2}. For comparison, solid rock has a value of μ near 10^{11} dyne cm^{-2} and Phobos has μQ of 10^{12} dyne cm^{-2} (Weidenschilling et al. 1989; Yoder 1981).

The values of μQ = 2.26 $\times$ 10^8 dyne cm^{-2} and $\tilde{\mu}$ = 1.66 $\times$ 10^4 dyne cm^{-2} were used to estimate basic timescales for orbit evolution of the simulated binaries. $R_{\rm pri}$ was set at 1 km and the initial starting separation used for the calculations was 1.0 $R_{\rm pri}$; this simplification is made because the starting separation is largely insignificant for the relevant timescales (Fig. 2.12). The smaller size ratios evolve very slowly, with a binary of size ratio = 0.1 taking 10 Myr to evolve from a separation of 1 $R_{\rm pri}$ out to 4 $R_{\rm pri}$. Larger size ratios evolve much faster (as shown in Fig. 2.12), but have a smaller maximum attainable

[2]The value constrained by Margot et al. (2002) was actually k_2/Q, where k_2 is the Love number and is related to rigidity by $k_2 = (3/2)/(1+\tilde{\mu})$.

$a/R_{\rm pri}$ based on a simple conversion of initial primary spin to orbital angular momentum. For example, Hermes is presumed to be in a doubly synchronous state at $< 5\ R_{\rm pri}$ with a primary rotation and orbital period of ~ 13.8 h (Pravec et al. 2003c; Margot et al. 2003). This binary represents a possible fully evolved system, with a small $a/R_{\rm pri}$ compared to a similar system with a smaller size ratio.

The calculations suggest that over a median NEA lifetime of 10 Myr the most observable effects of tidal evolution will be that binaries with near-equal-mass components approach a synchronous state quickly (Gladman et al. 2000). Orbital evolution is quite slow for smaller mass ratios, especially beyond $5\ R_{\rm pri}$.

Of the observed binary NEAs with known eccentricities, all but one have $e < 0.1$. The damping timescales of eccentricity due to tidal interactions is governed by,

$$\tau_e = -\frac{e}{\dot{e}} = \frac{4}{63}\left(\frac{R_{\rm sec}}{R_{\rm pri}}\right)^3\left(\frac{a}{R_{\rm sec}}\right)^5\frac{\tilde{\mu}_{\rm sec}Q}{n} \tag{2.3}$$

where n is the mean motion and $\tilde{\mu}_{\rm sec}$ is the effective rigidity of the secondary (Murray & Dermott 1999). This formalism is for a secondary with a spin period equal to its orbital period and considers only the effects of the tides raised by the primary on the secondary. Tides raised on the primary by the secondary, which play a greater role for larger mass ratios, can have the effect of raising the secondary's eccentricity (Goldreich 1963; Margot & Brown 2003). Most of the known binaries have relatively small separations and size ratios, which is the regime in which eccentricity damping may be very efficient. Figure 2.13 shows damping timescales as a function of size ratio and separation, with the simulated binaries and observed binaries indicated for reference. All but one observed binary has a damping timescale less than 10 Myr, and only 7 of the 24 have a damping timescale greater than 1 Myr. The outlier is 1998 ST_{27}, with a separation of $10\ R_{\rm pri}$ and an observed eccentricity > 0.3. This is the only NEA binary with an eccentricity measured to be greater than 0.1, and is the only one for which the estimated damping timescale is greater than 10 Myr (Benner et al. 2003). This suggests that large-separation binaries discovered

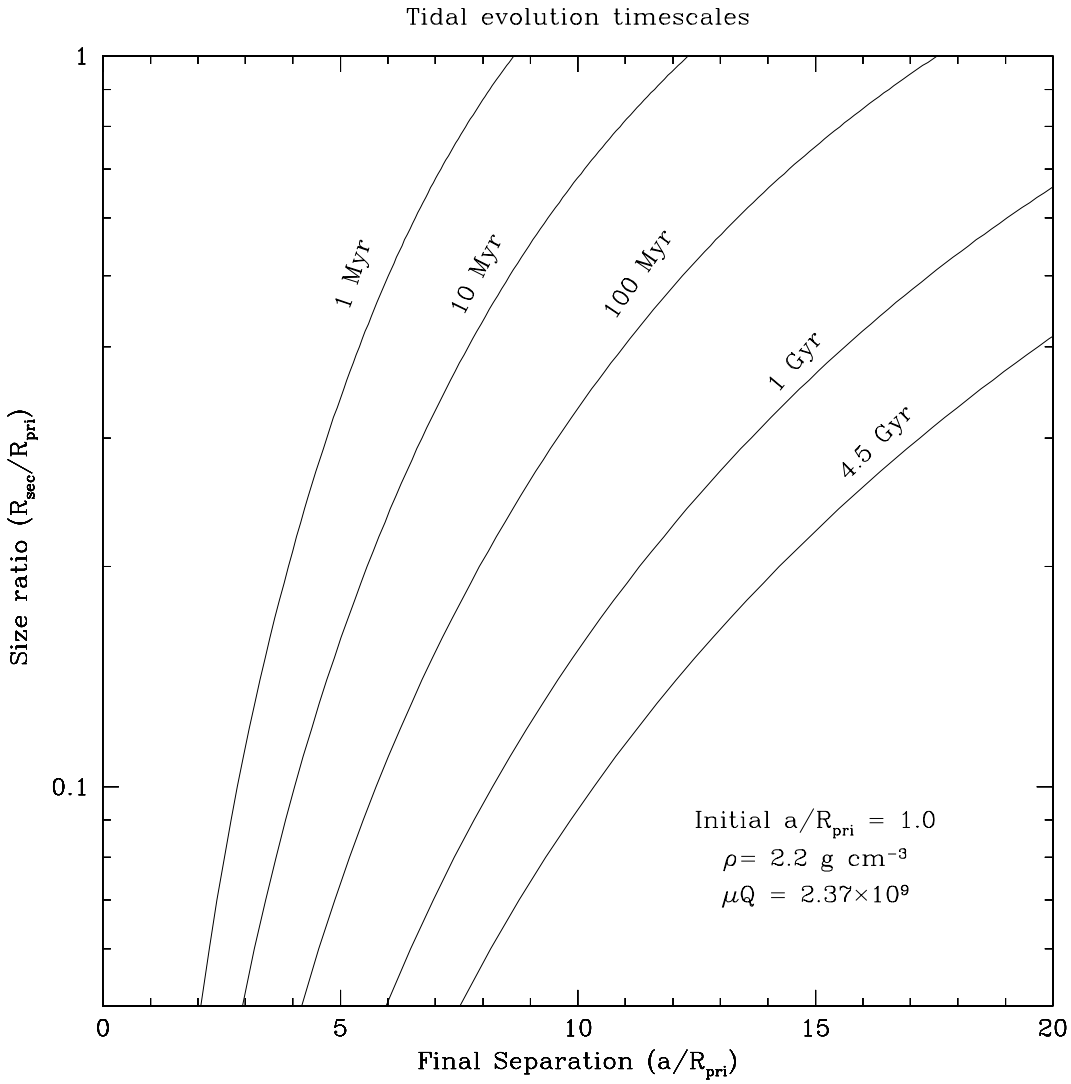

Figure 2.12: The final separations (a/R_{pri}) for different tidal evolution times for a binary starting at a separation of 1 R_{pri} as a function of their size ratio. The value for μQ used was 2.37×10^9 for a density of 2.2 g/cm^3.

in the future may also have high eccentricities.

These evolution calculations are very dependent on $\tilde{\mu}_{sec}$, for which the value used was derived from a single well-studied binary, 2000 DP_{107}. Not considered are other forces which may alter the binary on timescales comparable to those of mutual tidal forces, such as planetary tidal encounters or thermal effects. Previous work on binary encounters with Earth or Venus out to 8 planet radii showed that orbit properties of the binary can be al-

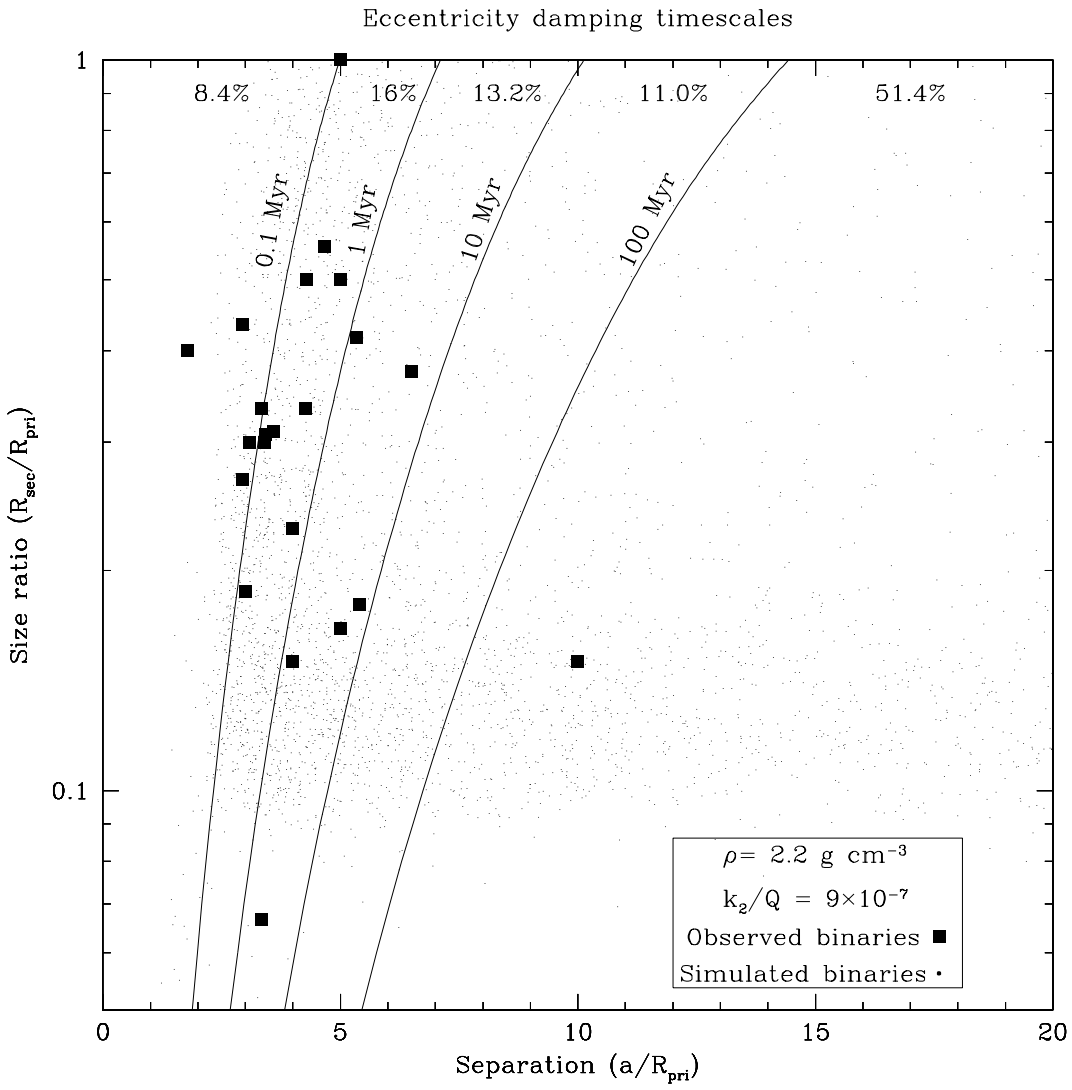

Figure 2.13: The eccentricity damping timescales for binaries as a function of their size ratio and separation (a/R_{pri}). Plotted as dots are the simulation-produced binaries and plotted as solid squares are the NEA binaries.

tered dramatically (Chauvineau & Farinella 1995; Bottke & Melosh 1996a). In addition, the thermal Yarkovsky and YORP effects have been identified as responsible for both orbital evolution and spin axis re-orientation of asteroids (Chesley et al. 2003; Vokrouhlický et al. 2003). Cuk & Burns (2004) propose that the YORP effect can alter the orbit of a synchronized secondary in a manner similar to how it affects a single body. Under ideal circumstances it may work on time scales as short as 10^5 years, dominating tidal

evolution in some situations.

2.4 Conclusion

This study used N-body simulations to model the tidal disruption of strengthless asteroids, or rubble piles, during close encounters with Earth. We presented distributions for the resultant physical and orbital properties of the binaries formed, citing similarities and differences with the observed population of NEA binaries. The spin of the primary body is bracketed in a similar fashion to the observed population, though the simulation's range of primary spin periods is centered on a somewhat slower spin period. Similarly, size ratios are smaller and less distributed than the observed binaries. Eccentricity poses one of the largest differences, with the simulations producing eccentricities greater than 0.1 for nearly all cases, whereas all observed binaries have eccentricity less than 0.1. Roughly half the simulated binaries had separations below 10 $R_{\rm pri}$, which is the upper limit for nearly all observed NEA binaries.

Due to the nature of the simulations, and the expensive computations involved, this many N-body runs cannot all be simulated forward to map the evolution of the overall population. Instead this task will have to be handled on a case-by-case basis, partly using analytical techniques developed by Scheeres (2002) to model evolution of binary systems with non-spherical primaries and secondaries. Other numerical techniques in development, such as freezing the rubble piles into rigid aggregates, thereby eliminating collision calculations, would reduce computation time making some stability and evolution simulations more practical.

As young binaries evolve and new binaries form, a steady-state distribution of properties may develop. Modeling this would help determine which binaries are created in the inner solar system via tidal disruption and which, if any, may have entered intact from the

Main Belt. Work by Chauvineau & Farinella (1995) and Bottke & Melosh (1996a) suggest further encounters of binaries with planets may increase the separation of binaries. Synthesis of these studies with this presented work could provide estimates of evolutionary tracks and help establish the steady-state distribution of properties.

An improvement in our knowledge of physical traits of small MBAs would help determine what effect tidal disruption has on the NEA population as a whole. Better determination of very small MBA shape and spin distributions will help set the initial conditions for future studies.

Overall this work points towards a population of NEA binaries yet to be discovered, those with small size ratio, and with separations greater than 10 $R_{\rm pri}$. This population could very well be formed in equal numbers as the current known small-separation binaries. These binaries may have elongated primaries, more eccentric orbits, and small size ratios. The long-term survival of such binaries is questionable as distant encounters with a planet will likely keep lifetimes very short.

Acknowledgments

The simulations were run on the `borg` and `vampire` computing clusters at the Department of Astronomy, University of Maryland. Thanks to Bill Bottke for providing encounter distributions and for manuscript comments. Thanks also to Doug Hamilton for manuscript comments. We thank the referees for helpful comments that improved the manuscript. This material is based upon work supported by the National Science Foundation under Grant No. AST0307549.

Chapter 3

Lightcurve Observations of Small Main Belt Asteroids

3.1 Overview

We report the results of an observing campaign to measure the lightcurves of small ($D < 5$ km) Main-Belt asteroids. Shape and spin information from lightcurve data is valuable for investigating the processes in the Main-Belt and near-Earth regions that affect these properties of asteroids. The targets of these observations all had $H > 16.5$, and were observed from the Kitt Peak National Observatory (KPNO) 2.1 m telescope. We have observed a total of 28 objects, constraining amplitudes for all, and periods for 15. We present the results of these observations, and compare them to previously known distributions of lightcurve amplitudes and periods for MBAs, small MBAs and NEAs. Previously there were only 60 published light curves for small MBAs. Overall no significant divergence is present between the distributions for small MBAs and all MBAs, with small MBAs not appearing to have the abundance of rapidly rotating bodies present among the NEAs.

The work presented here is essentially a continuation of the survey by Binzel et al.

(1992), with a target range of slightly smaller bodies. It is aimed at increasing the number of bodies with well-known lightcurves, allowing comparison between NEAs, SMBAs, and the population of larger MBAs. In section 3.2 we discuss the details of our observing campaign. The data reduction techniques are covered in section 3.3 and the results of the observations along with discussion are in section 3.4.

3.2 Observations

All observations were made at the KPNO 2.1m on the following dates,

1. December 7–9, 2004
2. March 4–13, 2005
3. December 27, 2005 – January 3, 2006
4. February 28, 2006 – March 4, 2006

Observations were made in *R* and *V* filters, with *V* used rarely for color measurements (though a surprisingly low number of photometric nights diminished the number of nights it was used). On non-photometric nights observations were typically only made in the *R* filter. Exposure time was typically adjusted to achieve a Signal-to-Noise ratio of 50, with most exposures between 30–120 seconds. Coverage time for each object was adjusted depending on target brightness and airmass throughout the night of observations. Many nights included observations of more than one target, and coverage for each was distributed according to initial estimates of any lightcurve period determined from real-time data reduction. During the course of one exposure the motion of the asteroid, around 0.5 arcsec per minute usually, was less than the size of the typical point spread function (PSF). Therefore the asteroids were not tracked during the exposure, instead tracking was at the sidereal rate.

H	D (km) p = 0.23	D (km) p = 0.05
16.0	1.7	3.8
16.5	1.4	3.0
17.0	1.1	2.4
17.5	0.9	1.9
18.0	0.7	1.5

Table 3.1: Estimated diameters for S-type asteroids with an albedo p = 0.23 and C-type asteroids with p = 0.05 for different values of H. The limit for this observing campaign $H = 16.5$.

The targets were exclusively asteroids in the Main Belt with an absolute magnitude $H > 16.5$, which roughly corresponds to $D < 3$ km for standard MBA albedos (see Table 3.1), where H is defined as the visual magnitude a body would have 1 AU from the Sun, 1 AU from the Earth and at zero phase angle. Targets were selected using the JPL Solar System Dynamics online tools, and were verified by motion vectors, and predicted brightness. The conversion from absolute magnitude H to diameter D depends on the albedo of a body. Generally for the target bodies observed in this group of targets, all are in the inner Main Belt, and therefore likely to be S-type asteroids (Ivezić et al. 2001). Assuming an albedo of $p = 0.23$ for S-type asteroids a set of transformations can be made using the formalism,

$$D = \frac{1329}{\sqrt{p}} 10^{-0.2H} \tag{3.1}$$

where p is albedo (see Table 3.1 for relevant conversions). Given more ideal observing conditions, where absolute photometry could be made for all, or even most of the objects, color measurements would strongly suggest the class of asteroid. Due to the large number of objects being targeted in relatively few nights, and the low number of photometric nights, this was not a realistic way to classify our targets. The limit of $H > 16.5$ was conservative, and even C-type asteroids at this absolute magnitude would be smaller than 5 km (Table 3.1).

The observations were made from the KPNO 2.1m located on Kitt Peak in Arizona. The camera used on the 2.1m was the T2KA chip which is a 2048 $\times$ 2048 CCD with 24 micron pixels. The pixel scale is 0.305 arcsec per pixel for a field of view for the entire chip of 10.2 $\times$ 10.2 arcminutes. All images were taken with no binning and a gain setting of 3.1 e/ADU.

3.3 Data Reduction and Photometry

All data reduction was done in the IRAF data reduction package. Prior to any analysis being performed, each image was bias subtracted and flatfielded. Biases were typically recorded at the beginning and end of each night. Flats were made in each filter for each night of observing, and usually consisted of 4–6 dome flats each, and occasionally included 2–3 additional twilight flats. Comparisons showed little difference between dome and twilight flats for any given nights, and were combined on nights when they were both obtained.

Photometry was performed using the `phot` package in IRAF. This package calculates the mode of the sky values found in a wide annulus (typically from 40–50 pixels), and subtracts this value from each pixel (including fractional pixels) within the area of the circular aperture. The remaining flux is converted into an instrumental magnitude, with the error of a given measurement being dominated by the standard deviation of the sky values.

On photometric nights all-sky photometry was performed, otherwise differential photometry was done with at least 3 field stars. For all-sky photometry, standard stars (Landolt 1992) were used to determine the extinction coefficient and zero point magnitude for that night of observing. These were then used to determine magnitude values for each image of each asteroid. For non-photometric or marginally photometric nights, differential

photometry was used. This required bright field stars present throughout all the observations of the asteroid. Assuming that any fluctuations in seeing or atmospheric conditions will affect the entire field of view similarly, the asteroid's magnitude relative to the field stars was used to determine its brightness fluctuations. Most object's periods were determined from a single night of observing, so field stars from the same object from different nights of observing were typically not compared.

In some rare cases the technique of aperture correction was used. This is a common technique for photometry on very dim objects, where most of the object's PSF is below the sky level, and field stars are used to estimate the total flux of an object (Howell 1989). Measurements were made on both the field stars and the object at a small aperture, and the average difference between the small and large aperture for the field stars was added to the measured small aperture magnitude for the object. Typically the large aperture used had a radius of 24 pixels, 7.32 arcsec, while the small aperture had a radius of 7 pixels, 2.135 arcsecs.

3.3.1 Phase dispersion minimization

The method of period determination using Phase Dispersion Minimization (PDM), within IRAF, was used to analyze the data set for each asteroid (Stellingwerf 1978). PDM bins the data according to phase for a given test period, and calculates the variance for each bin. The ratio of the average bin variance over the variance for the entire unbinned data determines the quality of the fit. This method is not optimized for any particular curve shape, or data spacing, which makes it well suited for asteroidal lightcurves. This fitting method also retains any secondary periods and also produces amplitude and epoch information.

When selecting a best-fit period for any given lightcurve, solutions were examined and the best double-peaked period was selected. Often the best PDM fit was for a single-

peaked period, with a lower significance fit for the double-peaked alias. In these situations the double-peaked period was selected after visual confirmation. Single-peaked lightcurves are possible for low-amplitude cases, where the brightness variations are dominated by albedo differences on the surface. This is expected to be possible only with amplitudes below $\sim$0.2 magnitudes (Sheppard & Jewitt 2004; Degewij et al. 1979). Most small-amplitude lightcurves in this study produced no reliable period fit and hence are not at risk of having an albedo-caused single-peaked lightcurve being mistaken for half of a shape-induced double-peaked lightcurve.

3.4 Results and Discussion

The discussion of individual asteroids below is divided according to the quality of the lightcurve obtained, those with well-determined lightcurves being discussed in Section 3.4.1, those where significant constraints on period or amplitude were made in Section 3.4.2 and those objects with only marginal constraints in Section 3.4.3. Many large-amplitude cases presented straight-forward analysis, with clearly defined periods and amplitudes. These were typically the exception, as there was a significant fraction of asteroids with small amplitudes that were close to the photometric error. These cases involved quite challenging analysis, sometimes giving ambiguous solutions.

Typically the best fit lightcurve would result from one night's observation, with a few exceptions where a long period would demand multiple nights. Observations are presented in Figs. 3.1–3.5 and are summarized in Table 3.2, and each object is discussed in turn below.

3.4.1 Well-determined lightcurves

2002 JS_{112} (Fig. 3.1a). Extensive observations of this object on 2 March, 2005 reveal a double-peaked lightcurve with a period of 5.7 h and an amplitude of 0.45 magnitudes. Additional observations on 3 March, 2005 recovered a minimum in agreement with the period.

2000 TO_{34} (Fig. 3.1b). A large amplitude lightcurve, Δm = 0.81, with a double-peaked period of 5.11 h. Observations were made on 7 March, 2005.

2000 CC_{33} (Fig. 3.1c). Observed extensively over two nights, 28 and 29 December, 2005, this asteroid's period and amplitude were both determined. Both nights of observations were needed to finalize a period of 2.57 h and an amplitude of 0.15 magnitudes. The asteroid is plotted with points from multiple nights phased to the best fit period.

2001 QL_{212} (Fig. 3.1d). Observations on 30 December, 2005, provided a solid PDM fit to a single-peaked lightcurve with a period of 2.47 h and amplitude of 0.2 magnitudes. Therefore we estimate a rotational period of $\sim$ 4.94 h for a double-peaked lightcurve.

2001 QZ_{156} (Fig. 3.1e). A short-period lightcurve was revealed in one night of observations on 30 December, 2005. The PDM routine revealed a double-peaked lightcurve of 2.98 h, with an amplitude of 0.16 magnitudes.

2001 UW_{121} (Fig. 3.1f). The amplitude and period of this object were determined on 1 January, 2006. This object had the largest amplitude of any observed object, at 1.04 magnitudes. Using the standard estimation for axis ratio from lightcurve amplitude, $\Delta m = 2.5 \log \frac{a}{b}$, the axis ratio for this body is $\sim$ 2.6 to 1.0, which is very extreme

and suggests that it is possibly a contact binary. The period was determined by the PDM routine to be 4.82 h.

1998 XS_{59} (Fig. 3.2a). One night of observations, 3 January, 2006, covered the entire period of this asteroid. The best fit double-peaked lightcurve has a period of 6.79 h with an amplitude of 0.23 magnitudes.

3.4.2 Detections with significant constraints

2002 AW_{151} (Fig. 3.2b). Limited observations on December 9, 2004 allowed for an upper limit of amplitude $\sim$ 1 mag to be determined. The PDM fits suggest a 2.843 h period, but we appear to have observed only one maximum, and therefore the actual double-peaked lightcurve period could be between two and four times that value. With such a large amplitude observed we estimate that we likely observed from minimum to minimum, thus a period $\sim$5.7 h is estimated.

2000 HX_{82} (Fig. 3.2c). Extensive observations on December 8, 2004 placed no constraints on the rotational period, but suggest an upper limit on amplitude around 0.6 magnitudes. All PDM fits were of very low significance.

1187 T-1 (Fig. 3.2d). Observations on 8 December, 2004 suggested a relatively large amplitude of 0.35 magnitudes when analyzed with the photometric technique of aperture correction. The PDM routine found a period of 2.848 h, but the quality of the fit was quite low. It does appear that the period may be slightly longer than the observational window, or longer than $\sim$ 4 h.

2002 JD_{50} (Fig. 3.2e). Observations on 3 March, 2005 revealed a small-amplitude lightcurve. Despite small photometry errors, the period is ambiguous. The PDM fitting routine best-fit period was 3.46 h, though the actual period is likely an integer factor of this, likely over 7 h.

2000 SB_{193} (Fig. 3.2f). Extensive observations on 10 March, 2005 were unable to reveal a definitive period for this object. The very long baseline of images of over 6 h allowed for a strong upper limit in the amplitude of ~ 0.25 magnitudes. The PDM routine finds a marginal period fit at 1.28 h, suggesting a double-peaked period at twice to four times that value.

2000 UE_{109} (Fig. 3.3a). Observations spread over a long baseline of two nights, 4 and 9 March, 2005 revealed a very flat lightcurve with amplitude fluctuations similar to the error in the photometry. The amplitude can be constrained below 0.1 magnitudes, but no constraints on the rotation period can be made.

1981 EJ_{27} (Fig. 3.3b). Observations over 3 and 4 March, 2005 revealed a large-amplitude lightcurve with a period ~ 13.56 h. The lightcurve was not covered in its entirety so the amplitude is estimated to be ≥ 0.7 magnitudes.

1981 EL_{31} (Fig. 3.3c). Observations on 8 March, 2005 revealed a low-amplitude lightcurve with a possible period ~ 6 h. The best PDM fit is for a 3.0 h single-peaked lightcurve with an amplitude of 0.07 magnitudes.

1998 HZ_{32} (Fig. 3.3d). This asteroid demonstrated a very long period and required spaced out observations over multiple nights, 8 and 10 March, 2005. Both nights of observations covered a baseline longer than 4 hours and only observed one maximum and no minimum. Combined, the two nights of observations suggest a period ~ 32 h, with an amplitude greater than 0.7 magnitudes.

1999 CM_{50} (Fig. 3.3e). One night of observations revealed a relatively low-amplitude lightcurve, 0.26 magnitudes. The best double-peaked period solution from PDM was 3.18 h, though it was only with a marginal significance.

2001 TZ_{50} (Fig. 3.3f). Observations on 4 March, 2006 were not enough to solidify a

fit for the period of the lightcurve. The PDM best fit was 4.22 h, but was very marginal. The amplitude of that fit was 0.38 magnitudes.

1998 VJ_{25} (Fig. 3.4a). Observations on the night of 5 March, 2006 were enough to establish a lower limit on lightcurve amplitude of 0.12 magnitudes. However, the best-fit period was only of marginal quality at 4.33 h.

3.4.3 Marginal detections

2000 QL_{73} (Fig. 3.4b). Limited observations on 9 and 10 December, 2004 revealed no discernible period. The lightcurve is constrained for short periods to be below 0.15 magnitudes. This faint asteroid required the use of aperture correction using an inner aperture of 7 pixels and an outer aperture of 24 pixels.

2000 QX_{15} (Fig. 3.4c). Observations on 8 December, 2004, with the aid of aperture correction, revealed some structure in the lightcurve. The amplitude is limited to below 0.3 magnitudes, and the best PDM solution for the period is $\sim$ 2 h, though it is a very marginal fit.

2001 BH_{22} (Fig. 3.4d). Observations on 10 March, 2005 revealed a low amplitude lightcurve, below 0.1 magnitudes, with an unidentified period. The lightcurve shows some possible structure, but no fits with significance are found with the PDM fitting routine.

2000 YE_{110} (Fig. 3.4e). Extensive observations over two nights, 8 and 9 March, 2005, was not enough to find a period in the heavily structured lightcurve. The significant coverage did allow for an estimate for the upper limit on the amplitude < 0.3 magnitudes.

1999 CR_{87} (Fig. 3.4f). Limited observations of this asteroid on 27 December, 2005 pro-

vided no significant constraint on the asteroid's period. The baseline of observations over 4 h suggests that the amplitude is no greater than 0.15 magnitudes.

2001 SA_{258} (Fig. 3.5a). Limited observations on 28, December 2005 found substantial structure in the lightcurve, but was insufficient to determine a period or place limits on the amplitude. The observations determined a lower limit for amplitude of 0.15 magnitudes.

2000 HZ_{47} (Fig. 3.5b). Observations on 2 March, 2006 were unable to determine the period of this object. A large gap in the observations due to poor conditions seriously limited the data. The extent of the observations would suggest a lower limit on amplitude of 0.6 magnitudes.

Kadlu (Fig. 3.5c,d,e). The most interesting object in the group was observed on three separate nights, was the only Mars-crossing asteroid observed and the only object observed with a previously published lightcurve. Pravec et al. (1995) estimated a period > 9 h and an amplitude of ≥ 0.30, while Mottola et al. (1995) determined a period of 50.6 ± 0.2 h and an amplitude > 0.4 magnitudes. During sparse observations on 3 March, 2005 Kadlu showed a rapidly brightening lightcurve, with a maximum range of ~ 0.5 magnitudes over just one hour of observations (Fig. 3.5c). The night of 5 March, 2006 (Fig. 3.5d) the object was quite stable showing periodic fluctuations. Observations on 6 March, 2006 also showed a night-long decline over 0.5 magnitudes, but over a 5 h timescale (Fig. 3.5e).

Table 3.2. Orbital, physical and lightcurve parameters for all targets.

Object	*a* (AU)	*e*	*H* (mag)	Amplitude (h)	Period	**Q**	*n*
2002 JS_{112}	2.26	0.11	16.8	0.45±.02	5.7±.2	3	72
2000 TO_{34}	2.25	0.14	16.8	0.81±.03	5.11±.2	3	65
2001 UW_{121}	2.44	0.15	16.6	1.04±.03	4.82±.1	3	80
2000 CC_{33}	2.18	0.13	16.6	0.15±.03	2.57±.2	3	125
2001 QZ_{156}	2.28	0.14	16.8	0.16±.03	2.98±.2	3	88
2001 QL_{212}	2.32	0.21	16.7	0.2±.03	4.94±1.0	3	63
1998 XS_{59}	2.30	0.13	16.8	0.23±.03	6.79±.2	3	95
2001 TZ_{50}	2.21	0.14	17.1	0.38±.03	∼4.2	2	50
1999 CM_{50}	2.31	0.16	16.6	≥0.26	∼3.2	2	81
1998 VJ_{25}	2.21	0.16	16.6	≥0.12	∼4.3	2	77
1981 EJ_{27}	2.28	0.20	16.6	≥0.7	13.58±.1	2	100
1981 EL_{31}	2.28	0.11	16.8	<0.07	∼6	2	51
1998 HZ_{32}	2.34	0.15	16.7	≥0.5	∼32	2	66
2002 AW_{151}	2.28	0.06	16.8	>1.0	∼5.7	2	29
2000 HX_{82}	2.18	0.18	16.8	≥0.22		2	67
1187 T-1	2.29	0.15	17.5	≤0.35	>4	2	34
2001 BH_{22}	2.35	0.13	16.6	<0.1		1	54
2002 JD_{50}	2.27	0.11	16.8	<0.1		1	33
2000 SB_{193}	2.18	0.08	16.8	<0.25		1	67
2000 YE_{110}	2.34	0.14	16.7	<0.3		1	91
2000 UE_{109}	2.31	0.13	16.6	<0.1		1	49
2000 QL_{73}	2.22	0.13	17.0	<0.15		1	36
2000 QX_{15}	2.25	0.17	17.2	≥0.3		1	40
1999 CV_{91}	2.36	0.17	16.6	<0.1		1	79
1999 CR_{87}	2.32	0.17	16.6	<0.15		1	38
2001 SA_{258}	2.35	0.17	16.7	>0.15		1	53
2000 HZ_{47}	2.16	0.03	16.7	>0.6		1	54
Kadlu	2.53	0.48	16.9	>0.5		1	80

Note. — The semi-major axis *a*, and eccentricity *e*, and quality rating of the lightcurve **Q** (see Section 1.3.1) are listed along with *n*, the number of observations for the object. Absolute magnitude *H* is defined as the absolute magnitude of an object at unit heliocentric and geocentric distance with zero phase angle. In many cases limits are placed on values due to insufficient data.

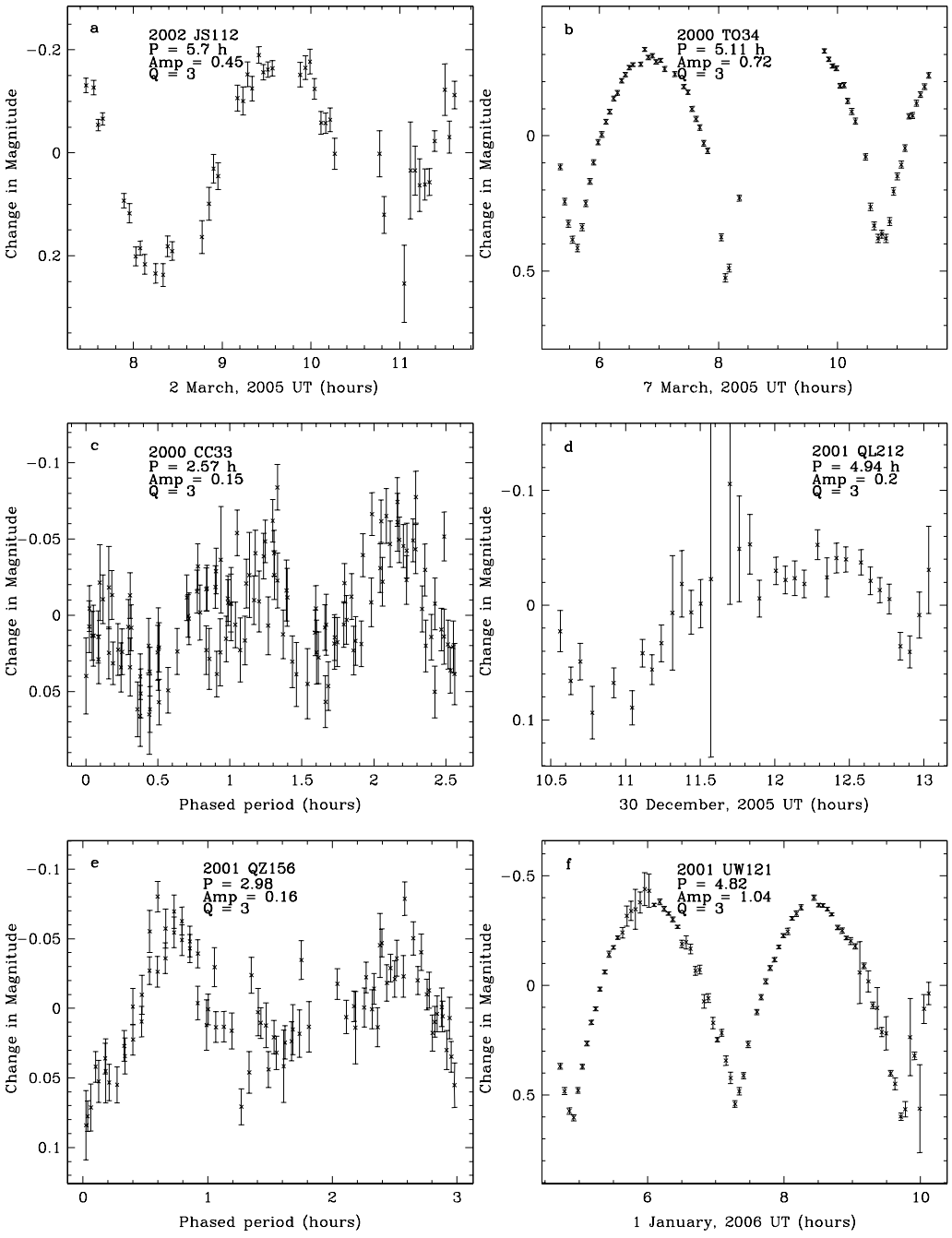

Figure 3.1: Asteroid lightcurves.

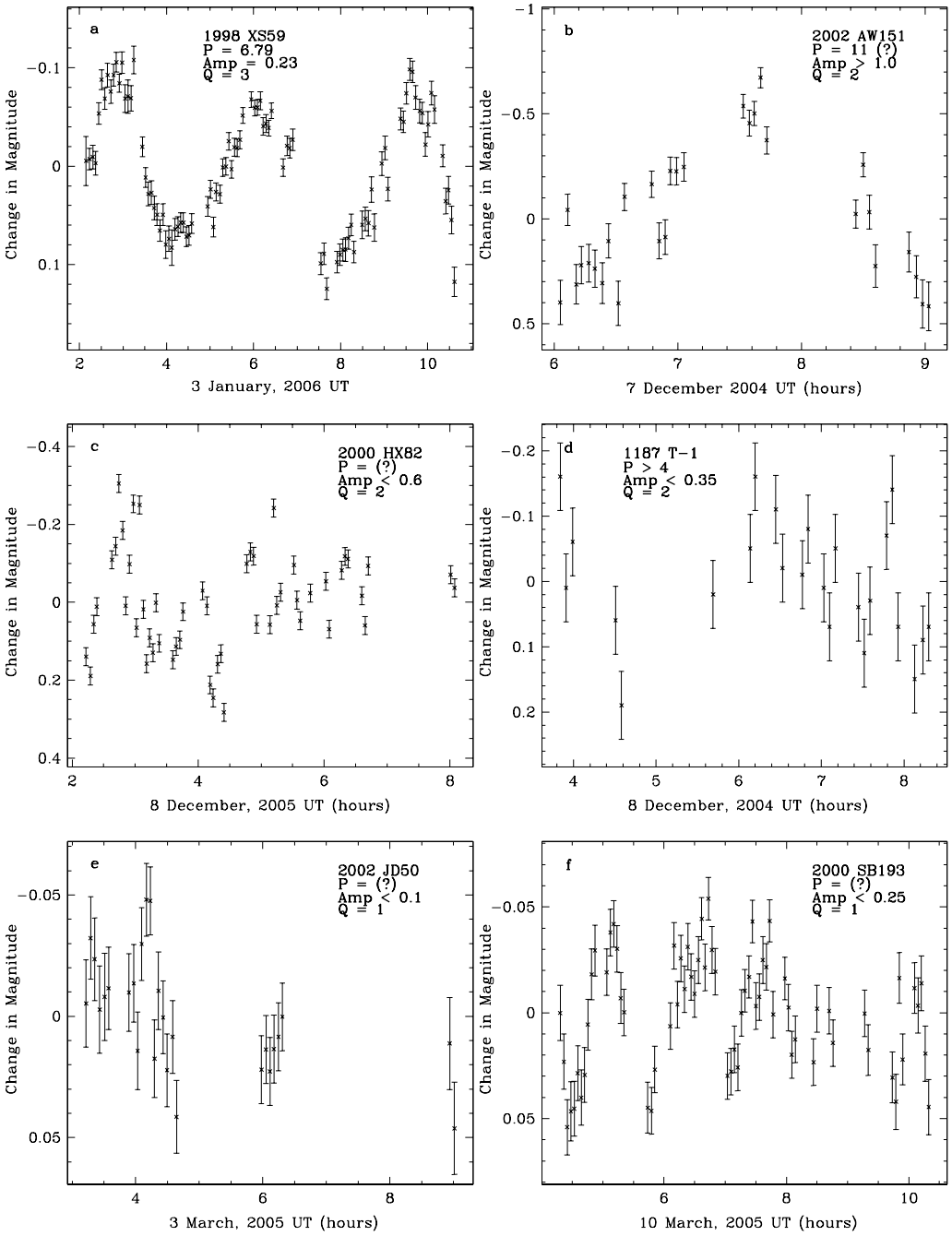

Figure 3.2: Asteroid lightcurves.

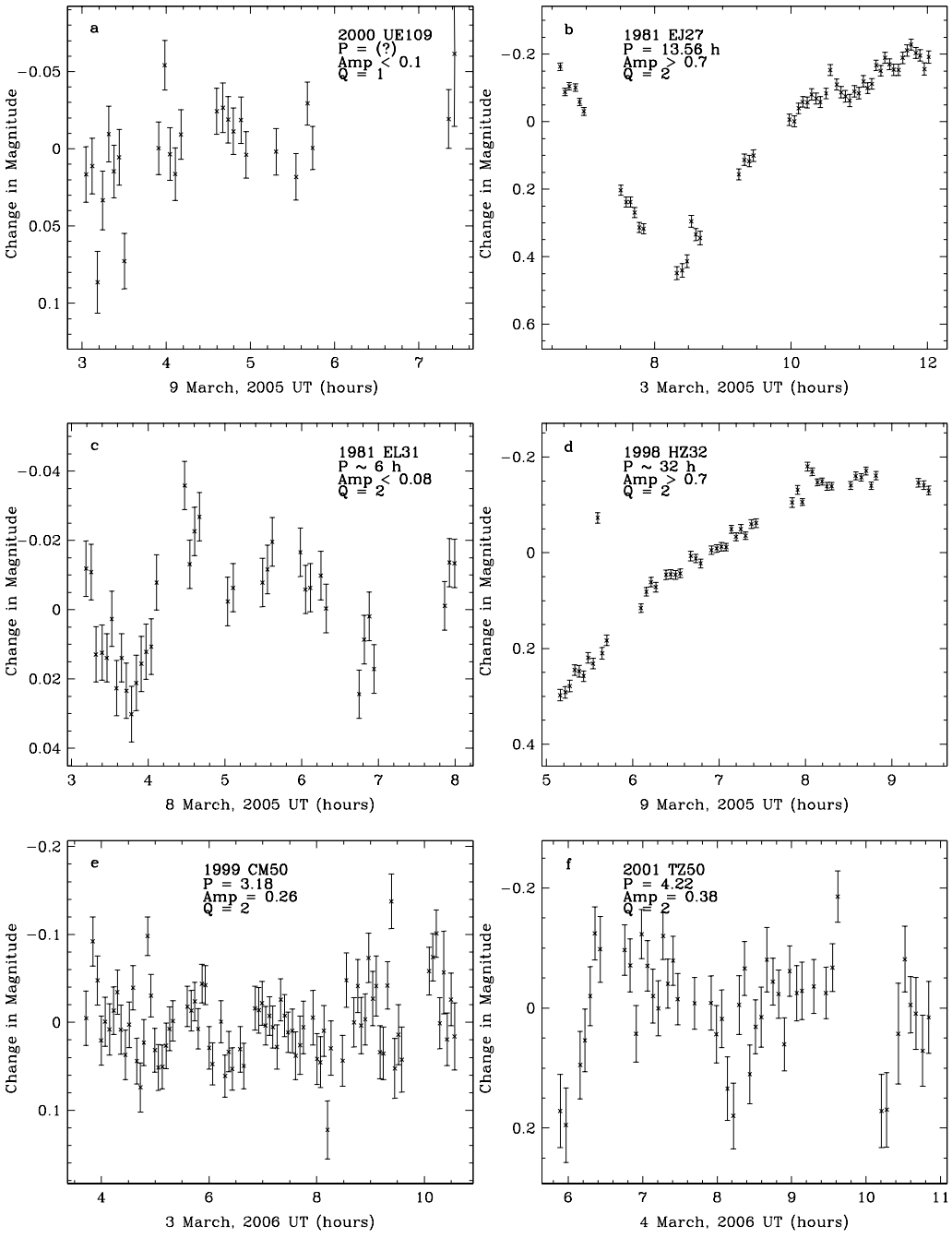

Figure 3.3: Asteroid lightcurves.

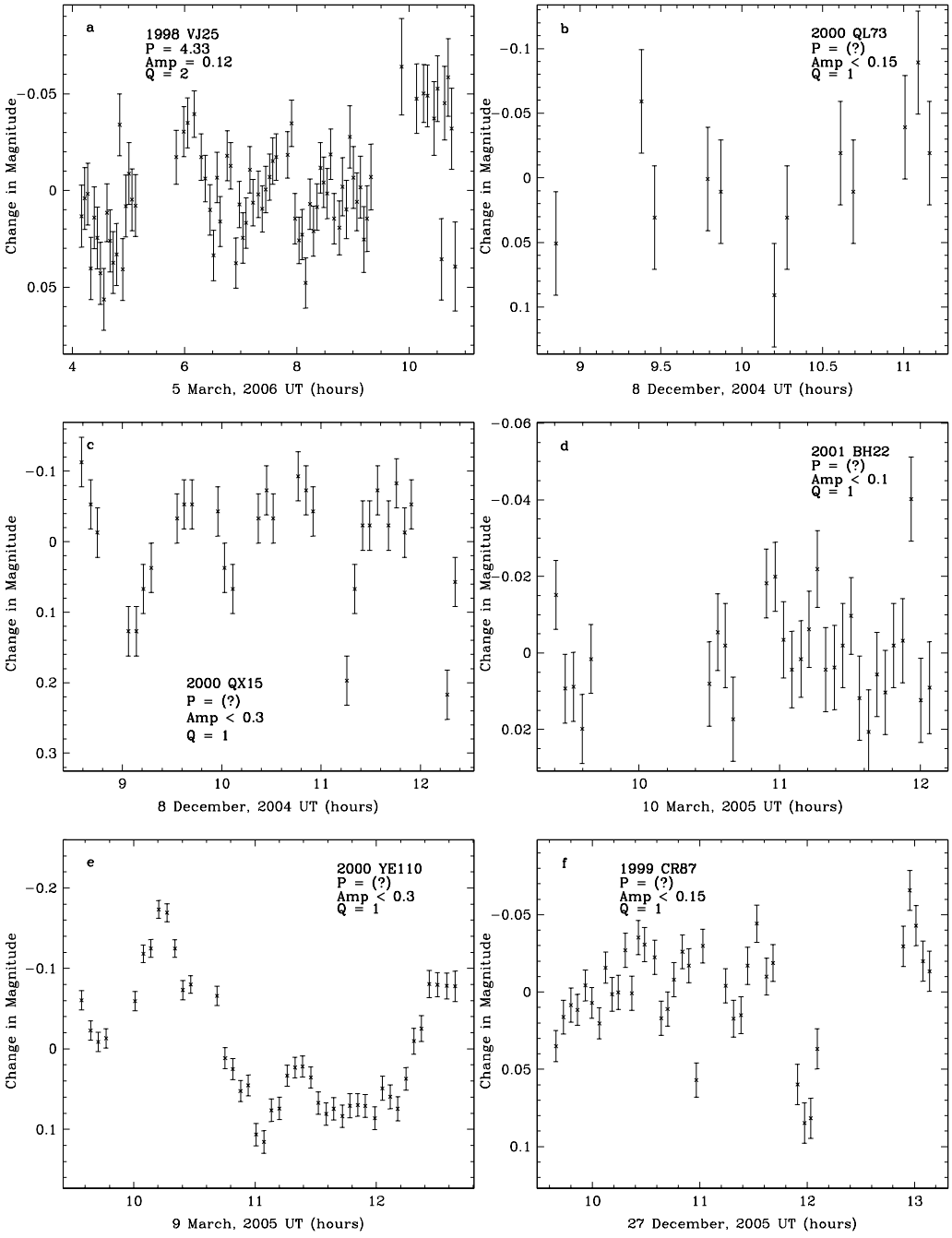

Figure 3.4: Asteroid lightcurves.

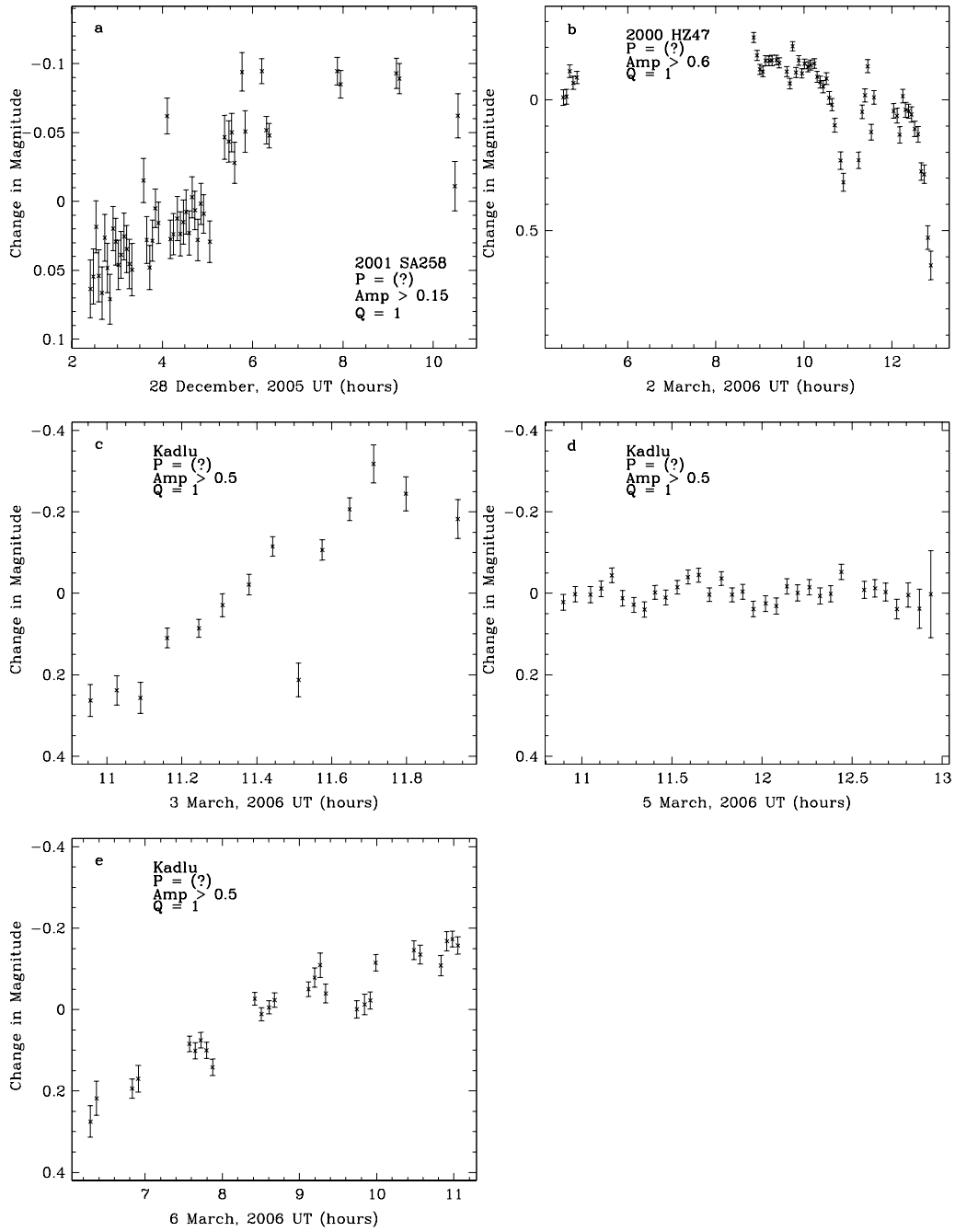

Figure 3.5: Asteroid lightcurves.

3.4.4 Spin and shape properties among small MBAs and NEAs

The lightcurve properties of MBAs with $D < 20$ km plotted in groups of $D < 20$, $D < 15$, $D < 10$ and $D < 5$ km (Fig. 3.6) show no major divergence in properties with size (where only asteroid lightcurves with a published $\mathbf{Q} \geq 2$ are considered). The smallest sizes plotted, 5 km, generally remain consistent with the distribution of the larger bodies, including the gap in intermediate lightcurve amplitude between 0.5–0.7 magnitudes. A Kolmogorov-Smirnov (KS) test of the distributions for both period and amplitude suggest that those with $D < 5$ km are very similar to $D < 10$ km. This test also suggests decreasing similarity with increasing size, so that the $D < 15$ km distributions match more closely than the $D < 20$ km. The match with $D < 20$ km is at a low significance, similar to that obtained in comparing the $D < 5$ km bodies with NEAs.

The SMBA lightcurve distributions do differ from those of NEAs (Fig. 3.7). These differences highlight the abundance of fast-rotating bodies in the NEA population, not observed amongst the SMBAs. This abundance has been noted in numerous works, and is still present with this increase in SMBA lightcurves (Pravec et al. 2002). This difference may be a combination of the increased intensity of thermal effects and/or the influence of planetary encounters for NEAs. Given the short dynamical lifetime for NEAs (median lifetime of 10 Myr) any environmental difference would have to be strong enough to significantly alter the population on equally short timescales (Gladman et al. 2000). The strength of thermal effects also varies with size, affecting smaller bodies much faster. The NEA lightcurve distributions in Fig. 3.7 include bodies significantly smaller than those in the SMBA distribution. To verify that size differences are not involved we imposed a cutoff of $H < 17$ on the NEA distribution, and replot the comparison of spin periods in Fig. 3.8. This limits the two populations to essentially the same lower limit on size, allowing a comparison of truly similar sized bodies with diameter between $\sim$ 1–5 km (see

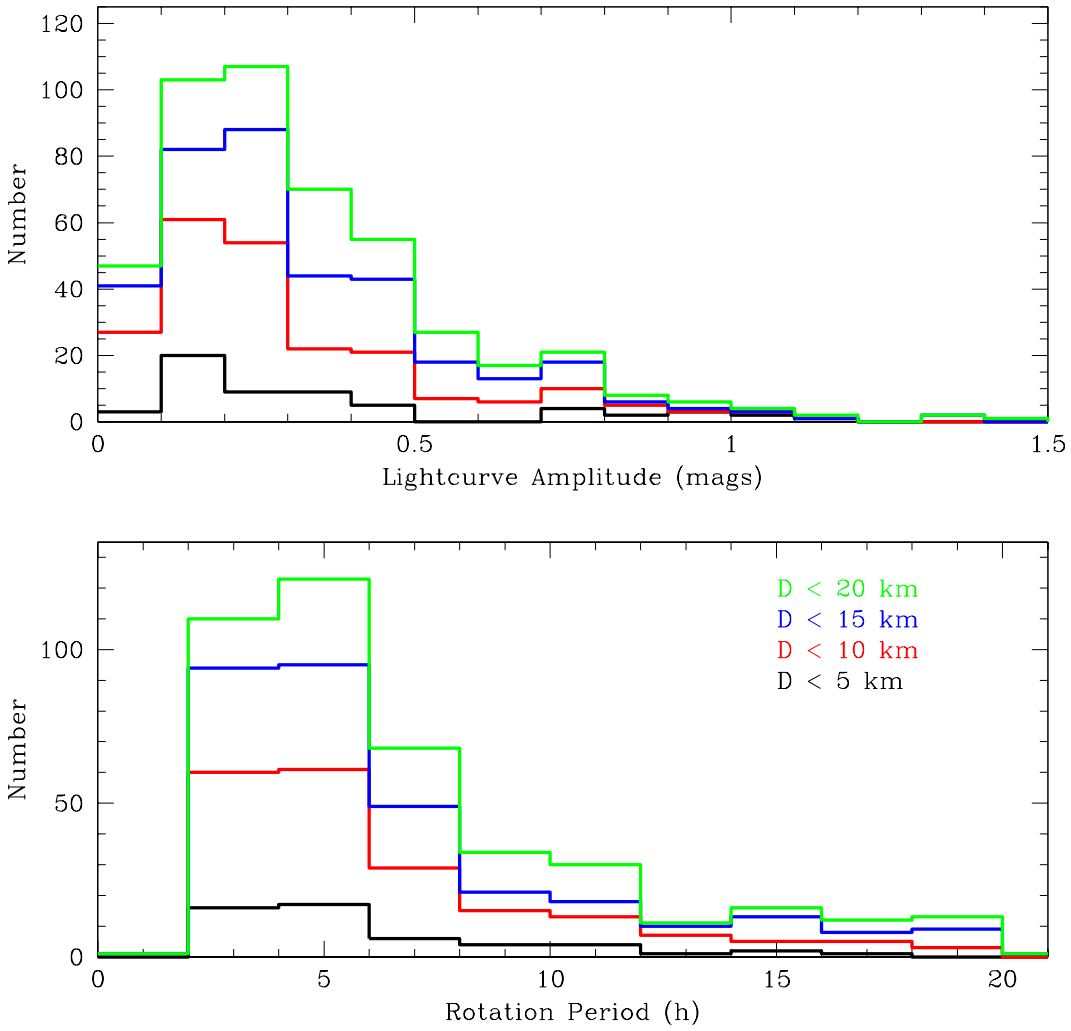

Figure 3.6: The four histograms show the distribution of rotation period and lightcurve amplitude for MBAs with $D < 5$ km (Black), 10 km (Red), 15 km (Blue) and 20 km (Green).

Fig. 3.8 for H distributions). Even with this lower limit on size, the NEAs still appear to have a larger population of rapid rotators than is observed among SMBAs. Generally the K-S test of the period and amplitude distributions of the NEAs with $H < 17$ and the SMBAs show a low significance statistical match, similar to that when the SMBAs are compared with $D < 20$ km MBAs. This statistical test suggests the SMBAs and NEAs are drawn from different populations, due to the excess of fast rotators among the NEAs.

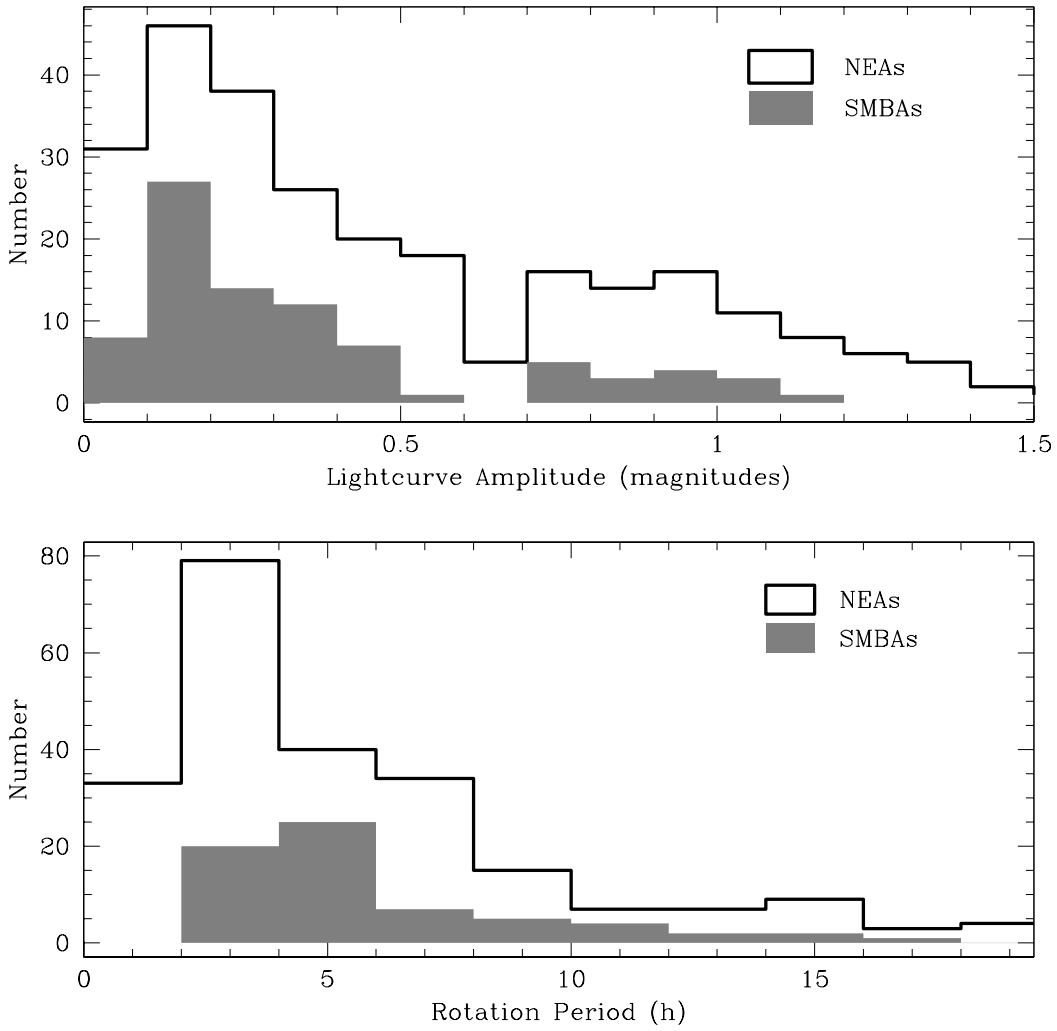

Figure 3.7: The lightcurve amplitude and period for observed NEAs (outline) and small MBAS (shaded) with a lightcurve quality $\mathbf{Q} \geq 2$.

The overall coverage for each target was not extensive enough to definitively discover or rule out binaries in the sample. From the group of targets observed, the very high amplitude objects would make the most likely candidates for further study as possible binaries, or contact binaries. Previous theoretical work has suggested an upper limit for lightcurve amplitude for non-binary strengthless bodies at 0.91 magnitudes, and even smaller amplitudes for bodies with long rotational periods (Leone et al. 1984; Sheppard

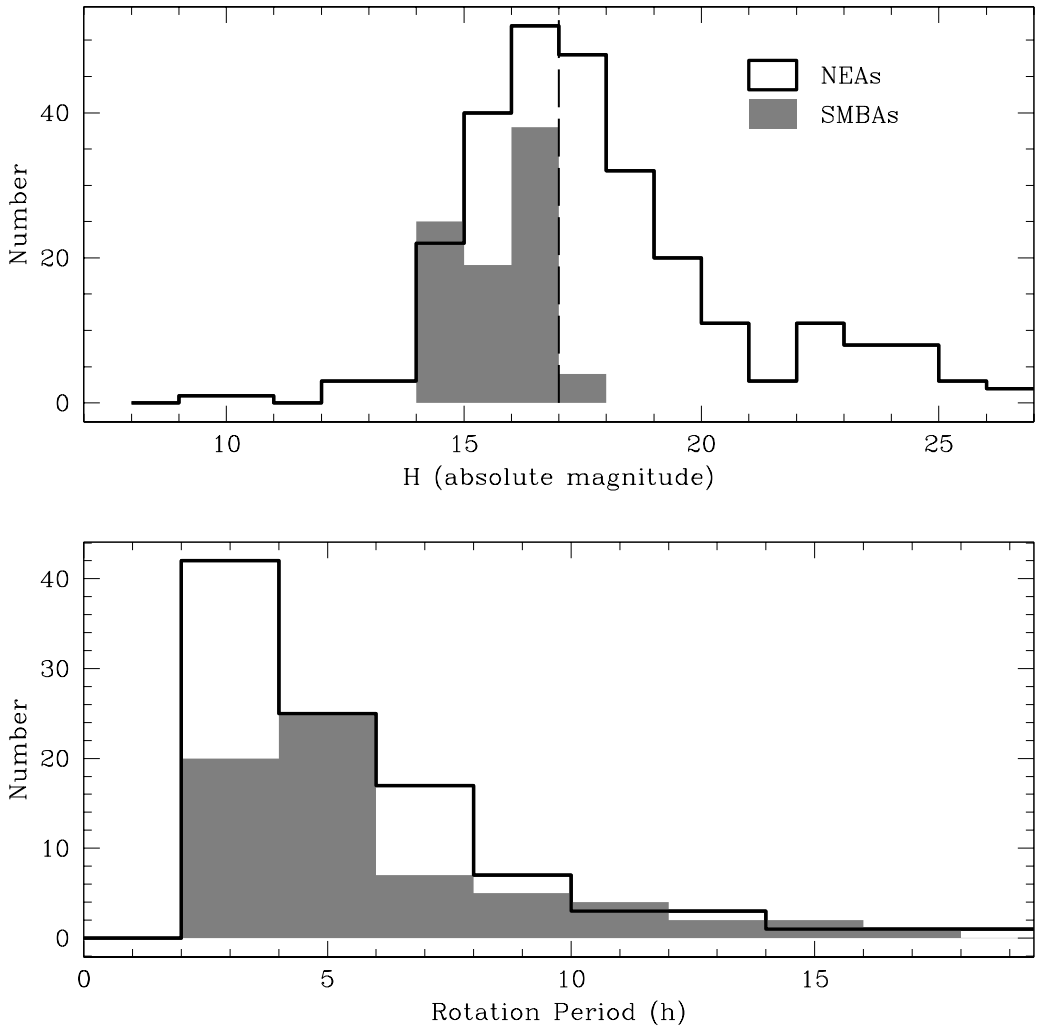

Figure 3.8: The *H* distribution for all the bodies in Fig. 3.7, where the dotted line at *H* = 17, shows where the NEA distribution was cut off for the lightcurve period plot on the bottom panel.

& Jewitt 2004). Among our sample 2001 UW_{121} and 2000 TO_{34} both have similar shaped lightcurves, with sharp minima and rounded maxima. The former has an amplitude of 1.04, the latter 0.72 magnitudes. 2002 AW_{151} showed a large amplitude of at least 1 magnitude, though the spotty coverage did not allow a close analysis of its shape, or detection of a minimum. Both 1981 EJ_{27} and 1998 HZ_{32} both had long periods and amplitudes greater than 0.7 magnitudes.

Typically observations of eclipse or occultation events are necessary to solidly establish binarity via lightcurve observations. Amongst the NEAs all the binaries discovered with this technique have been asynchronous, where two separate periods are distinct in the lightcurve, and any events are correlated with the secondary period. Recently Behrend et al. (2006) reported 4 new binary MBAs out of a search of 10 km and larger bodies. All 4 detections were made of fully synchronous systems, where sharp, V-shaped minima with a depth of 0.5 magnitudes or greater suggested total eclipses. These events happen at each minimum on the lightcurve, as each body's rotational period is the same as the orbital period of the system. These V-shaped minima are significantly more dramatic than those exhibited by the large amplitudes cases in this work, but these shapes also depend on viewing geometries. Hence further observations are required to further understand these suspicious targets from our observations.

3.5 Conclusions

We presented lightcurve observations for 27 small Main Belt asteroids and one Mars-crossing asteroid. Amplitudes and periods were determined for seven objects, while constraints were placed on these properties for the rest for the objects.

The lightcurve period and amplitude distributions were added to those previously reported with similar sizes increasing the sample from 60 to 87, and then compared to the distribution of large MBAs and NEAs. In multiple size increments from 20 km down to this sample of 5 km MBAs, no significant divergence in properties is seen. However, this work does help to solidify the excess of fast rotating NEAs observed in comparison to similar size MBAs. Continued work on this will help to define the role that thermal effects and tidal disruption play in altering asteroid spin states. Recent discoveries of binaries among SMBAs via lightcurve observations also motivate further observations of

this population.

Chapter 4

Steady-State Model of the Binary Near-Earth Asteroid Population

Overview

In this chapter we present a Monte Carlo simulation of a steady-state binary near-Earth asteroid (NEA) population. This study combines previous work on tidal disruption of gravitational aggregates (Chapter 2) with a statistical treatment of NEA planetary encounters and includes evolutionary effects such as tidal evolution and binary disruption from close planetary encounters. Though tidal disruption is capable of creating binaries with properties similar to those observed in the NEA population, it must make them frequently given that the best observed estimate of a binary NEA fraction is 15%,

We also present the expected distribution of binary orbital and physical properties for the steady-state binary NEAs formed by tidal-disruption. We discuss the effects on binary fraction and properties due to changes in the least constrained parameters, and other possible effects on our model that could account for differences between the presented results and the observed binary population. Finally, we model possible effects of a significant

population of binaries migrating to the near-Earth population from the Main Belt.

In Section 4.1 we describe the details of the Monte Carlo steady-state model. We present the results of the simulations in detail in Section 4.2 and discuss the implications of these results in Section 4.3.

4.0.1 Previous work

Substantial modeling work has been done on the tidal disruption of rubble pile asteroids in regards to the formation of binary NEAs. Richardson et al. (1998) investigated tidal disruption outcomes in terms of the body's close approach distance and speed, shape and spin, spin-axis and body-axis orientation. This work suggested that tidal disruption could account for 1–2 observed crater chains on the Moon, as well as the population of binary NEAs. Using similar but improved methods Chapter 2 presented an exhaustive set of simulations of tidal disruption to characterize the properties of binaries formed during a disruption.

Chapter 2 found that binary asteroids formed during a tidal disruption event share many characteristics with the observed population of binary NEAs, namely

1. The semi-major axis distribution of the binaries is strongly peaked below 10 $R_{\rm pri}$, though the simulations also show a long tail out beyond the 1 AU Hill sphere at 130 $R_{\rm pri}$. Large separations are neither expected nor observed in the NEA population because close planetary encounters will easily separate very wide binaries and all but one of the observed binary NEAs have semi-major axes smaller than 10 $R_{\rm pri}$, with all but 4 smaller than 5 $R_{\rm pri}$.

2. The size ratios in the simulations are peaked between $R_{\rm sec}/R_{\rm pri}$ = 0.1 – 0.2, with a significant tail towards higher values, i.e. equal size components. The observed population, though biased against size ratios below $R_{\rm sec}/R_{\rm pri} \sim 0.2$, almost all have

values between 0.2–0.6. There is only one observed binary with equal-sized components, also a rarity in simulations.

3. The rotation rate of the primary body is narrowly bracketed between 4–6 h in the simulations. Nearly all binary NEAs have rapidly rotating primaries though they typically have somewhat faster rotation rates between 2.2–3.5 h.

Some questions either unanswered or subsequently raised in Chapter 2, are;

1. What is the overall steady-state binary fraction for NEAs caused by tidal disruption?

2. Why do simulations not match the rapid rotation rates of the primary bodies?

3. Will the binaries created by tidal disruption, which generally start with high eccentricity, survive long enough to have their eccentricity tidally damped to the observed low values (almost all observed below 0.1 for the few well-measured systems)?

4. Do binary NEAs with large semi-major axes exist unobserved as Chapter 2 suggests, or are they disrupted during subsequent close approaches with Earth?

The main focus of the current work is to apply the results of Chapter 2 to determine how many present-day NEA binaries may be tidal disruption outcomes, and what the population of this subset of binaries will look like in steady-state. We use these results in a Monte Carlo routine to simulate the transport of bodies from the Main Belt to the near-Earth population, their encounters with Earth, and the formation and subsequent evolution of binaries. We also determine the effect of pre-existing binary MBAs migrating into the near-Earth population.

4.1 Steady-State Model

The steady-state model consists of a set number of asteroids (usually 2000), simulated over 1 Gyr to estimate the number and properties of the steady-state binary NEA population. During each timestep (typically 0.01 Myr), each asteroid may be removed and replaced, have a close encounter with a planet, evolve (if it is already a binary), or not change. The model uses recent estimates from the literature for NEA lifetimes, planetary encounter probabilities, binary asteroid formation via tidal disruption, Main Belt binary formation via catastrophic collision, and tidal evolution (details are given below). This model does not consider NEA orbits directly; rather it is a statistical approach that does not account for resonant encounters or the different dynamics of the NEA orbital classes.

4.1.1 Initial shape and spins

One of the main results of previous tidal disruption work is the strong dependence on the shape and spin of a progenitor on the outcome of a disruption (Richardson et al. 1998; Walsh & Richardson 2006). Elongated and/or faster-rotating asteroids are more likely to disrupt and form binaries. However, due to NEAs' frequent interactions with terrestrial planets, the observed distribution of shape and spin properties for NEAs is likely different from its source population. Scheeres (2002) quantified the changes to the rotational states of asteroids for a steady-state population of NEAs (assuming rigid bodies, and a distribution of spin rates for the source bodies from collisional experiments) and found that an overall spin–up of the population might be expected, with a minimum spin period for any given body close to the observed maximum $\sim$ 2 h (near the estimated critical spin rate).

Main Belt asteroids of a similar size as NEAs, for the sake of this model, qualify as NEA progenitors. However, obtaining lightcurves to estimate shape and spin of 1–3 km

asteroids in the Main Belt is sufficiently challenging that these properties remain a point of some uncertainty. The archived data of asteroid lightcurves (Harris et al. 2005b) and recent results (Chapter 3) provide data for 86 MBAs with $D < 5$ km. This data provided relative frequencies for each of the parameters contained in the tidal disruption database (shape and spin, see Fig. 4.1).

Different distributions of shape and spin were tested in the simulation, with the outcomes varying accordingly. The distributions used were: (a) one derived from the SMBA lightcurve data described above; (b) and one based on only NEA spin and shape data.

4.1.2 NEA lifetimes and planetary encounters

Recent numerical results place the median NEA lifetime around 10 Myr. The simulations by Gladman et al. (2000) show a rapid decay in surviving particles with a tail of long-lived particles surviving for the length of the 60 Myr integration. The lifetimes of asteroids in each of the present work's simulations are assigned when they are created, with a distribution designed to match Gladman et al. (2000) exactly up to 60 Myr. Beyond 60 Myr the number of asteroids surviving is made to tail off to zero at 100 Myr, which is the longest lifetime used (see Fig. 4.2). When an asteroid or binary exceeds its lifetime it is removed from the simulation and replaced by an asteroid/binary with properties designated for the SMBA population (small MBA, see Section 4.1.1).

The encounter probabilities used were a combination of those for Earth and Venus. The probabilities for an NEA encounter with the two planets differ, as do the encounter parameter probability distributions. However, the gravitational properties of Venus are quite similar to those of Earth, with a density of 5.2 g cm^{-3} and comparable radius $\sim$ 6000 km. For these reasons the tidal effects of close encounters are quite similar in terms of close approach distance in units of planetary radii. Due to these similarities the same tidal disruption database is used, and planetary encounters are not distinguished as being

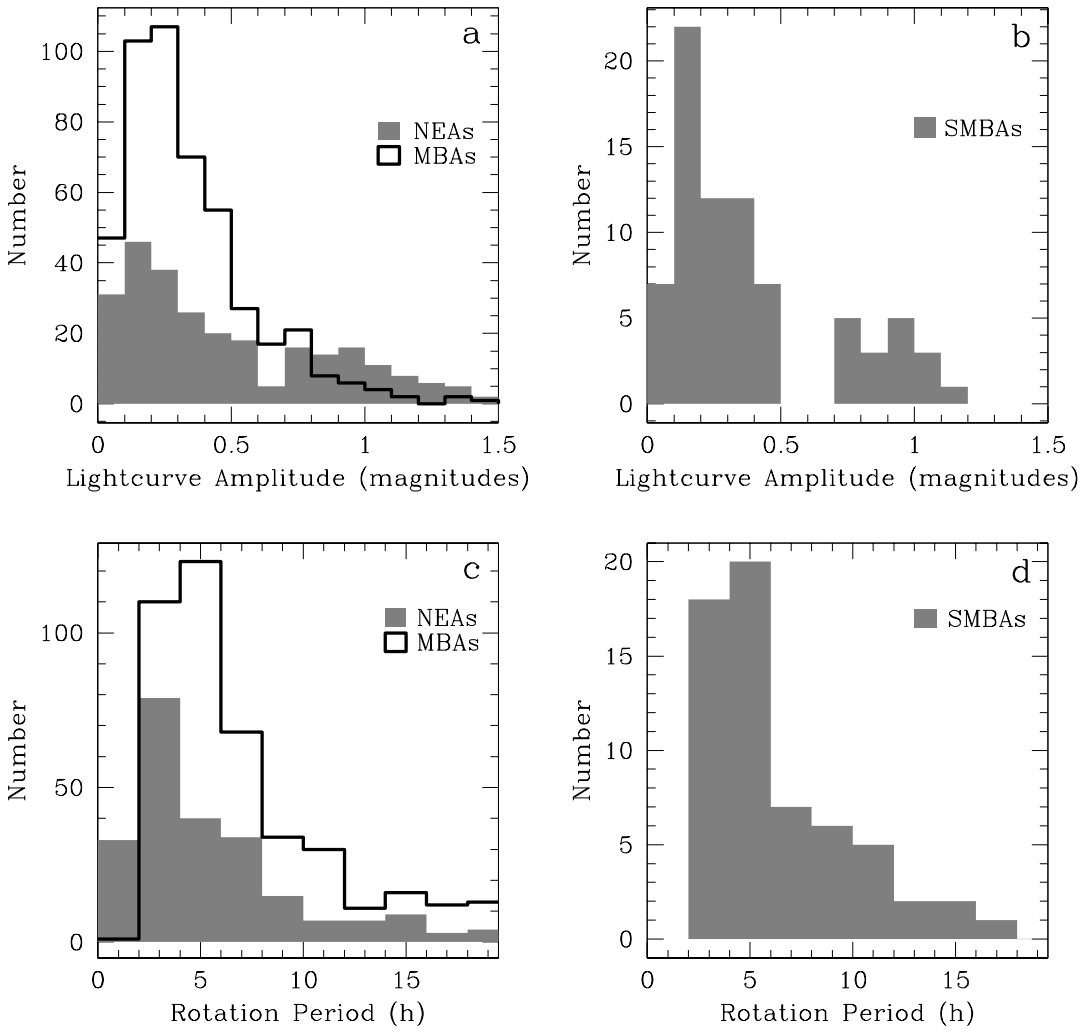

Figure 4.1: Comparison of amplitude and rotation period data from asteroid lightcurves: (a) distribution of lightcurve amplitude for all NEAs and MBAs with a diameter less than 20 km; (b) lightcurve amplitude for small MBAs (diameter less than 5 km); (c) rotation period of NEAs and MBAs and (d) rotation period of small MBAs. The distributions for small MBAs have significantly fewer known lightcurves, hence they are plotted separately. Data compiled from Harris et al. (2005b).

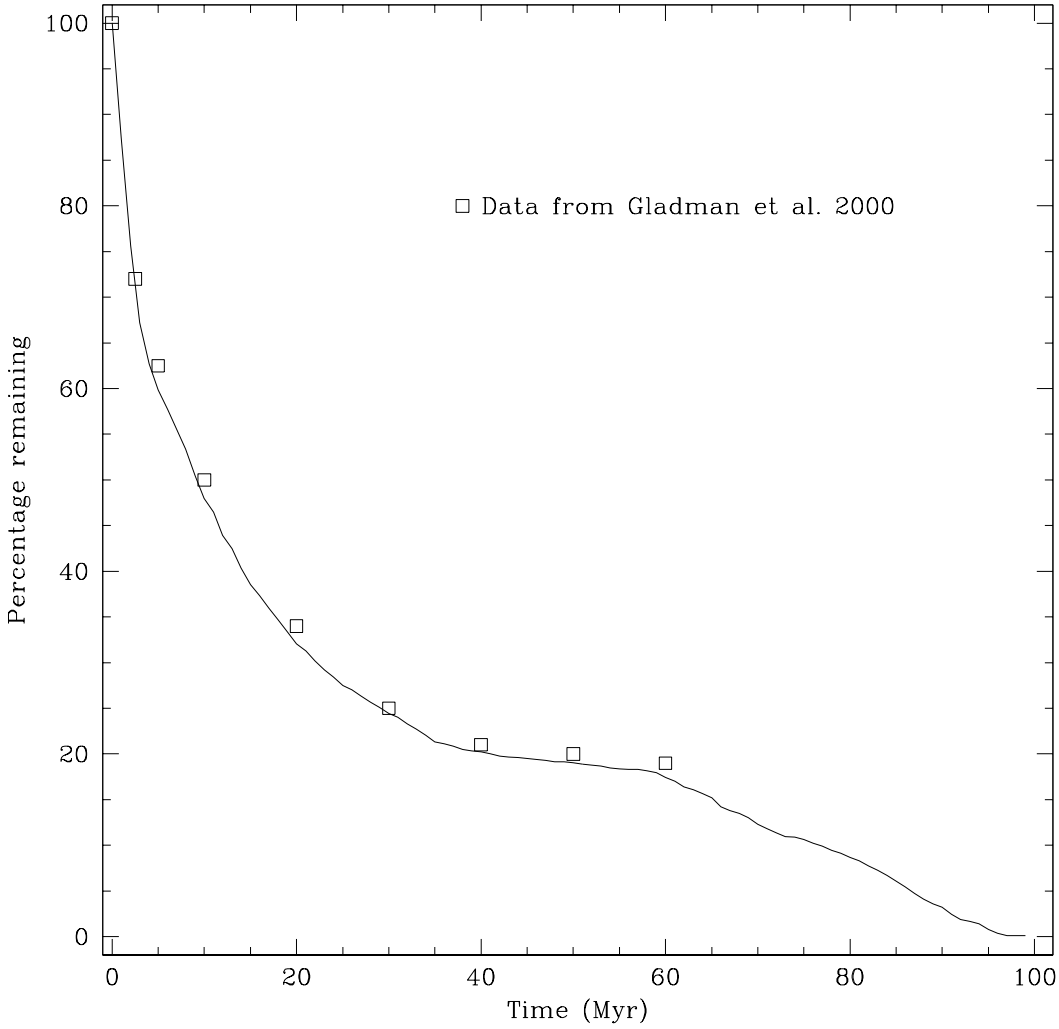

Figure 4.2: Percent of surviving NEAs used to assign lifetimes in the steady-state model. The squares are data from Figure 2 of Gladman et al. (2000).

with Earth or Venus, as differences would be small in this work. We generally refer to encounter distances in terms of Earth radii ($R_{\oplus}$), as the tidal disruption simulations were done in a geocentric system.

At each timestep the probability for each asteroid to encounter a planet was calculated. Encounters within 3 planetary radii were the maximum distance for a binary forming by tidal disruption, so the probability of an encounter for each asteroid was

$$P_{\rm enc} = (< P_{\oplus} > + < P_{\female} >)\, \pi\, q^2\, \Delta t \tag{4.1}$$

where

$$< P_{\oplus} > = 1.12 \times 10^{-16}\ {\rm km}^{-2}\ {\rm yr}^{-1} \tag{4.2}$$

and

$$< P_{\female} > = 2.02 \times 10^{-16}\ {\rm km}^{-2}\ {\rm yr}^{-1} \tag{4.3}$$

with q being the close approach distance and Δt the timestep (Bottke et al. 1994). These encounter probabilities predict a 3 $R_{\oplus}$ encounter with Earth or Venus every $\sim$ 3 Myr. Binary asteroids in the simulation were tested for encounters out to 24 $R_{\oplus}$ at each timestep by the same method.

Fundamentally the model presented here is a statistical model of asteroid lifetimes and planetary encounters in the NEA population. A more accurate approach could include actual integrated orbits of a population of asteroids, tracking the close approaches for each. This method would include resonant encounters, and bodies in longer-lived orbits. However, we do not expect this method to diverge significantly from the model presented here due to the dominance of tidal disruption of a binary as compared with tidal disruption of a single body. Encounters out to 3 $R_{\oplus}$ can disrupt a single body, whereas encounters out to 24 $R_{\oplus}$ can disrupt a binary. With the more distant encounters statistically occuring 64 times more frequently, this effect is expected to dominate the simulations, possibly limiting the steady-state binary NEA population to below 2% of the overall NEA population.

4.1.3 Binary evolution

Basic stability limitations

Two strict limitations were placed on the binaries: their mutual pericenter distance had to be outside the radius of the primary body, and the semi-major axis had to be smaller than the mutual Hill sphere. When a binary was formed that violated these requirements, or evolved to a disallowed state, it was immediately removed and replaced by a new asteroid/SMBA binary.

Tidal evolution

Tidal forces between the primary and secondary will affect the binary in most cases by: changing the semi-major axis of the secondary's orbit, synchronizing the secondary's rotation with its orbital period, and changing the eccentricity of the secondary. Weidenschilling et al. (1989) published formalisms for the change of the semi-major axis of a tidally evolving binary asteroid, and this formalism was used in Chapter 2 (Eq. 3) to estimate evolutionary timescales for the simulated binaries. In this work the formula is applied during each timestep to evolve each binary's semi-major axis.

All but one of the observed binary NEAs with known eccentricities have $e < 0.1$. The damping timescale of eccentricity due to tidal interactions used in Chapter 2 was adapted to recalculate the binary's eccentricity during each timestep in the steady-state model,

$$de = -e \times \frac{1}{\tau_e} \times \Delta t \tag{4.4}$$

where de is the change in eccentricity based on the eccentricity damping timescale τ_e over the timestep Δt (Murray & Dermott 1999). This formalism is for a secondary with a spin period equal to its orbital period and considers only the effects of the tides raised by the primary on the secondary. Tides raised on the primary by the secondary, which

play a greater role for larger mass ratios, can have the effect of raising the secondary's eccentricity (Goldreich 1963; Margot & Brown 2003).

An evolutionary factor not included in this simulation is the binary YORP (BYORP) effect (Cuk & Burns 2004). Similarly to how the YORP effect can change asteroid spin rates and obliquities, BYORP can potentially alter binary eccentricity and semi-major axis on timescales significantly faster than tidal evolution. BYORP, similar to the YORP effect's dependency on obliquity, depends on the binary's inclination. Because binary inclination is not tracked in our model this effect is not included. However, any effect which increases binaries' semi-major axes, as we expect BYORP to do rapidly in many cases, will only decrease the binary fraction in steady-state as their susceptibility to disruption via a planetary encounter increases quickly with increased a.

Binary encounter with a planet

In order to consider the possibly disruptive effects that a planetary encounter could have on a binary asteroid, direct 3-body encounters were simulated and incorporated into the steady-state model. These simulations were done separately and compiled into a look-up table and then used in the steady-state model via interpolation. In a separate test explained below, 3-body encounters were simulated directly within the model.

For integer values of close approach in Earth radii from 1 to 24 $R_{\oplus}$, and the same speeds used in the tidal disruption simulations of Chapter 2 (v_{∞} = 8, 12, 16, 20, 24 km s^{-1}), a series of simulations were run over a range of binary mass ratio (M_{sec}/M_{pri} = 1.0, 0.5, 0.1, and 0.01) and semi-major axis (a = 2, 4, 6, 8, 10, 15, and 25 R_{pri}). The simulations were performed with an N-body code, `HNBODY`, using a Runge-Kutta algorithm modified for close encounters (Rauch & Hamilton in preparation; Gültekin et al. 2004; see also Gültekin 2006). For each set of parameters 1000 simulations were run with orbit orientation randomized assuming zero eccentricity (zero eccentricity is a safe assumption

Table 4.1. Lifetimes for binary NEAs.

Semi-Major Axis (R_{pri})	Critical q for 50% ejection	Lifetime (Myr)
2	1.6	10.
4	3.0	2.
6	4.0	1.6
8	5.0	1.0
10	6.0	0.7
15	8.0	0.4
25	12.5	0.17

Note. — Predicted lifetimes for NEA binaries for systems with encounters of v_∞ = 16 km/s and a mass ratio of 0.1. The limiting close approach distance, q, was selected for the distance at which 50% of the randomly oriented binaries were disrupted as a result of the close approach. The lifetime is then how often an encounter at that critical distance is expected to occur.

due to the relative quickness of tidal eccentricity damping). Thus each set of parameters assumed a probability for binary disruption, which was then used in the Monte Carlo simulation to determine the fate of binary encounters. This code was tested against the results in Bottke & Melosh (1996a,b), for the case of v_∞ = 12 km s^{-1}, a = 6 km and mass ratio of 0.125, yielding very close matches (see Fig. 4.3). The results also match well with the analytical calculation of Agnor & Hamilton (2006), relating the Hill sphere of the binary and its semi-major axis,

$$r_{td} \approx \frac{a}{R_{\rm pri}} R_\oplus \tag{4.5}$$

where r_{td} is the tidal disruption distance for a binary encounter with Earth.

A statistical estimate for binary lifetimes against separation due to planetary encounters is calculated for binaries of various semi-major axes (assuming a relatively average binary encounter scenario with v_∞ = 16 km s^{-1} and a mass ratio of 0.1). A critical en-

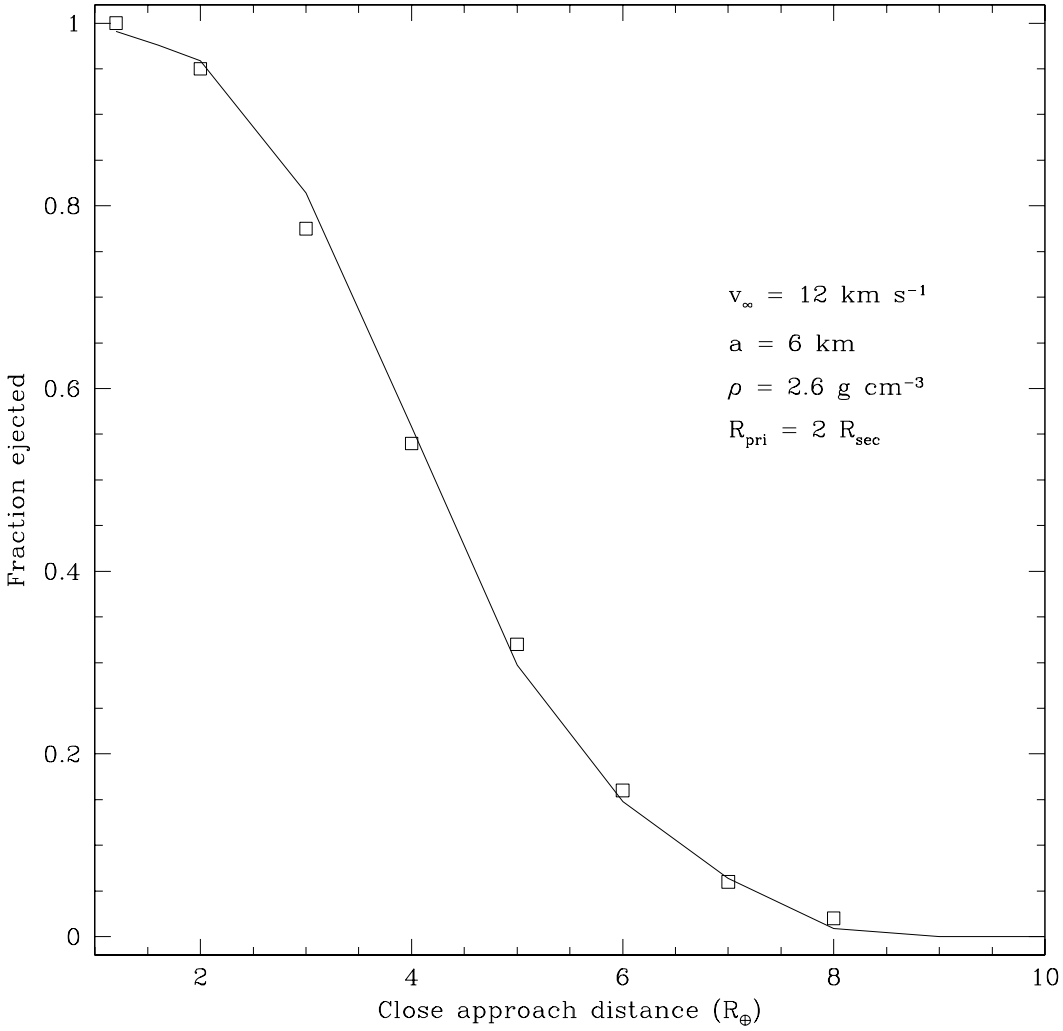

Figure 4.3: Comparison of this work, using HNBODY to calculate binary disruption probability (solid line), with results presented in (Bottke & Melosh 1996a, squares).

counter distance is determined for each binary semi-major axis as the distance at which 50% of randomly oriented binaries disrupt due to the tidal forces of the close encounter. The statistical encounter probabilities for each critical distance then determine lifetime between binary-disrupting encounters (Table 4.1). The lifetime for very close binaries of 4 or 6 $R_{\rm pri}$ is only 2 or 1.6 Myr, suggesting that many of the observed NEA binaries are potentially quite young. The NEA binary Hermes has a semi-major axis of 5 $R_{\rm pri}$,

which means it should have a critical encounter every 1.75 Myr, despite requiring similar timescales to tidally revolve to its doubly synchronous state. This result for Hermes highlights the nature of this calculation, that it is a statistical average, and does not consider resonant encounters, or dynamically stable orbits within the NEA population.

A second implementation of the code included inline 3-body integrations to model a binary encounter with a planet within the simulation itself. In this implementation the exact semi-major axis and mass ratio of the binary is used to setup and run a 3-body integration in `pkdgrav` of that binary with Earth with randomly selected encounter parameters of close approach distance and speed. Again, no eccentricity is given to this initial binary. After the encounter the new semi-major axis and eccentricity of the binary replace the pre-encounter values. If the binary was disrupted the resultant body is treated as a single asteroid again. This implementation offers a level of sophistication greater than the previously described runs via the lookup table by providing binary orbital changes induced by the encounter, rather than just indicating whether or not the binary was disrupted. However, the overall results in this work are not very sensitive to which method of 3-body encounters was used, and generally we would only expect inclusion of this to decrease the binary fraction due to the increases in eccentricity that are tracked.

4.1.4 Migrating binary MBAs

A large unknown in the study of binary NEAs is the extent of any migration of binary asteroids from the Main Belt population. If binary asteroids can migrate successfully from MBA orbits into NEA orbits then the numbers and properties of these binaries may be extremely important in shaping the binary NEA population.

In this work binary MBAs were included in the steady-state simulation as a variable percentage of the incoming asteroids. The binary properties were drawn from a previous study of a family-forming collisions modeled with SPH code and `pkdgrav` (Durda

et al. 2004). The binaries with primaries having $D < 5$ km were used, however a large portion of these were EEBs[1] with a mass ratio of unity, where the bound particles were at the resolution limit of the simulation. Durda et al. (2004) presented results with these unit-mass-ratio systems removed, considering them more a function of the numerical resolution rather than actual dynamics. The distribution used in this work also excludes unit-mass-ratio systems, when both components are at the resolution limit.

Another difficulty with the MBA binary population is the potential for a very large range in binary ages, and hence a wide range of tidal evolution end states. Therefore just using the raw binaries from a collision simulation may represent newly formed binary MBAs that will not account for any post-collision evolutionary effects. Thus a second population of binary MBAs is also considered, those with the basic selection effects applied (pericenter distance $q > 2.0\ a/R_{\rm pri}$ and semi-major axis $a < R_{\rm Hill}$, where $R_{\rm Hill}$ is the Hill sphere), and 100 Myr of tidal evolution while the binaries are migrating into the NEA population (see Fig. 4.4, and Section 4.1.3 for full description of the tidal evolution formalisms used).

Observations are just starting to constrain the binary fraction among the SMBA population, with current work estimating a fraction close to the NEA fraction of $\sim 15\%$, and properties similar to the binary NEAs (Harris & Pravec 2006). The survivability during transport from a Main Belt orbit to an Earth-crossing orbit is unknown as these binaries possibly have to survive multiple perturbations.

[1]Escaping Ejecta Binaries are binaries formed during a catastrophic collision. As some material is ejected from the system entirely, two or more escaping pieces may remain bound to each other. The EEBs differ from the binaries formed around the target body as they can be loosely bound small fragments of the collision, with small sizes that are similarly sized.

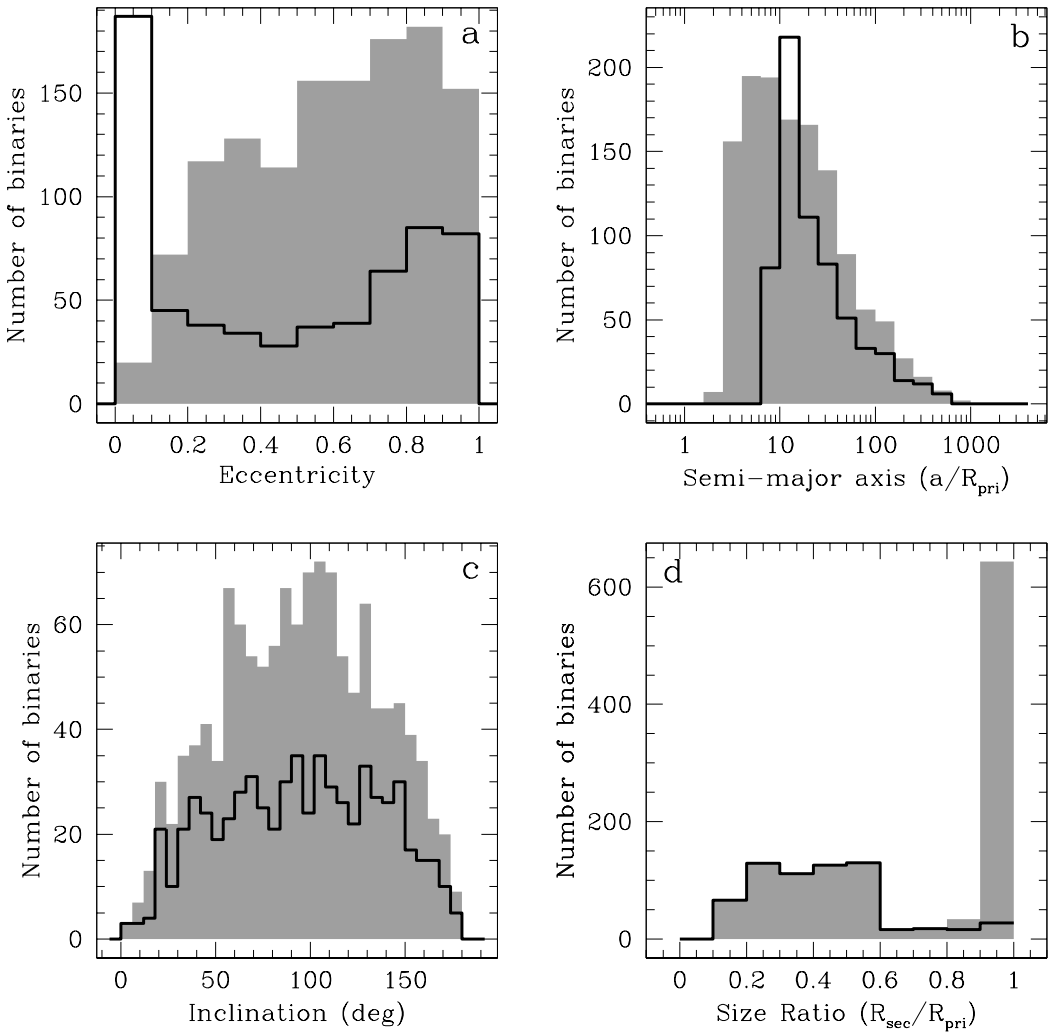

Figure 4.4: The total number of binary MBAs for the (shaded) original distribution and (outline) the distribution with 100 Myr of tidal evolution and single particle pairs removed. The original distribution is from Durda et al. (2004) simulations of a 34 km diameter impactor striking a 100 km diameter target at 3 km s^{-1} at an impact angle of 30°. Shown are the: (a) eccentricity of the binaries; (b) semi-major axis of the binaries in units of the primary radii; (c) inclination; and (d) size ratio.

4.2 Steady-State Results and Discussion

We first present the nominal case, which includes the best estimate for each of the many variable parameters included in the steady-state model. In subsequent sections we examine the individual effects of each of the main model parameters, and their overall effect on the results. Our nominal case has the following properties:

1. Progenitors follow the shape and spin distributions discussed above (section 4.1), matching estimates for SMBAs,
2. Tidal evolution actively changes binary properties, with parameters from Chapter 2,
3. 10% of Main Belt asteroids entering the simulation are binaries, with properties from Durda et al. (2004) (excluding unit-mass-ratio systems) with 100 Myr of tidal evolution,
4. Binary encounters with Earth are handled via a look-up table of 3-body encounters.

4.2.1 Nominal case

The nominal case is a 1 Gyr simulation using 2000 asteroids. Figure 4.5 shows the evolution of binary number over time for the simulation, showing the quick decline in the number of remaining MBA binaries. This rapid decline is due to the comparatively large semi-major axes of the binary MBAs and their very short lifetimes against disruption. The steady-state number of MBA binaries in the population hovers close to 0.2%. The fraction of binaries formed via tidal disruption is 1.2% and has comparable small fluctuations in numbers throughout the simulation.

The properties of the binaries show strong effects of tidal evolution. There is a very strong peak in eccentricity between 0.0–0.1, which shows significant tidal damping of

the original eccentricity distribution and matches the observed population well (Fig. 4.6). The distribution of semi-major axes is mildly dependent on the formation mechanism, tidal disruption, or collisional remnant in the Main Belt. The tidal disruption remnants have semi-major axes almost entirely below 10 $R_{\rm pri}$, where the binaries from the Main Belt have a number of bodies with larger semi-major axis.

The low steady-state percentage of both NEA and MBA binaries is due to short lifetimes against disruption during planetary encounters. The average lifetime before a NEA binary is disrupted is $\sim$ 1.2 Myr, while for an MBA formed binary that time is $\sim$ 0.3 Myr (Fig. 4.7). While increasing the percentage of MBA binaries will increase the number migrating into the population (see Sec. 4.2.2), the properties of the binaries will determine their lifetime, and the sustainable binary fraction. Hence, for the distribution of binary properties used in this nominal case for both the tidal disruption and MBA migrated binaries, the steady-state fraction is dominated by short binary lifetimes against disruption.

4.2.2 Influence of MBA binary percentage

Tests were run varying the binary percentage of MBA progenitors between 10 (the nominal case), 20, 50, and 80%. The contribution to the NEA binary population from migrated MBA binaries is quite low for the binary properties used, below 1.2% for all four tests values run (Fig. 4.8).

The binaries that migrate in from the MBA population are disrupted via a close encounter with Earth quite quickly. The average lifetime for a migrated binary is $\sim$ 0.3 Myr. The properties of the binary MBAs will drastically affect their lifetime, and also their overall contribution to the steady-state population (see Fig. 4.7). The properties for the binary MBAs in this work from Durda et al. (2004) represent the results of the most recent asteroid collision simulations. A different formation mechanism for producing smaller-separation binary MBAs could theoretically provide a different set of binary

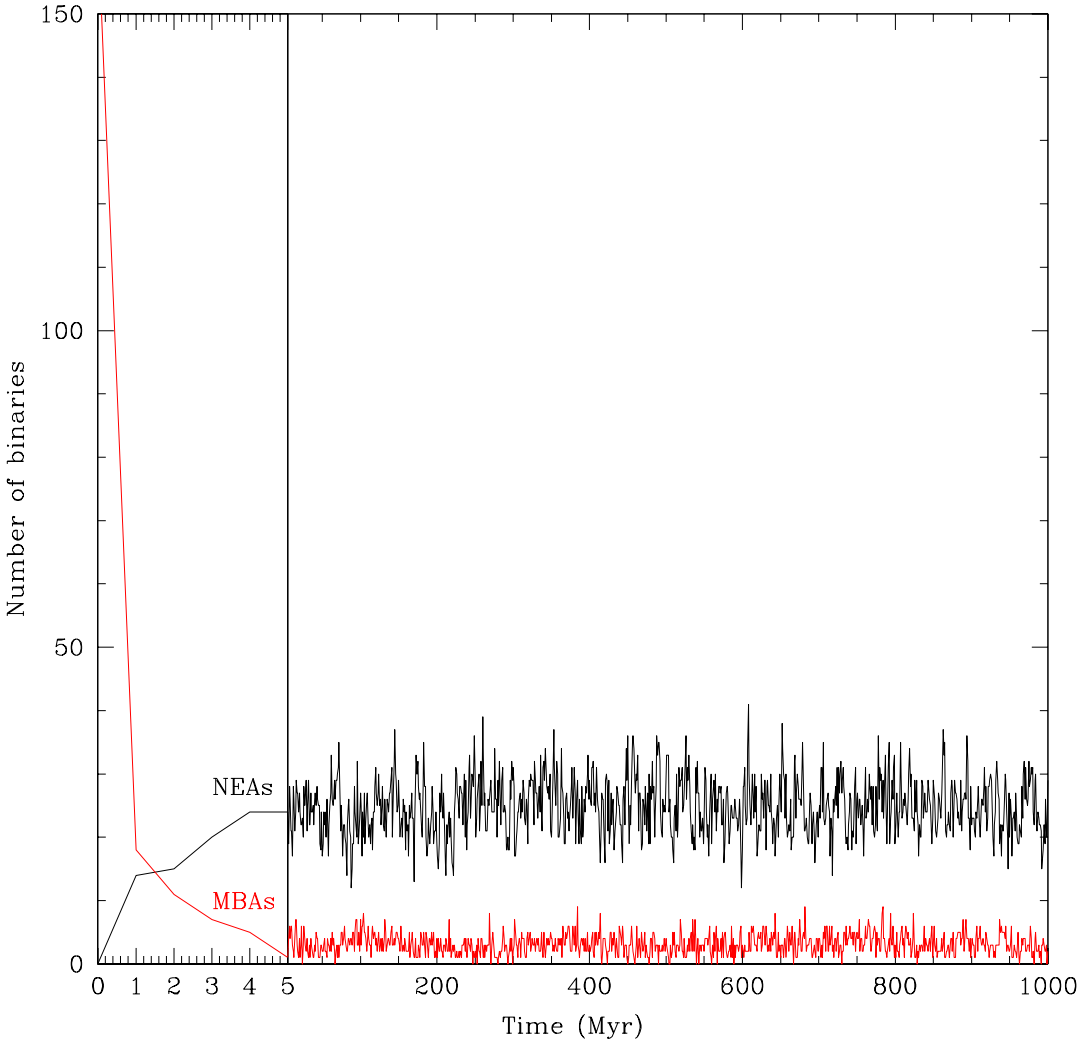

Figure 4.5: The number of binaries as a function of time out of a total of 2000 asteroids in the nominal steady-state simulation, showing those formed by tidal disruption (black), and those injected into the simulation from the MBAs (red).

properties to test. As well, detailed observations of binary MBAs could also provide new data to include in the simulations.

The test simulation producing the highest overall steady-state binary fraction is when the properties of MBA binaries take the properties of the observed NEA binaries. In this test simulation, with the the MBA binary fraction increased to 80%, the steady-state binary population increases to 5%. Due to the decreased separations of the migrating

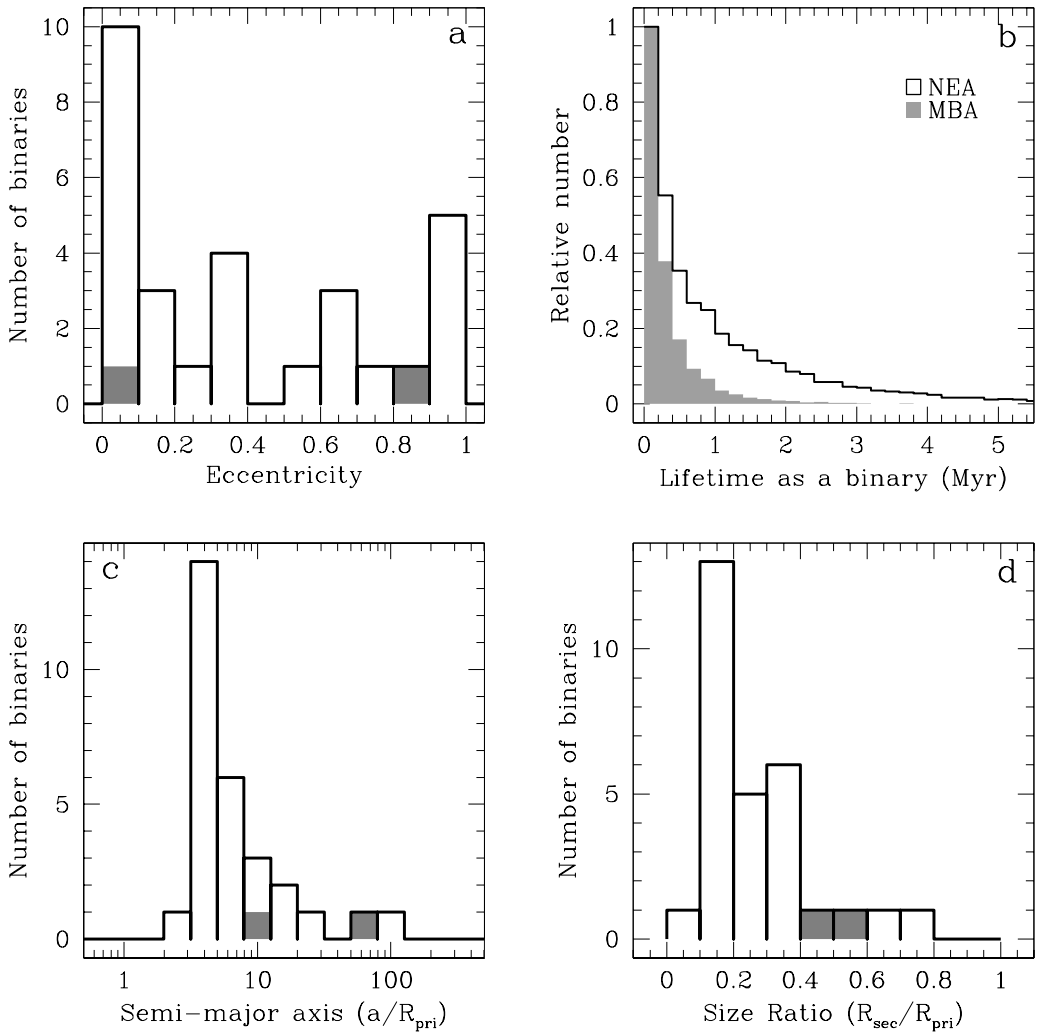

Figure 4.6: Properties of the binary population at the end of the 1 Gyr nominal steady-state simulation: (a) eccentricity; (b) cumulated lifetimes of tidal disruption formed and migrated MBA binaries; (c) semi-major axis in terms of $R_{\rm pri}$; and (d) size ratio. The histograms (a), (c), and (d) show just the instantaneous state of the (outline) tidal disruption formed binaries and those (shaded) that migrated from the MBA population, hence the near absence of migrated binary MBAs.

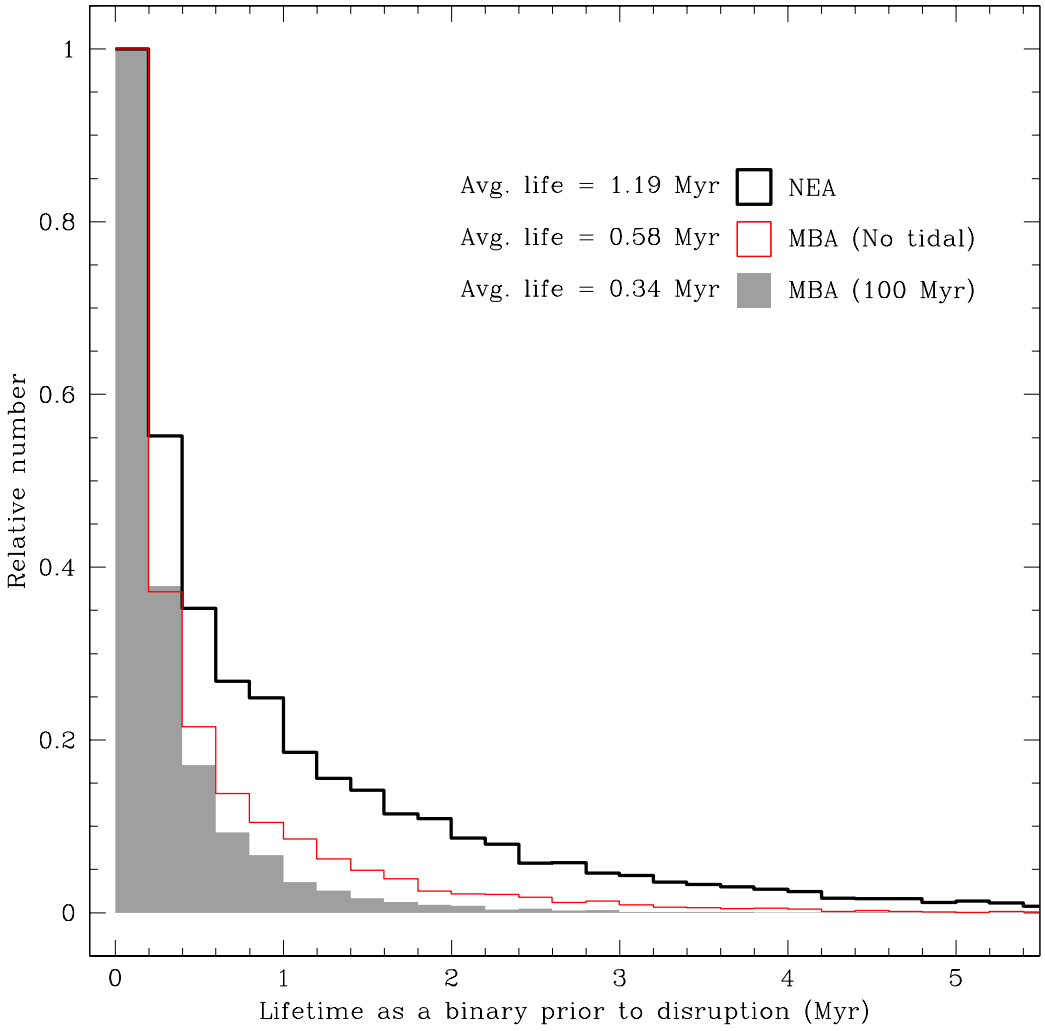

Figure 4.7: Time between binary introduction/formation, and its disruption due to a close encounter. The MBAs (shaded) are swapped out after a shorter time than the tidally formed NEA binaries (outline). The binary MBAs which weren't tidally evolved for 100 Myr years before incorporation into the simulation (red), survived longer than the evolved ones as their semi-major axes were generally smaller making them less susceptible to disruption during a planetary encounter.

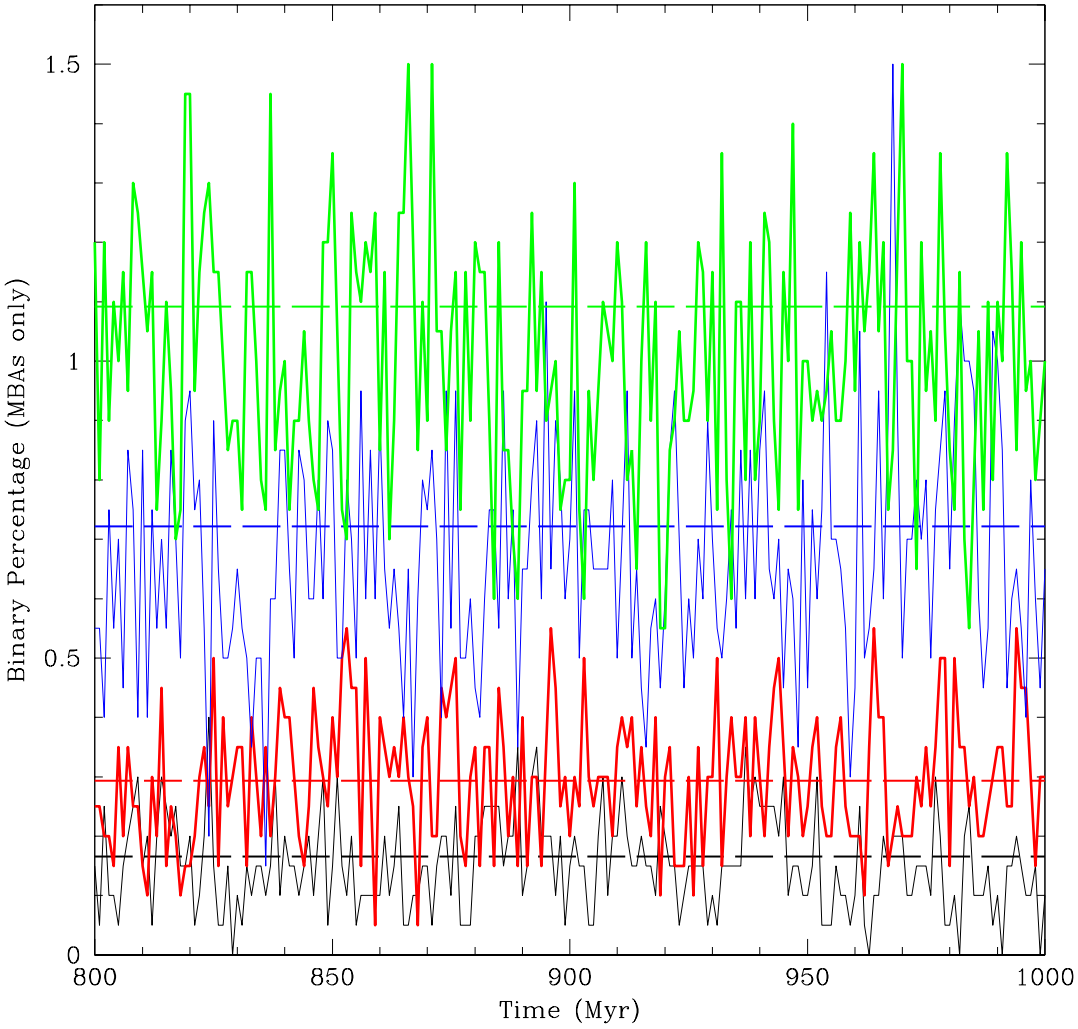

Figure 4.8: Binary percentage for migrated MBAs in the simulation for the last 200 Myr, up to the conclusion at 1 Gyr, with the thick dotted line representing the average value for the entire simulation. Varying binary percentages were used for the source population, from top to bottom on the plot: 80% (Green); 50% (Blue); 20% (Red) and 10% (Black).

binaries (3–5 $R_{\rm pri}$), their lifetimes increase dramatically, allowing for the increased steady-state fraction.

4.2.3 Influence of MBA shape/spin properties

The two different shape/spin distributions used produced similar results. Using the distributions derived for SMBA shape and spin from lightcurve data, as in the Nominal case (see section 4.2.1), the steady-state binary fraction for tidal disruption formed binaries was 1.2% (Table 4.2). This fraction increased slightly when the shape/spin distribution for NEAs was used, increasing to 1.4%. The faster spinning NEAs generally are more effective at producing binaries via tidal disruption, but within this steady-state model where disruption by planetary encounters dominated, the overall affect is minimal.

4.2.4 Influence of tidal evolution

Tidal evolution during the simulation strongly change the eccentricity and semi-major axes of the binaries (Fig. 4.9). The lifetimes against disruption due to close encounters are greater for closer binaries, and for these binaries the eccentricity damping time-scales are relatively short. The effects of eccentricity damping is quite noticeable with a strong peak of nearly half the binaries at 0–0.1 eccentricity with small numbers spread out at higher values. This is vastly different than a simulation with no tidal effects where the bulk of the eccentricity values are greater than 0.1.

Similarly the semi-major axis distribution is noticeably increased for the simulation with tidal effects compared to the one without (Fig. 4.9). The peaks of the distribution are pushed from 3–5 $R_{\rm pri}$ towards 5–8 $R_{\rm pri}$. This does move some bodies out beyond 10 $R_{\rm pri}$, though time scales to move any beyond that are very long, and the lifetime of the binary against disruption will decrease rapidly with increasing a.

The overall binary fraction increases slightly from 1.2% to 1.7% (Table 4.2), though the size ratio between the two components is essentially unchanged (Fig. 4.9). Though the tidal effects noticeably affect a and e they are not strong enough to increase a so rapidly

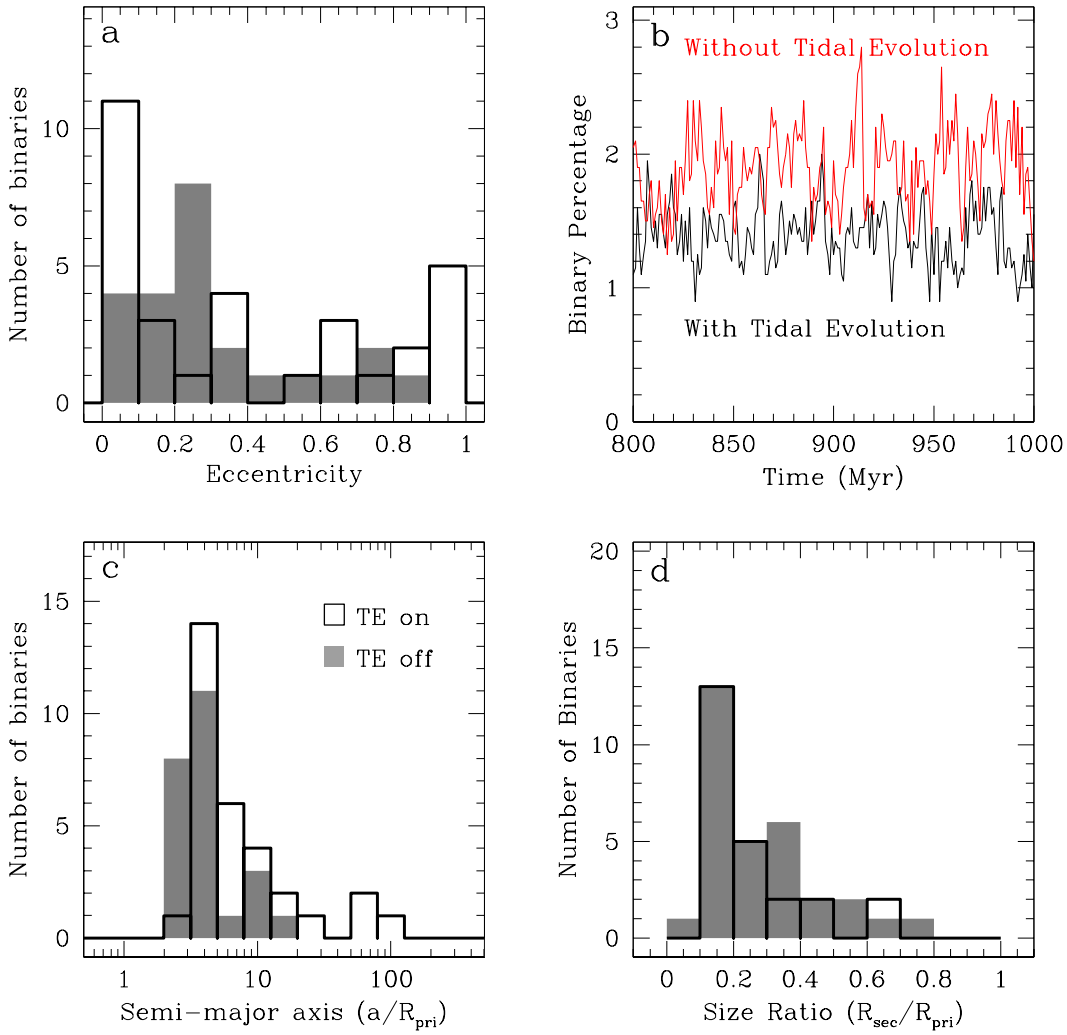

Figure 4.9: Effects of tidal evolution on the binaries during the nominal steady-state simulation comparing their properties with tidal evolution (outline, TE on) and with no tidal evolution (shaded histogram, TE off): (a) eccentricity; (b) number of binaries; (c) the semi-major axis; and (d) the size ratios.

that the lifetimes of binaries decrease dramatically, instead they only slightly lower the binary fraction. Therefore it is essentially a shift in the basic properties only.

Table 4.2. Binary fractions for all simulations.

Progenitor distribution	Tidal evolution	MBA binaries	Tidal disruption binaries	Migrated binaries	Total binaries
SMBA (10%)	ON	100 Myr	1.2%	0.2%	1.4%
NEA (10%)	ON	100 Myr	1.4%	0.3%	1.7%
SMBA (10%)	**OFF**	100 Myr	1.7%	0.1%	1.8%
SMBA (10%)	ON	0 Myr	1.2%	0.2%	1.4%
SMBA (20%)	ON	100 Myr	1.2%	0.3%	1.5%
SMBA (50%)	ON	100 Myr	1.2%	0.7%	1.8%
SMBA (80%)	ON	100 Myr	1.1%	1.0%	2.1%

Note. — Binary fraction of both NEA and MBA binaries are listed with respect to the primary model parameter setting. The column "Progenitor distribution" refers to the shape and spin distribution of the asteroids being injected into the system, with the percentage of binary progenitors in parentheses. Tidal Evolution refers to whether or not binary systems would actively be altered tidally throughout the simulation. One simulation was run where the binary MBA population did not have any tidal evolution (compared to the nominal case of 100 Myr); it is listed as 0 Myr under the "MBA binaries" column. The final three columns list the percentage of asteroids in the simulation that were formed from tidal disruption, migrated from the Main Belt, and the total combined percentage of binaries.

4.2.5 Estimates on the properties of binary NEAs formed by tidal disruption

The properties of the steady-state binaries are largely dominated by the preference of planetary encounters to eliminate widely separated systems. This effect is so strong that it may eliminate any significant fingerprint of the formation mechanism that exists in the population (possibly other than primary spin and shape). The eccentricities are damped substantially, with values between 0 and 0.1 dominating the distribution.

The binaries in the steady-state system otherwise retain the fast spinning primary. This potentially diagnostic property may be the only significant observable property not

quickly altered, or involved in binary lifetimes. However, with all observed NEA binaries having fast rotation rates it certainly appears that a rotational spin-up origin for most systems is likely. Similarly the observed primaries generally appear quite spherical, which could be a diagnostic feature in future work.

Differentiating between tidally disrupted binaries and those formed from another mechanism will be quite difficult. Any binaries observed are likely to have survived due to selected binary properties, namely a small semi-major axis. Primary spin and shape may also be diagnostic, but currently all the observed binaries look the same with fast-spinning and spherical primaries, both of which are seen in tidal disruption simulations (Walsh & Richardson 2006).

4.2.6 Estimates of migrated binaries' numbers and properties

The properties assumed for migrating MBA binaries is such that their lifetime against disruption from a planetary encounter is very short. Thus the steady-state number of binaries having migrated from the MBA population is very small, nearly zero at any given time. However, as mentioned above, this value is highly dependent on the MBA binary properties used in the model. If a formation mechanism is found to create MBA binaries with consistently small separations, their lifetime against disruption would increase dramatically, allowing for a significant presence in the steady-state population.

One factor working in the favor of migrating binaries could be the ability to avoid resonant encounters with planets. Binaries created by tidal disruption by definition have planet-crossing orbits, and therefore an increased chance for future encounters. It may be possible that binaries migrating from the Main Belt could survive longer than is calculated in this study by avoiding close planetary encounters, therefore increasing their contribution to the steady-state population.

4.2.7 Doublet craters

Currently any encounter of an asteroid or binary at less than 1 $R_{\oplus}$ is flagged with the asteroid or binary parameters, allowing investigation of doublet crater formation. While the ratio of doublet to singlet craters would be expected to roughly correspond to the ratio of binary to single asteroids in the NEA population, doublets may still be diagnostic of the binary population.

For a nominal simulation with 20% binary MBAs, approximately 10% of all craters were doublet. When the MBA percentage was increased up to 80%, the doublet percentage increased to 15%. For the second case, about 14% of the impacting binaries had a semi-major axis greater than ten times the combined radii of their components ($a > 10 \times R_{\rm pri} + R_{\rm sec}$) roughly approximates the necessary separation needed for an impacting binary to form two separate identifiable craters). Thus only about 2% of the craters would likely be detectable as doublets.

Tracking ratios of singlet to doublet craters will be significantly more relevant when the steady-state population of binaries is at the observed level around 15%. With a clear deficit of binaries in the NEA population in this steady-state simulation it is not surprising that we find such a low percentage of impacts as possibly observable doublets. Currently it is estimated that at least 10% (3 of 28) of craters on Earth are doublets (Bottke & Melosh 1996a).

4.3 Conclusion

This study focused on uncovering how tidal disruption affects the population of NEA binaries. It is clear from the discussions above that tidal disruption provides only a small fraction of the observed binary population. We have shown that these binaries appear similar to those observed, suggesting that some of these systems were in fact formed via

tidal disruption. However, the implications of such a small contribution of binaries formed from tidal disruption as well as the even smaller numbers of surviving MBA binaries, are quite dramatic. We can essentially account for very few of the NEA binaries observed, and require an unknown source or mechanism to create them.

The major constraints on any formation mechanism are a rapidly rotating primary body, as observed for nearly all NEA binaries, and a small semi-major axis to survive planetary encounters. Close planetary encounters are the dominant factor in the low steady-state fraction of binaries found in this work, and even introducing migrating binaries at an 80% rate was ineffective at increasing the total binary fraction. Thus any new means of introducing binaries into the NEA population must provide significant numbers with small separations.

Lightcurve observations/discoveries of binary MBAs will continue to establish the similarities and differences between the two populations of binary asteroids. This method of binary discovery allows for direct comparison between the NEA population and similar-sized MBAs. With the two populations having different dynamical, collisional and thermal environments the differences between the two should provide strong constraints on any new binary formation mechanisms proposed. Continued observations will also provide a different set of SMBA binaries that can be used for modeling of binary migration from the Main Belt.

Thermal spin-up (the YORP effect) as a binary formation mechanism could solve many outstanding issues by creating binaries and spinning up primaries in both the NEA and MBA population without the need for close planetary encounters. The YORP effect has been been shown to be a potentially important mechanism to modify spin rates and obliquities of asteroids, but no systematic study of YORP as a mechanism for fission and binary creation has yet been carried out (Bottke et al. 2006). Spin-up timescales by YORP depend on the shape and size of an asteroid as well as its distance from the Sun

and its axis orientation and therefore should operate at different timescales on the NEA and MBA populations. The scenario for successfully losing mass while retaining some in a stable orbit is unknown, but small separations and fast spinning primaries are likely resulting properties, making this the most likely mechanism to supply the large percentage of observed binaries.

Chapter 5

Conclusions

A general conclusion to this entire work is that tidal disruption is not a sufficient formation mechanism to create the observed binary NEAs. More specifically, in Section 1.6 three questions were posed to be answered in this dissertation, and each in turn was answered in the following chapters.

What are the properties of tidal-disruption-formed binaries and how do they compare to the observed NEA and MBA binaries? The semi-major axis distribution is strongly peaked below 10 $R_{\rm pri}$, with about half of the binaries with larger separations. The simulations do produce systems similar to the observed binaries, as all observed NEA binaries have semi-major axes less than 10 $R_{\rm pri}$, with the majority below 5 $R_{\rm pri}$. The size ratios are peaked between $R_{\rm sec}/R_{\rm pri}$ = 0.1–0.2. Similar to the observed population, few systems are made with equal sized components. The simulations produced a tight bracket of primary rotation rates between 4–6 h. The observed NEA binaries are similarly bracketed, but at a more rapid rotation rate between 2.2–3.5 h.

What is the spin and shape distribution for small MBAs? Small MBAs appear to have a distribution of shape and spin most similar to that of MBAs with $D < 20$ km. NEAs generally have an excess of rapid rotators not observed among the small MBAs.

What is the overall steady-state binary fraction for NEAs caused by tidal disruption? 1–2%. The steady-state simulations demonstrated that the average lifetime of a tidal disruption-formed binary was too short (1.2 Myr) to have a higher binary fraction. Tidal evolution had a significant impact on the simulations, damping eccentricities rapidly, making most of the population of binaries have values below 0.1. Planetary encounters removed wide binaries quite rapidly, resulting in a distribution that closely resembles that of the observed population, with separations near 5 $R_{\rm pri}$ and below. Overall, tidal disruption can only account for a 1–2% binary fraction among NEAs.

5.1 Future Work

The questions raised by this work, to be answered by future work include,

1. What are the properties of binaries formed by the YORP thermal spin-up mechanism?

2. Can the addition of YORP as a formation mechanism explain all of the observed NEA binaries?

3. How closely do sub-kilometer MBAs resemble NEAs, in both spin and shape, but also binary fraction and properties?

Many of the simulation techniques used in this work will be directly applicable to these new questions. N-body simulations are an ideal way to simulate a YORP spin-up. The steady-state model that was constructed to model the binary fraction caused by tidal disruption can be easily modified to include YORP or another binary formation mechanism. First steps towards a YORP spin-up model have been taken utilizing a rubble pile model of a strengthless asteroid being slowly spun-up. This is implemented via very

small additions to the angular momentum of the body and spaced out to allow the body to reshape or settle after every boost.

Preliminary results from YORP simulations for an initial tri-axial ellipsoid that is nearly spherical with a 4 h rotation, show that the first mass is lost after serious shape deformations, which occur beyond the limit for cohesionless proloids with a friction angle of 40° (see Fig. 5.1, Holsapple 2001). This limit has been shown to govern the breakup of numerically modeled rubble piles, whereas the traditional Jacobi sequence of ellipsoids governs the reaccumulation of a rotationally-disrupted body (Richardson et al. 2005; Holsapple 2001). This simulation was run until 20% of the initial mass was lost from the primary body. At the end of the simulation all mass bound to the central body was in single particles, none had accumulated into larger companions.

Though this simulation did not provide a stable large companion from a gradual spin-up, it does establish the framework for a more realistic set of simulations. Unlike tidal disruptions, which are by nature substantially more impulsive, the internal makeup of each body will have a large impact on the evolution of its shape and spin. As well, due to a significantly smaller parameter space to explore (initial shape and spin, spin-up rate, resolution, and particle size distribution), more exotic and computationally time-consuming body structures can be explored. Experiments with particle size distributions are needed, as are tests of rubble piles consisting of particle aggregates. Introducing a numerical "strength" to the model may permit super-critical spin, allowing for a more substantial disruption and a larger release of mass per breakup. These advances may be necessary to quantify how efficient the YORP effect is as a binary formation mechanism.

Lastly, a new observing campaign utilizing larger telescopes will be needed to more closely examine sub-kilometer MBAs. Currently the bulk of NEA lightcurves are measured by amateurs who are directed and organized by scientists. The relative proximity of NEAs allows for their study with modest, commercially-available telescopes. Re-

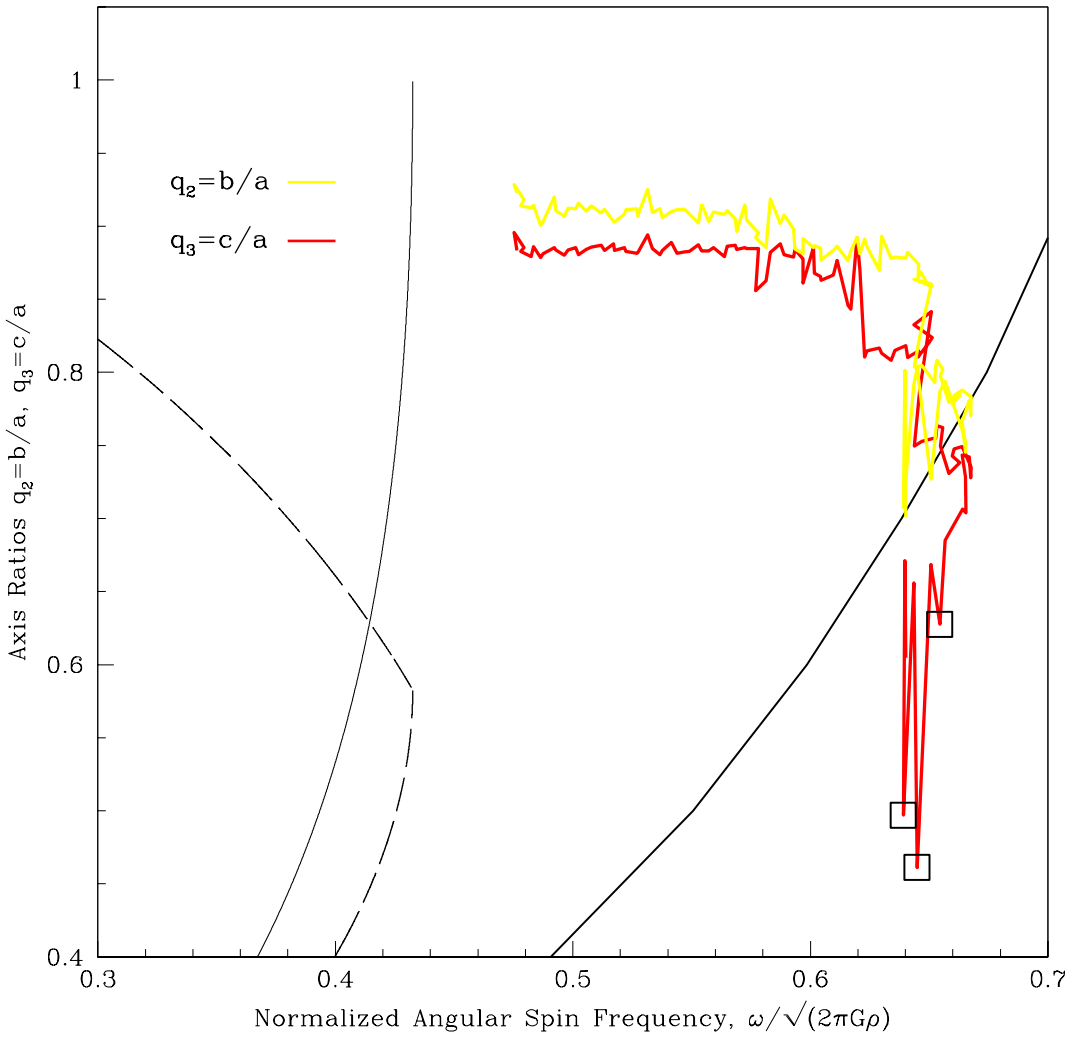

Figure 5.1: The axis ratios of a strengthless body as it is slowly spun-up are plotted against the normalized angular spin frequency. The red line represents the short over the long axis, and the yellow line is the intermediate over the long axis. The thin solid line and dashed line on the left are the classical limits for Jacobi and Maclaurin ellipsoids, and the thick solid line on the right is the spin limit for cohesionless solid proloids with an angle of friction of $\phi = 40°$. The open boxes represent places where mass was lost from the spinning body.

cently this large pool of observers has started studying MBAs, though larger apertures are needed to approach kilometer-sized targets. There are two anticipated changes that have the potential to greatly increase the number of well-determined lightcurves. The first is the increase in dedicated survey telescopes. In the next decade multiple survey telescopes will come online that are capable of imaging the entire observable sky over periods of days. Outfitted with enormous CCD's with instantaneous readout times, fields of view of many square degrees, and moderate to large apertures, these telescopes will discover millions of asteroids and increase the coverage on all small bodies enormously. Depending on the exact observing strategy of each telescope, many asteroids will be observed frequently enough to have lightcurves constructed over very long baselines.

The second possible advance in this field may come from the increasing number of extremely wide field of view imagers on 4–10 m class telescopes. The advance in CCD technology and the subsequent increase in the availability of wide field cameras has made possible the simultaneous observation of hundreds of asteroids. We have initiated trial observations using the MOSAIC camera on the KPNO 4m telescope observing a single ecliptic field containing 22 asteroids. The MOSAIC camera has a 36'$\times$36' field of view, and with a 90-second exposure, can get a signal-to-noise ratio of 50 on 21st visual-magnitude targets. Thus many sub-kilometer bodies will be sufficiently bright for lightcurves in any asteroid-rich field of view. This trial study suggests that large scale observations using more recent instruments, which boast 4–10 times the field of view of MOSAIC, may prove to be the most efficient way to study lightcurves of small MBAs, as well as to discover binaries in these populations.

Appendix A

Parameter Tests

In an effort to examine the systematics in the simulations completed is Chapter 2 a series of tests were performed to examine certain parameters which had remained fixed previously, namely bulk density, number of particles or resolution, and porosity. Observations continue to increase the number of bodies with well-constrained bulk densities, but using a value anywhere between 1–3 g cm^{-3} could be justified. Changing this parameter could affect all the results globally, and therefore tests were run to estimate the effect of such a change (Section A.1). Similar tests were performed on the resolution (number of particles) of the progenitor, which was also previously a fixed number (Section A.2). Finally tests were carried out on a non-close-packed progenitor body, to analyze how initially decreased bulk density may affect important properties (Section A.3).

A.1 Bulk Density of Progenitor

Recent observations indicate that near-Earth asteroids have a wide range of bulk density, with values sometimes as low as 1 g cm^{-3} (Pravec et al. 2006). The results in Chapter 2 were based on simulations where progenitors had a bulk density of 2.2 g cm^{-3}. In light of a population with a range of bulk densities, a test was performed to measure significant

differences in results when a lower-density, 1.0 g cm^{-3} progenitor is used. Previous work by Asphaug & Benz (1996) suggests that lowering bulk density of a progenitor makes a more dramatic disruption, with more fragments and less mass in the largest remnant, which should increase in the number of binaries formed.

The subset selected for testing covered a narrower range of parameters than previously examined, but focused on the closest approaches ($q < 2.0\ R_{\oplus}$) which were found to be most effective in forming binaries. The progenitor spin rates of 4 and 6 h were used, with elongations (elongation is defined as the ratio of the long axis, a to the short axis, c, of a tri-axial ellipsoid) of 1.0, 1.5 and 2.0. The encounter parameters used were close approach distances, q, or 1.2, 1.4, 1.6, 1.8 $R_{\oplus}$, with v_{∞} of 8, 16, and 24 km/s. As in Chapter 2 each set of parameters was simulated 100 different times with the spin axis of the progenitor body randomly positioned each time. This creates a distribution of outcomes for each set of parameters.

The low-density subset simulations show no differences in binary properties or binaries formed as a function of progenitor or encounter parameter. However, they show a uniform increase in number of binaries formed, producing 2.5 times the binaries for the same parameters.

As was seen earlier (Chapter 4), the dominant force in shaping the binary NEA fraction are binary-disrupting planetary encounters. This effect has a similar dependence on asteroid density as tidal disruption of a single body, and therefore any binary production gains from low densities are expected to be offset by increases in binary disruption.

A.2 Resolution of Progenitor

The resolution, or number of particles per progenitor, was about 1000 in our standard runs, designed to represent a $\sim$ 3 km aggregate consisting of $\sim$ 150 m sized particles. The evidence for 150 m building blocks comes from numerical simulations and the observed spin frequency cutoff for asteroids (Benz & Asphaug 1999; Pravec et al. 2002). However, this logic would demand that progenitors with smaller diameters have a lower resolution in simulations, and similarly require higher resolution for larger-diameter objects. Our ignorance about the true makeup of a gravitational aggregate justifies experiments with higher- and lower-resolution bodies. Thus a test of resolution over an order of magnitude was run, using progenitors with 200, 500, and 2000 particles over a subset of parameters.

The parameters used for these simulations are the same as those in Section A.1, except the 6 h spin rate. The resulting size ratios for the simulations all peak at a higher value (larger secondaries) for lower resolution and at lower values (smaller secondaries) for higher resolution (see Fig. A.1).

The number of binaries produced at each resolution differed by over a factor of three (see Table A.1). The disparity in binaries formed is likely due to the numerical technique used to find companions (Leinhardt & Richardson 2005). Only clumps with 3 or more particles were entered into the search, and each companion around a primary counts as a binary. Thus for higher-resolution runs it is significantly easier to have debris in the form of a 3+ particle clump orbiting a large primary thereby driving up the number of total binaries.

Also listed in Table A.1 is the count of the number of simulations in which a binary is produced. This statistic should reduce the advantage that higher-resolution simulations have in creating multiple binaries, and just count situations that produce at least one binary. This number still increases with resolution, but not as dramatically, as the 2000

Table A.1. Number of binaries produced at varying resolutions.

Number of particles per progenitor	Total binaries	Sims with binaries
200	686	543
500	962	648
1000	1549	921
2000	2262	939

Note. — The number of binaries produced for each subset of runs testing progenitor resolution.

particle runs produce less than twice as many as the 500 particle simulations.

The properties of the binaries show minor changes in primary spin rate and semi-major axis with resolution. Lower resolution pushes secondaries towards faster spin, and smaller semi-major axis. The shape of the primary is also affected, with lower resolution producing slightly more spherical primaries.

A.3 Packing Efficiency of Progenitor

In tidal disruption simulations, binaries are formed from reaccumulation of disrupted debris. Previously the progenitors were constructed using hexagonal closest packing of spheres for simplicity, meaning the particles were organized very precisely and the resulting assemblage had a lower porosity than a random assemblage of identical spheres[1].

[1]The densest arrangement of similar-sized spheres is a problem that dates back to Kepler, when he hypothesized in 1611 that the maximum density for packing comes from cubic or hexagonal close packing with a packing density $\pi/(3\sqrt{2}) \approx 74.408\%$. Many attempts to prove this culuminated in a published proof by Hales (2005), making extensive use of computer calculation and 12 reviewers *attempting* to verify its validity (Conway & Sloane 1993).

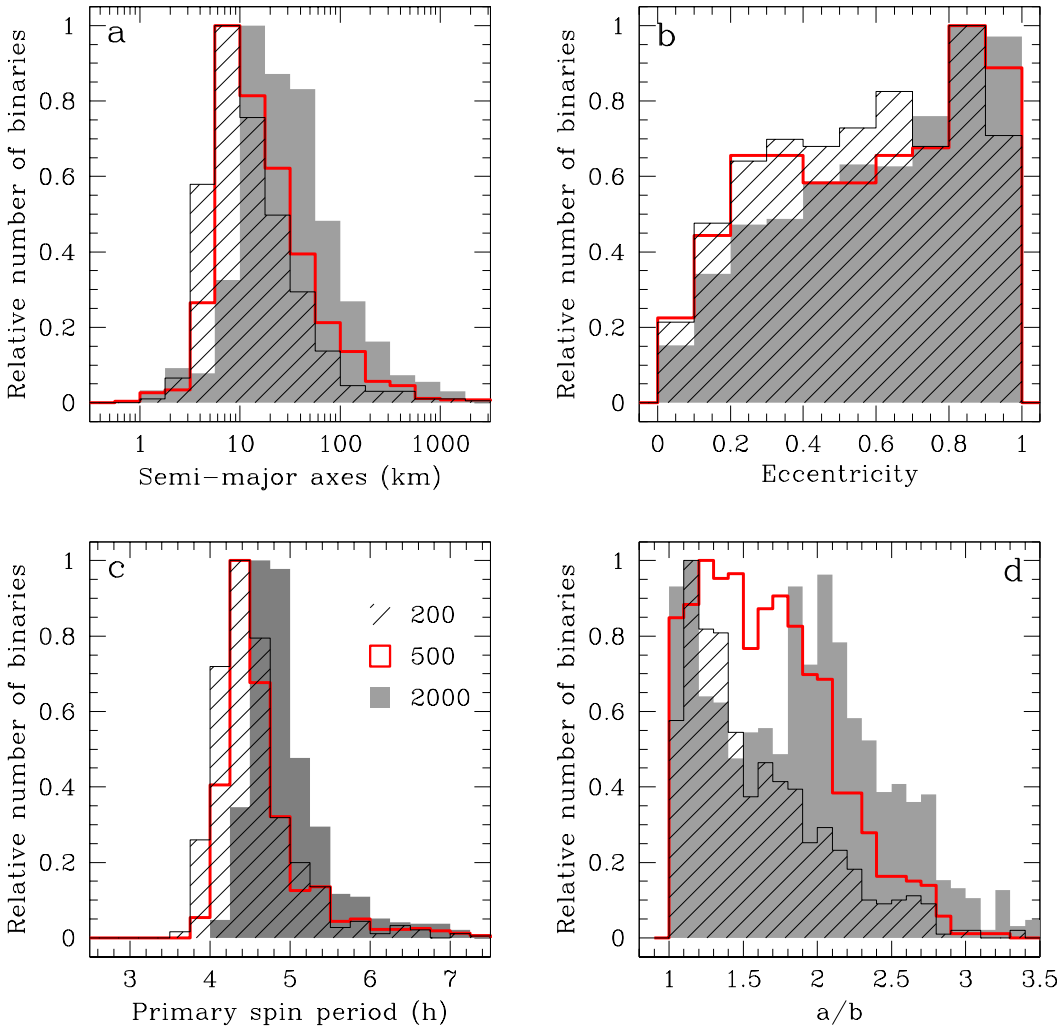

Figure A.1: Plot showing the effects of resolution on resultant binary properties: (a) is the semi-major axis of the binary; (b) the eccentricity; (c) the primary spin period; and (d) the primary shape given as the ratio of the long axis *a* to the intermediate axis *b*. Note that different numbers of binaries were formed at each resolution, and the histograms shown are each normalized with their maximum bin equal to unity.

Thus the reaccumulated bodies in the simulations would necessarily have a higher porosity and lower bulk density than the progenitor. The inability to collapse to an equally dense state as the progenitor was considered a possible reason for disparity in primary spin rate in previous simulations, and is tested here. New progenitors were taken from tidal disruption runs, where the bodies were disturbed or distorted but not disrupted. These new progenitors matched the original axis ratios closely, and had bulk densities $\sim$ 1.8 g cm^{-3}compared to $\sim$ 2.2 g cm^{-3}.

The subset of parameters used for these tests was the same as that used in the previous sections. Overall the slight density change had a minimal effect on binary production and properties (Figure A.3).

A.4 Conclusions on Parameter Tests

None of the previous three tests provided definitive solutions to discrepancies observed between the results of Chapter 2 and the observed binary NEAs. Altering the bulk density of the progenitor had an expected effect in dramatically changing the number of binaries produced. Such an effect may become increasingly important as measurements of asteroid bulk densities become more common. The dramatic increase in binary production for a 1.0 g cm^{-3} progenitor suggests that the overall binary production of NEAs by tidal disruption could depend on this property, but because binaries are disrupted by planetary encounters in a similar manner it is unlikely to change the steady-state binary fraction.

Varying the resolution of the simulations does change the resultant binary properties. *However, the changes are not dramatic, and do not affect the outcome of this steady-state simulation.* These differences could become important in a more sophisticated model in which the size distribution of the Main Belt and NEA populations is included and simulations are performed at each step, using different resolution bodies to correspond to

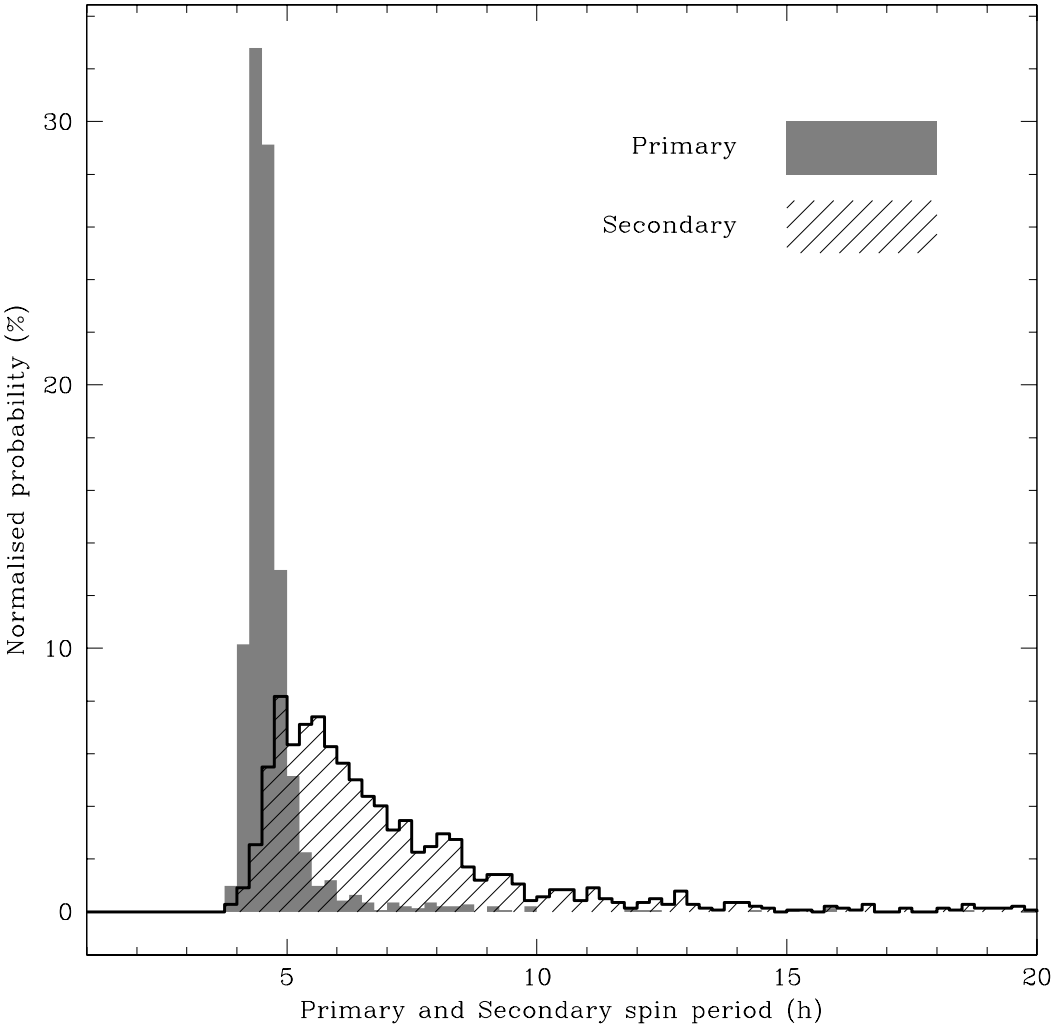

Spin rate of the primary and secondary bodies for binaries formed from the low-density-progenitor subset of simulations. The spin rates are comparable to those found from the results in Chapter 2 (Fig. 2.7)

different sized asteroids. This effect would be quite subtle and would be important only if the binary fraction contributed by tidal disruption was significant (which is does not appear to be).

Using progenitors with similar porosity/density as a reaccumulated body had relatively small effects on primary spin rate. This remains a point of concern, as the simulations do not reproduce primary spins nearly as rapid as those observed. The upper limit

of 2.2 h observed is significantly faster than the 3.0 h from simulations.

Bibliography

Agnor, C. B. & Hamilton, D. P. 2006, Nature, 441, 192

Asphaug, E. & Benz, W. 1996, Icarus, 121, 225

Behrend, R. 2004, IAU Circ., 8354

Behrend, R., Bernasconi, L., Klotz, A., & Durkee, R. 2004a, IAU Circ., 8389

Behrend, R., Bernasconi, L., Roy, R., Klotz, A., Colas, F., Antonini, P., Aoun, R., Augustesen, K., Barbotin, E., Berger, N., Berrouachdi, H., Brochard, E., Cazenave, A., Cavadore, C., Coloma, J., Cotrez, V., Deconihout, S., Demeautis, C., Dorseuil, J., Dubos, G., Durkee, R., Frappa, E., Hormuth, F., Itkonen, T., Jacques, C., Kurtze, L., Laffont, A., Lavayssière, M., Lecacheux, J., Leroy, A., Manzini, F., Masi, G., Matter, D., Michelsen, R., Nomen, J., Oksanen, A., Pääkkönen, P., Peyrot, A., Pimentel, E., Pray, D., Rinner, C., Sanchez, S., Sonnenberg, K., Sposetti, S., Starkey, D., Stoss, R., Teng, J.-P., Vignand, M., & Waelchli, N. 2006, A&A, 446, 1177

Behrend, R., Roy, R., Rinner, C., Antonini, P., Pravec, P., Harris, A. W., Sposetti, S., Durkee, R., & Klotz, A. 2004b, IAU Circ., 8265

Behrend, R., Roy, R., Sposetti, S., Waelchli, N., Pray, D., Berger, N., Demeautis, C., Matter, D., Durkee, R., Klotz, A., Starkey, D., & Cotrez, V. 2004c, IAU Circ., 8292

Belton, M. & Carlson, R. 1994, IAU Circ., 5948

Benner, L. A. M., Nolan, M. C., Margot, J. L., Ostro, S. J., & Giorgini, J. D. 2003, Bull. Am. Astron. Soc., 35, 959 (abstract)

Benner, L. A. M., Nolan, M. C., Ostro, S. J., Giorgini, J. D., & Margot, J. L. 2001a, IAU Circ., 7730

Benner, L. A. M., Nolan, M. C., Ostro, S. J., Giorgini, J. D., Margot, J. L., & Magri, C. 2004, IAU Circ., 8329

—. 2005, IAU Circ., 8563

Benner, L. A. M., Ostro, S. J., Giorgini, J. D., Jurgens, R. F., Margot, J. L., & Nolan, M. C. 2001b, IAU Circ., 7632

Benz, W. & Asphaug, E. 1999, Icarus, 142, 5

Binzel, R. P., Xu, S., Bus, S. J., & Bowell, E. 1992, Icarus, 99, 225

Bottke, Jr., W. F. & Melosh, H. J. 1996a, Icarus, 124, 372

—. 1996b, Nature, 381, 51

Bottke, Jr., W. F., Morbidelli, A., Jedicke, R., Petit, J., Levison, H. F., Michel, P., & Metcalfe, T. S. 2002, Icarus, 156, 399

Bottke, Jr., W. F., Nolan, M. C., Greenberg, R., & Kolvoord, R. A. 1994, in Gehrels, T., Matthews, M. S. (Eds.), Hazards Due to Comets and Asteroids. Univ. Arizona Press, Tucson, 337–357

Bottke, Jr., W. F., Richardson, D. C., Michel, P., & Love, S. G. 1999, Astron. J., 117, 1921

Bottke, Jr., W. F., Vokrouhlický, D., Rubincam, D. P., & Nesvorný, D. 2006, Annual Review of Earth and Planetary Sciences, 34, 157

Brown, M. E., Margot, J. L., de Pater, I., & Roe, H. 2001, IAU Circ., 7588

Burns, J. A. 1975, Icarus, 25, 545

Chandrasekhar, S. 1969, Ellipsoidal figures of equilibrium (The Silliman Foundation Lectures, New Haven: Yale University Press, 1969)

Chauvineau, B. & Farinella, P. 1995, Icarus, 115, 36

Chesley, S. R., Ostro, S. J., Vokrouhlický, D., Čapek, D., Giorgini, J. D., Nolan, M. C.,

Margot, J., Hine, A. A., Benner, L. A. M., & Chamberlin, A. B. 2003, Science, 302, 1739

Conway, J. H. & Sloane, N. J. 1993, Sphere Packings, Lattices, and Groups, 2nd ed. (Springer-Verlag), 3–9

Cuk, M. & Burns, J. A. 2004, Bull. Am. Astron. Soc., 36, 1184 (abstract)

Degewij, J., Tedesco, E. F., & Zellner, B. 1979, Icarus, 40, 364

Donnison, J. R. & Wiper, M. P. 1999, MNRAS, 302, 75

Durda, D. D. 1996, Icarus, 120, 212

Durda, D. D., Bottke, Jr., W. F., Enke, B. L., Merline, W. J., Asphaug, E., Richardson, D. C., & Leinhardt, Z. M. 2004, Icarus, 170, 243

Gladman, B., Michel, P., & Froeschlé, C. 2000, Icarus, 146, 176

Goldreich, R. 1963, MNRAS, 126, 257

Grieve, R. A. F. & Shoemaker, E. M. Hazards Due to Comets and Asteroids, ed. , T. GehrelsM. S. Matthews & A. M. Schumann, 417

Guibout, V. & Scheeres, D. J. 2003, Celestial Mechanics and Dynamical Astronomy, 87, 263

Gültekin, K., Miller, M. C., & Hamilton, D. P. 2004, ApJ, 616, 221

Gültekin, K. G. 2006, Ph.D. Thesis

Hales, T. C. 2005, Ann. Math., 162, 1065

Hamilton, D. P. & Burns, J. A. 1991, Icarus, 92, 118

Harris, A. W. 1996, in Lunar and Planetary Institute Conference Abstracts, 493–+

Harris, A. W. & Pravec, P. 2006, AAS/Division for Dynamical Astronomy Meeting Abstracts, 37

Harris, A. W., Warner, B. D., & Pravec, P. 2005a, NASA Planetary Data System, EAR-A-5-DDR-DERIVED-LIGHTCURVE-V7.0:LCREF_TAB, 35, 4

—. 2005b, NASA Planetary Data System, EAR-A-5-DDR-DERIVED-LIGHTCURVE-

V7.0:LCREF_TAB, 35, 4

Harris, A. W., Young, J. W., Dockweiler, T., Gibson, J., Poutanen, M., & Bowell, E. 1992, Icarus, 95, 115

Holsapple, K. A. 2001, Icarus, 154, 432

Howell, S. B. 1989, PASP, 101, 616

Ivezić, Ž., Tabachnik, S., Rafikov, R., Lupton, R. H., Quinn, T., Hammergren, M., Eyer, L., Chu, J., Armstrong, J. C., Fan, X., Finlator, K., Geballe, T. R., Gunn, J. E., Hennessy, G. S., Knapp, G. R., Leggett, S. K., Munn, J. A., Pier, J. R., Rockosi, C. M., Schneider, D. P., Strauss, M. A., Yanny, B., Brinkmann, J., Csabai, I., Hindsley, R. B., Kent, S., Lamb, D. Q., Margon, B., McKay, T. A., Smith, J. A., Waddel, P., York, D. G., & the SDSS Collaboration. 2001, AJ, 122, 2749, arXiv:astro-ph/0105511

Jeffreys, H. 1947, MNRAS, 107, 260

Landolt, A. U. 1992, AJ, 104, 340

Leinhardt, Z. M. & Richardson, D. C. 2002, Icarus, 159, 306

—. 2005, Icarus, 176, 432

Leinhardt, Z. M., Richardson, D. C., & Quinn, T. 2000, Icarus, 146, 133

Leone, G., Paolicchi, P., Farinella, P., & Zappala, V. 1984, A&A, 140, 265

Magnusson, P. 1990, Icarus, 85, 229

Marchis, F., Berthier, J., Clergeon, C., Descamps, P., & Hestroffer, D. 2005a, Asteroids, Comets, and Meteors: ACM 2005, in preparation

Marchis, F., Descamps, P., Hestroffer, D., & Berthier, J. 2005b, Nature, 436, 822

Marchis, F., Descamps, P., Hestroffer, D., Berthier, J., & de Pater, I. 2004a, AAS/Division for Planetary Sciences Meeting Abstracts, 36

Marchis, F., Descamps, P., Hestroffer, D., Berthier, J., Vachier, F., Boccaletti, A., de Pater, I., & Gavel, D. 2003, Icarus, 165, 112

Marchis, F., Laver, C., Berthier, J., Descamps, P., Hestroffer, D., de Pater, I., Behrend,

R., Roy, R., & Baudoin, P. 2004b, IAU Circ., 8264

Margot, J. L. 2003, IAU Circ., 8182

Margot, J.-L. & Brown, M. E. 2001, IAU Circ., 7703

Margot, J. L. & Brown, M. E. 2003, Science, 300, 1939

Margot, J. L., Nolan, M. C., Benner, L. A. M., Ostro, S. J., Jurgens, R. F., Giorgini, J. D., Slade, M. A., & Campbell, D. B. 2002, Science, 296, 1445

Margot, J. L., Nolan, M. C., Negron, V., Hine, A. A., Campbell, D. B., Howell, E. S., Benner, L. A. M., Ostro, S. J., Giorgini, J. D., & Marsden, B. G. 2003, IAU Circ., 8227

Merline, W. J., Close, L. M., Dumas, C., Chapman, C. R., Menard, F., Tamblyn, P. M., & Durda, D. D. 2003a, AAS/Division for Planetary Sciences Meeting Abstracts, 35

Merline, W. J., Close, L. M., Dumas, C., Chapman, C. R., Roddier, F., Menard, F., Slater, D. C., Duvert, G., Shelton, C., Morgan, T., & Dunham, D. W. 1999, IAU Circ., 7129

Merline, W. J., Close, L. M., Dumas, C., Shelton, J. C., Menard, F., Chapman, C. R., & Slater, D. C. 2000a, Bull. Am. Astron. Soc., 32, 1017 (abstract)

Merline, W. J., Close, L. M., Shelton, J. C., Dumas, C., Menard, F., Chapman, C. R., & Slater, D. C. 2000b, IAU Circ., 7503

Merline, W. J., Close, L. M., Siegler, N., Dumas, C., Chapman, C., Rigaut, F., Menard, F., Owen, W. M., & Slater, D. C. 2002a, IAU Circ., 7827

Merline, W. J., Close, L. M., Tamblyn, P. M., Menard, F., Chapman, C. R., Dumas, C., Duvert, G., Owen, W. M., Slater, D. C., & Sterzik, M. F. 2003b, IAU Circ., 8075

Merline, W. J., Dumas, C., Siegler, N., Close, L. M., Chapman, C. R., Tamblyn, P. M., Terrell, D., Conrad, A., Menard, F., & Duvert, G. 2003c, IAU Circ., 8165

Merline, W. J., Menard, F., Close, L., Dumas, C., Chapman, C. R., & Slater, D. C. 2001, IAU Circ., 7703

Merline, W. J., Tamblyn, P. M., Chapman, C. R., Nesvorny, D., Durda, D. D., Dumas, C.,

Storrs, A. D., Close, L. M., & Menard, F. 2003d, IAU Circ., 8232

Merline, W. J., Tamblyn, P. M., Dumas, C., Close, L. M., Chapman, C. R., & Menard, F. 2003e, IAU Circ., 8183

Merline, W. J., Tamblyn, P. M., Dumas, C., Close, L. M., Chapman, C. R., Menard, F., Owen, W. M., Slater, D. C., & Pepin, J. 2002b, IAU Circ., 7980

Merline, W. J., Tamblyn, P. M., Dumas, C., Menard, F., Close, L. M., Chapman, C. R., Duvert, G., & Ageorges, N. 2004, IAU Circ., 8297

Merline, W. J., Weidenschilling, S. J., Durda, D. D., Margot, J. L., Pravec, P., & Storrs, A. D. 2002c, in Bottke Jr., W .F., Cellino, A., Paolicchi, P., Binzel, R. P. (Eds.), Asteroids III. Univ. of Arizona Press, Tucson, 289–312

Michel, P., Benz, W., & Richardson, D. C. 2004, Icarus, 168, 420

Michel, P., Benz, W., Tanga, P., & Richardson, D. C. 2001, Science, 294, 1696

Michel, P., Migliorini, F., Morbidelli, A., & Zappalà, V. 2000, Icarus, 145, 332

Migliorini, F., Michel, P., Morbidelli, A., Nesvorny, D., & Zappala, V. 1998, Science, 281, 2022

Morbidelli, A. & Nesvorny, D. 1999, Icarus, 139, 295

Mottola, S., de Angelis, G., di Martino, M., Erikson, A., Hahn, G., & Neukum, G. 1995, Icarus, 117, 62

Mottola, S., Hahn, G., Pravec, P., & Šarounová, L. 1997, IAU Circ., 6680

Mottola, S. & Lahulla, F. 2000, Icarus, 146, 556

Murray, C. D. & Dermott, S. F. 1999, Solar system dynamics (Cambridge Univ. Press, New York), 166–173

Neish, C. D., Nolan, M. C., Howell, E. S., & Rivkin, A. S. 2003, American Astronomical Society Meeting Abstracts, 203

Nolan, M. C., Hine, A. A., Howell, E. S., Benner, L. A. M., & Giorgini, J. D. 2003a, IAU Circ., 8220

Nolan, M. C., Howell, E. S., & Hine, A. A. 2004, IAU Circ., 8336

Nolan, M. C., Howell, E. S., Magri, C., Beeney, B., Campbell, D. B., Benner, L. A. M., Ostro, S. J., Giorgini, J. D., & Margot, J.-L. 2002a, IAU Circ., 7824

Nolan, M. C., Howell, E. S., Ostro, S. J., Benner, L. A. M., Giorgini, J. D., Margot, J.-L., & Campbell, D. B. 2002b, IAU Circ., 7921

Nolan, M. C., Howell, E. S., Rivkin, A. S., & Neish, C. D. 2003b, IAU Circ., 8163

Nolan, M. C., Margot, J.-L., Howell, E. S., Benner, L. A. M., Ostro, S. J., Jurgens, R. F., Giorgini, J. D., & Campbell, D. B. 2000, IAU Circ., 7518

Opik, E. J. 1966, Irish Astronomical Journal, 7, 141

Ostro, S. J., Benner, L. A. M., Giorgini, J. D., Nolan, M. C., Hine, A. A., Howell, E. S., Margot, J. L., Magri, C., & Shepard, M. K. 2005, IAU Circ., 8627

Ostro, S. J., Hudson, R. S., Benner, L. A. M., Giorgini, J. D., Magri, C., Margot, J. L., & Nolan, M. C. 2002, Asteroids III, 151

Ostro, S. J., Margot, J.-L., Nolan, M. C., Benner, L. A. M., Jurgens, R. F., & Giorgini, J. D. 2000, IAU Circ., 7496

Ostro, S. J., Nolan, M. C., Benner, L. A. M., Giorgini, J. D., Margot, J. L., & Magri, C. 2003, IAU Circ., 8237

Pravec, P., Benner, L. A. M., Nolan, M. C., Kušnirák, P., Pray, D., Giorgini, J. D., Jurgens, R. F., Ostro, S. J., Margot, J.-L., Magri, C., Grauer, A., & Larson, S. 2003a, IAU Circ., 8244

Pravec, P. & Hahn, G. 1997, Icarus, 127, 431

Pravec, P. & Harris, A. W. 2000, Icarus, 148, 12

Pravec, P. & Harris, A. W. 2006, in AAS/Division for Planetary Sciences Meeting Abstracts, #65.01

Pravec, P., Harris, A. W., & Michalowski, T. 2002, in Bottke Jr., W .F., Cellino, A., Paolicchi, P., Binzel, R. P. (Eds.), Asteroids III. Univ. of Arizona Press, Tucson, 113–

122

Pravec, P., Kušnirá, P., Hicks, M., Holliday, B., & Warner, B. 2000a, IAU Circ., 7504

Pravec, P., Kušnirá, P., Šarounová, L., Brown, P., Esquerdo, G., Pray, D., Benner, L. A. M., Nolan, M. C., Giorgini, J. D., Ostro, S. J., & Margot, J.-L. 2003b, IAU Circ., 8216

Pravec, P., Kušnirá, P., & Warner, B. 2001, IAU Circ., 7742

Pravec, P., Kušnirá, P., Warner, B., Behrend, R., Harris, A. W., Oksanen, A., Higgins, D., Roy, R., Rinner, C., Demeautis, C., van den Abbeel, F., Klotz, A., Waelchli, N., Alderweireldt, T., Cotrez, V., & Brunetto, L. 2003c, IAU Circ., 8233

Pravec, P., Kušnirák, P., Šarounová, L., Brown, P., Kaiser, N., Masi, G., & Mallia, F. 2004a, IAU Circ., 8316

Pravec, P., Scheirich, P., Kušnirák, P., Šarounová, L., Mottola, S., Hahn, G., Brown, P., Kaiser, N., Krzeminski, Z., Esquerdo, G., Galád, A., Gajdoš, S., Kornoš, L., Világi, J., Harris, A. W., Hicks, M. D., Pray, D. P., Warner, B., Holliday, W., Behrend, R., DeGraff, D. R., Tholen, D., Whiteley, R., Larson, S., Grauer, A., Funkhouser, G. M., Knight, B. L., Slivan, S. M., Oksanen, A., Higgins, D., Velichko, F. P., Masi, G., Cooney, W. R., Kirsch, K., Dyvig, R., Stephens, R., & Snyder, L. 2004b, AAS/Division for Planetary Sciences Meeting Abstracts, 36, 1131 (abstract)

Pravec, P., Scheirich, P., Kušnirák, P., Šarounová, L., Mottola, S., Hahn, G., Brown, P., Esquerdo, G., Kaiser, N., Krzeminski, Z., Pray, D. P., Warner, B. D., Harris, A. W., Nolan, M. C., Howell, E. S., Benner, L. A. M., Margot, J.-L., Galád, A., Holliday, W., Hicks, M. D., Krugly, Y. N., Tholen, D., Whiteley, R., Marchis, F., Degraff, D. R., Grauer, A., Larson, S., Velichko, F. P., Cooney, W. R., Stephens, R., Zhu, J., Kirsch, K., Dyvig, R., Snyder, L., Reddy, V., Moore, S., Gajdoš, Š., Világi, J., Masi, G., Higgins, D., Funkhouser, G., Knight, B., Slivan, S., Behrend, R., Grenon, M., Burki, G., Roy, R., Demeautis, C., Matter, D., Waelchli, N., Revaz, Y., Klotz, A., Rieugné, M., Thierry,

P., Cotrez, V., Brunetto, L., & Kober, G. 2006, Icarus, 181, 63

Pravec, P., Šarounová, L., Rabinowitz, D. L., Hicks, M. D., Wolf, M., Krugly, Y. N., Velichko, F. P., Shevchenko, V. G., Chiorny, V. G., Gaftonyuk, N. M., & Genevier, G. 2000b, Icarus, 146, 190

Pravec, P., Wolf, M., & Šarounová, L. 1998, Icarus, 136, 124

Pravec, P., Wolf, M., & Šarounová, L. 1999, in IAU Colloq. 173: Evolution and Source Regions of Asteroids and Comets, 159

Pravec, P., Wolf, M., Varady, M., & Barta, P. 1995, Earth Moon and Planets, 71, 177

Rabinowitz, D. L. 1994, Icarus, 111, 364

—. 1997a, Icarus, 127, 33

—. 1997b, Icarus, 130, 287

Rauch, K. P. & Hamilton, D. P. in preparation, AJ

Reddy, V., Dyvig, R., Pravec, P., & Kušnirák, P. 2005, IAU Circ., 8483

Richardson, D. C., Bottke, Jr., W. F., & Love, S. G. 1998, Icarus, 134, 47

Richardson, D. C., Elankumaran, P., & Sanderson, R. E. 2005, Icarus, 173, 349

Richardson, D. C., Leinhardt, Z. M., Melosh, H. J., Bottke, Jr., W. F., & Asphaug, E. 2002, in Bottke Jr., W .F., Cellino, A., Paolicchi, P., Binzel, R. P. (Eds.), Asteroids III. Univ. of Arizona Press, Tucson, 501–515

Richardson, D. C., Quinn, T., Stadel, J., & Lake, G. 2000, Icarus, 143, 45

Richardson, D. C. & Walsh, K. J. 2006, Annual Review of Earth and Planetary Sciences, 34, 47

Roche, E. A. 1847, Acad. Sci. Lett. Montpelier. Mem. Section Sci., 1, 243

Ryan, W. H., Ryan, E. V., & Martinez, C. T. 2004, Planet. Space Sci., 52, 1093

Ryan, W. H., Ryan, E. V., Martinez, C. T., & Stewart, L. 2003, IAU Circ., 8128

Scheeres, D. J. 2002, Icarus, 159, 271

Scheeres, D. J., Marzari, F., & Rossi, A. 2004, Icarus, 170, 312

Shepard, M. K., Schlieder, J., Nolan, M. C., Hine, A. A., Benner, L. A. M., Ostro, S. J., & Giorgini, J. D. 2004, IAU Circ., 8397

Sheppard, S. S. & Jewitt, D. 2004, AJ, 127, 3023, arXiv:astro-ph/0402277

Solem, J. C. 1994, Nature, 370, 349

Solem, J. C. & Hills, J. G. 1996, Astron. J., 111, 1382

Sridhar, S. & Tremaine, S. 1992, Icarus, 95, 86

Stadel, J. G. 2001, Ph.D. Thesis, 126 p

Stanzel, R. 1978, A&AS, 34, 373

Stellingwerf, R. F. 1978, ApJ, 224, 953

Storrs, A., Vilas, F., Landis, R., Wells, E., Woods, C., Zellner, B., & Gaffney, M. 2001, IAU Circ., 7599

Tamblyn, P. M., Merline, W. J., Chapman, C. R., Nesvorny, D., Durda, D. D., Dumas, C., Storrs, A. D., Close, L. M., & Menard, F. 2004, IAU Circ., 8293, 3

van Flandern, T. C., Tedesco, E. F., & Binzel, R. P. 1979, in Gehrels, T. (Eds.), Asteroids. Univ. of Arizona Press, Tucson, 443–465

Vokrouhlický, D., Nesvorný, D., & Bottke, Jr., W. F. 2003, Nature, 425, 147

Walsh, K. J. & Richardson, D. C. 2006, Icarus, 180, 201

Walsh, K. J., Richardson, D. C., & Rettig, T. W. 2003, in ASP Conf. Ser. 291: Hubble's Science Legacy: Future Optical/Ultraviolet Astronomy from Space, 415–418

Warner, B., Pravec, P., Harris, A. W., Galád, A., & Kušnirák, P. 2005a, Asteroids, Comets, and Meteors: ACM 2005, in preparation

Warner, B., Pravec, P., Kušnirák, P., Pray, D., Galád, A., Gajdoš, S., Brown, P., & Krzeminski, Z. 2005b, IAU Circ., 8511

Warner, B. D. 2004, The Minor Planet Observer

Weidenschilling, S. J., Paolicchi, P., & Zappala, V. 1989, in Binzel, R. P., Gehrels, T., Matthews, M. S. (Eds.), Asteroids II. Univ. of Arizona Press, Tucson, 643–658

Wetherill, G. W. 1979, Icarus, 37, 96

—. 1988, Icarus, 76, 1

Wisdom, J. 1983, Icarus, 56, 51

Yoder, C. F. 1981, Bull. Am. Astron. Soc., 13, 710 (abstract)